Design Methods for Triangle-based 3D Origami

March　２０１８

Yan Zhao

Design Methods for Triangle-based 3D Origami

Graduate School of Systems and Information Engineering

University of Tsukuba

March　２０１８

Yan Zhao

Abstract

Paper, a kind of everyday material, has shown its ability to form three-dimensional (3D) structures as we can see in origami. Origami, also known as paper folding, has a long history, which maybe since the invention of paper. Such operations continue to this day and most of us have the experience of folding crane and frog in our childhood. Recently, origami, the centuries-old art forms, has taken off to new heights. Benefiting from the developing mathematical understanding, more and more complex and detailed origami pieces emerged. In addition, designing an origami becomes more efficient with the help of the computer-aided-design software, using which the user can preview the final shape.

Origami also gained much attention in science and engineering owing to its unique properties, e.g., developability, flat-foldability, and scale-independent. It has already provided solutions in nature, e.g., tree leaves and insect wings. The material for folding is not limited to paper, but can be metal, plastic, and shape memory polymers for specific applications. Applying origami-concepts has lead to lots of applications in various areas, e.g., DNA origami, self-folding robots, and foldable solar panels. Despite the growing attention, designing an origami considering its geometric constraints is still difficult.

The 3D origami, which is a kind of origami with a 3D structure, is a relatively new area comparing to flat-foldable origami (2D origami). It can generate geometrically elegant 3D structures and could be applied in engineering. The 3D origami focused in this study contains a set of polygons, and thus a planar constraint, which requires all vertices of a polygon lie on the same plane, should be satisfied. Triangle-based 3D origami is the simplest polygon-based 3D origami. It does not need to consider the planar constraint, however geometric constraints still limit its design space and make it hard to design. This thesis presents several design methods for the triangle-based 3D origami. Our work illustrates the ability for generating 3D structures using triangle-based origami, which not only provides variations of paper folding but also gives greater opportunity for applications.

Axisymmetric 3D origami is preferred by designers because it is relatively easy to fabricate and more stable. On the other hand, non-axisymmetric 3D origami is more flexible and thus can produce many types of shapes. In this thesis, three methods for the axisymmetric 3D origami and a method for axisymmetric or non-axisymmetric 3D origami are proposed. In particular, the proposed methods contain four parts: (1) a design method for axisymmetric 3D origami based on rotationally-symmetric crease patterns, (2) a design method for tucking axisymmetric 3D origami based on rotationally-symmetric crease patterns, (3) a design method for axisymmetric 3D origami with generic six-crease bases, (4) a method for approximating 3D surfaces with varying or constant curvatures using generalized waterbomb tessellations.

Firstly, a design method for axisymmetric 3D origami based on rotationally-symmetric crease patterns is proposed. First, the geometric definition of the crease pattern is given. Based on the type of the crease pattern, the developable constraint can be satisfied. Then,

the 3D geometry is analytically calculated. Furthermore, the proposed method explores the variations of the geometry by changing parameters, which lead to two rigid motions.

Secondly, a design method for tucking the axisymmetric 3D origami based on rotationally-symmetric crease patterns is proposed. This method can handle the crease pattern consisting of interior vertices having non-zero angle deficit generated during the 3D editing. Those interior vertices having non-zero angle deficit could lead to blank spaces, which contain no creases and thus hinder us from folding. Here, a procedure to place flaps outside or tucks inside to handle the blank spaces is proposed. The flaps or tucks make the edited shape realizable.

Thirdly, a method to design axisymmetric 3D origami with generic six-crease bases is proposed. Inspired by the conventional six-crease bases, i.e., waterbomb base or Yoshimura base, where six regular crease lines meet at an interior vertex, this method generalizes the base so that the lengths of the creases can be regular or irregular. First, the crease pattern consisting of such generic bases is interactively generated. Then, our method analytically calculates the 3D geometry with an axisymmetric structure. Furthermore, exploring various configurations, i.e., sets of input parameters, are demonstrated. The 3D origami can have multiple degrees of freedom, but by continually changing one parameter, a motion that can axisymmetrically deploy or flatten the shape is presented.

Fourthly, a method for approximating target surfaces, which can be axisymmetry or non-axisymmetry, using generalized waterbomb tessellations is proposed. The target surfaces are represented as parametric surfaces. First, a base mesh by tiling the target surface using waterbomb bases is generated. Then, by applying a simple numerical optimization algorithm to the base mesh, a developable waterbomb tessellation is achieved. Owing to the high degree of freedom of the waterbomb tessellation, orientable or non-orientable target surfaces can be handled.

We conduct results of origami pieces and demonstrate that our methods enable us to fabricate 3D structures by folding. Finally, we conclude this thesis and outlook the future.

Acknowledgements

First and foremost, I would like to thank my supervisors, Professors Jun Mitani, Yoshihiro Kanamori, and Assistant Professor Yuki Endo who give insightful comments and suggestions. This thesis has been done under the direction of them, and would not have been possible without their helpful advice and encouragement.

I am sincerely and extremely grateful to Professor Jun Mitani, for he taught me a lot about approaching and solving research problems. I also thank him for bringing me into his research group at the University of Tsukuba when I was achieved my master degree at Iwate University. During my doctoral course, I have not only published my research papers but also got the chances of interview and exhibition, which spurred me to further my research.

I would like to thank Yoshihiro Kanamori, for the countless hours he spent reading the drafts of my research papers line by line. His comments always inspired me to improve my research. I also want to thank Yuki Endo, for his enthusiasm and attitude toward research, and so many members of the non-numerical processing algorithms laboratory for giving me constructive comments and warm encouragement. My gratitude also goes to the Japanese Government and MEXT for the scholarship during the last year of my doctoral course.

I am grateful to great faculty members, Professor Hiroyuki Kudo, Professor Toshimasa Yamanaka, and Professor Shin Takahashi for reviewing this thesis and giving insightful comments.

Finally, I would like to thank my parents and wife for always believing in me and encouraging me.

Contents

1 Introduction **1**

1.1 Motivation . . . 2
1.2 Principal Contributions . . . 3
1.3 Outline . . . 6
1.4 Publications and Awards . . . 6
1.4.1 Reference papers . . . 6
Journal papers (with peer review) . . . 6
International poster (without peer review) . . . 7
Domestic conference papers (without peer review) . . . 7
1.4.2 Other papers . . . 7
International conference paper (with peer review) . . . 7
Domestic conference paper (with peer review) . . . 7
1.4.3 Grants and awards . . . 8

2 Related Work **9**

2.1 Preliminaries . . . 9
2.2 Mathematical principles of origami . . . 11
2.2.1 Huzita-Hatori axioms . . . 11
2.2.2 Constraint of developability . . . 12
2.2.3 Constraint of flat-foldability . . . 13
2.3 Design methods of origami . . . 13
2.3.1 Design methods for flat-foldable origami . . . 13
2.3.2 Design methods for 3D Origami . . . 15
2.4 Origami-inspired applications . . . 19
2.5 Triangle-based origami designs and applications . . . 20

3 Axisymmetric 3D origami based on rotationally-symmetric crease patterns **21**

3.1 Designing crease pattern . . . 22
3.2 Calculation of 3D origami . . . 23
3.2.1 Calculation of $\mathbf{P_1}$ . . . 23
3.2.2 Calculation of $\mathbf{P}_i(i > \mathbf{1})$ . . . 24

3.2.3 Special Case in Calculation of $\mathbf{P}_i(i > \mathbf{1})$ . . . 26
3.3 Effects on geometry . . . 27
3.3.1 Changing angle φ . . . 27
3.3.2 Changing angle Θ . . . 28
3.4 Results . . . 30
3.5 Summary . . . 31

4 Tucking axisymmetric 3D origami 35
4.1 Methodology . . . 36
4.1.1 Calculating 3D Origami with flaps or tucks . . . 36
4.1.2 Special case of 3D flaps . . . 40
4.2 Results . . . 41
4.3 Summary . . . 42

5 Axisymmetric 3D Origami with Generic Six-crease Bases 45
5.1 Designing 3D origami . . . 46
5.1.1 Designing crease pattern . . . 46
5.1.2 Calculation of each 3D point . . . 47
5.2 Motion analysis . . . 52
5.2.1 Calculation of degree of freedom . . . 52
5.2.2 Kinematic behavior . . . 53
5.3 Results . . . 55
5.4 Summary . . . 56

6 Approximating 3D Surfaces using Generalized Waterbomb Tessellations 59
6.1 Approximating target surfaces . . . 60
6.1.1 Generation of base mesh . . . 60
6.1.2 Numerical optimization . . . 62
6.2 Results . . . 63
6.3 Summary . . . 67

7 Conclusion and Future work 70
7.1 Summary of Contributions . . . 70
7.2 Future Work . . . 72

References 74

List of Figures

1.1 Examples of conventional triangle-based origami patterns. (a) A waterbomb tessellation, where the top shows a crease pattern and the bottom shows an origami piece. (b) A Yoshimura pattern, where the top shows a crease pattern and the bottom shows an origami piece. (c) A Nojima pattern. Image adopted from [75]. (d) A Resch's pattern. Image adopted from [70]. 2

1.2 Contributions of the design method for axisymmetric 3D origami based on rotationally-symmetric crease patterns. (a) A rotationally-symmetric crease pattern. (b) A rigid motion from a folded state to a flat state. The 3D origami is folded from the crease pattern shown in (a). (c) A motion that can flat fold the shape about a common axis. 4

1.3 Contributions of the tucking axisymmetric 3D origami. (a) A crease pattern with blank spaces. (b) A calculated 3D origami with flaps outside. 5

1.4 Contributions of the design method for axisymmetric 3D origami with generic six-crease bases. (a) A mirror-symmetric crease pattern with generic six-crease bases. (b) A calculated axisymmetric 3D origami. 5

2.1 Examples of origami diagrams and crease pattern for a paper crane. (a) Origami diagrams by Andrew Hudson. (b) A crease pattern exported by ORIPA [55]. 10

2.2 A crease pattern may be folded as a mountain (in red) or a valley (in blue). . 10

2.3 Huzita-Hatori (Huzita-Justin) axioms. 11

2.4 Flat-foldable vertex [78]. 12

2.5 TreeMaker software sequence (Images adopted from [8]). 14

2.6 Examples of flat-foldable origami design systems. (a) Tess: origami tessellation software. (b) ORIPA: origami pattern editor. (c) Origaminista: a browser-based application which generates simple origami pieces. (d) CP finder. 15

2.7 Examples of 3D origami design methods proposed by Tachi. (a) Origamizer software applied to Stanford bunny, where the real-world folding shown on the left and the computed crease pattern shown on the right. Images adopted from [19]. (b) Freeform origami used to edit a waterbomb tessellation in 3D. Image adopted from [78]. (c) Freeform origami tessellations by generalizing Resch′s patterns. Images adopted from [81]. 16
2.8 Examples of curved-crease origami. (a) The Bauhaus model [32]. (b) David Huffman and his "hexagonal column with cusps" [14]. (c) A lamp design [38]. (d) Reconstruction of the car model designed by Gregory Epps [41]. 17
2.9 Examples of 3D origami design methods proposed by Mitani. (a) A design method for 3D origami based on rotational sweep. Images adopted from [58], where the left shows a smooth curved polyline as an input, the middle shows the calculated 3D shape, and the right shows its crease pattern. (b) An interactive design of planar curved folding by reflection. Images adopted from [62]. (c) A column-shaped origami design based on mirror reflections. Images adopted from [61], where the left shows profile polyline, the middle shows the trajectory polyline, and the right shows the resulting shape. 18
2.10 Generalized Miura-ori tessellations fitting target surfaces. The top row depicts calculated 3D surfaces, while the bottom row shows physical models. Images adopted from [20]. 19
2.11 Triangle-based origami designs and applications. (a) A backpack design. Image adopted from [29]. (b) An adaptive freeform surface. Image adopted from [82]. (c) An origami stent graft made from a semi-rigid sheet. Image adopted from [93]. (d) A deformable wheel robot. Image adopted from [49]. 20

3.1 An overview of our method. 22
3.2 Designing rotationally-symmetric crease pattern consisting of triangular facets. 23
3.3 Calculation of P_1. 24
3.4 Calculation of $P_i(i = 2)$. 25
3.5 Calculation of $P_i(i = 3)$. 25
3.6 Calculation of $P_i(i = 4)$ 26
3.7 Special case in calculation. 27
3.8 Various origami designs obtained by changing φ from 0° to 180°: (a) $\varphi = 0°$, (b) $\varphi = 66°$, (c) $\varphi = 83°$, (d) $\varphi = 90°$, (e) $\varphi = 97°$, (f) $\varphi = 115°$, (g) $\varphi = 135°$, (h) $\varphi = 180°$. 28
3.9 Preparation for along-arc flat-folding. 29
3.10 A prototype system implemented our algorithm. 30
3.11 Resulting origami pieces with triangular facets. 31

3.12 Flat-folding motion. 32
3.13 Resulting origami pieces with flat center area and triangular facets. 33
3.14 Along-arc flat-folding sequences. 34
3.15 Along-arc flat-folding of real origami pieces. 34

4.1 An overview of our method. 36
4.2 Designing origami in 3D space. 37
4.3 Recalculating crease pattern. 38
4.4 Updated crease patterns corresponding to the operations shown in Figure 4.2. 38
4.5 Calculate 3D shape of flap. 39
4.6 Variation of 3D flaps. 39
4.7 Calculating 3D flaps folded from polygonal blank spaces. 40
4.8 Special case of 3D flaps. 41
4.9 A graphical user interface for supporting 3D editing. 42
4.10 Resulting origami pieces with 3D flaps or tucks. 43
4.11 Resulting origami pieces with two types of 3D flaps. 44
4.12 Resulting origami pieces with shape of stool. 44
4.13 Load bearing experiment on stool shape-like origami with tucks inside. . . 44

5.1 Origami consisting of four-crease bases. (a) Miura-ori. (b) Generalized Miura-ori pattern. For each origami, the left shows the crease pattern and the right shows a partially folded state. In the crease pattern, mountain creases are indicated by solid lines and valley folds by dashed lines. Fold lines of the same colour have the same fold angle. Images adopted from [24]. 45
5.2 An overview of our method. 46
5.3 Designing crease pattern. 47
5.4 Determination of P_1. 48
5.5 Calculation of P_2. 49
5.6 Calculation of $P_i (i > 2)$, where $i = 5$. 50
5.7 Variations in 3D origami by changing configuration. 51
5.8 Satisfaction of Kawasaki's theorem for each interior vertex. 53
5.9 Along-arc flat-folding with self-intersection-free test. 53
5.10 Kinematic behavior of P_5. 54
5.11 Kinematic behavior of P_6. 54
5.12 A prototype system implemented our algorithm. 55
5.13 Resulting origami pieces with different 'global' Gaussian curvature. 56
5.14 Resulting origami pieces. 57
5.15 Folding sequences with self-intersection-free test. 58
5.16 Self-intersections occur during folding motion. 58
5.17 Modification to enable the origami be flat folded. 58

6.1 Geometry of generalized waterbomb origami 59
6.2 An overview of our method. 60
6.3 Initial approximation using quads 61
6.4 Modification of waterbomb base 62
6.5 Merging waterbomb bases to achieve base mesh 63
6.6 Graphs of convergence created during optimization for producing developable surface 64
6.7 Approximations with variable resolutions for same target surface 65
6.8 Fabricated origami pieces 68
6.9 Developable approximations consisting of generalized waterbomb tessellations 69

Chapter 1

Introduction

This chapter gives an introduction in terms of origami and the main goals of this thesis. Then, it summarizes methods and results contributed by the thesis. Finally, it concludes with a short overview of the organization of this document.

Origami, the centuries-old art forms, is also known as paper folding. The term of origami has the Japanese roots "ori" meaning "folded" and "kami" meaning "paper" [46]. Traditional origami usually involves straight folds on a square piece of paper. Tearing, cutting or gluing are not allowed. Although it has a long history, origami continue to this day and most of us have the experience of folding crane and frog in our childhood. The resultant origami piece is achieved through a series of folding operations. Formally, the folding is a continuum of isometric embeddings of the paper in $\mathbb{R}^3$ and it permits to touch but not cross each paper [15]. Despite its simplicity, origami have produced lots of geometric shapes and some of them can be very complex and detail.

Recently, origami has taken off to new heights. Benefiting from a developing mathematical understanding, more and more complex and detailed origami pieces emerged. Some of the designs contain hundreds of folding and thus cannot be easily fabricated through a trial-and-error process. In addition, designing an origami becomes more efficient with the help of the computer-aided-design (CAD) software, using which the user can preview the final shape.

Origami can provide elegant solutions in nature, e.g., tree leaves and insect wings. It has been of growing interest to the scientific and engineering community due to its unique properties, e.g., developability, flat-foldability, and scale-independent. Developability enables an origami to be unfolded as a flat plane without stretching. Flat-foldability makes an origami be folded flat. Scale-independent enables the crease pattern of an origami to be folded at centimeter scale or meter scale. Besides, the material for folding is not limited to paper, but can be metal, plastic, and shape memory polymers for specific applications. Applying origami-concepts has lead to lots of applications in various areas.

The 3D origami, which is a kind of origami with a 3D structure, is a relatively new area comparing to flat-foldable origami (2D origami). The 3D origami focused in this study contains a set of polygons and can generate geometrically elegant 3D structures, some of which could be applied in architecture. Triangle-based 3D origami is the simplest polygon-based 3D origami. Several conventional triangle-based origami patterns, e.g., waterbomb tessellation [1], Yoshimura pattern [92, 36, 83], Nojima pattern [67], and Resch's pattern [69, 70], have been proposed (Figure 1.1). Besides, by applying such patterns, lots of applications have been achieved.

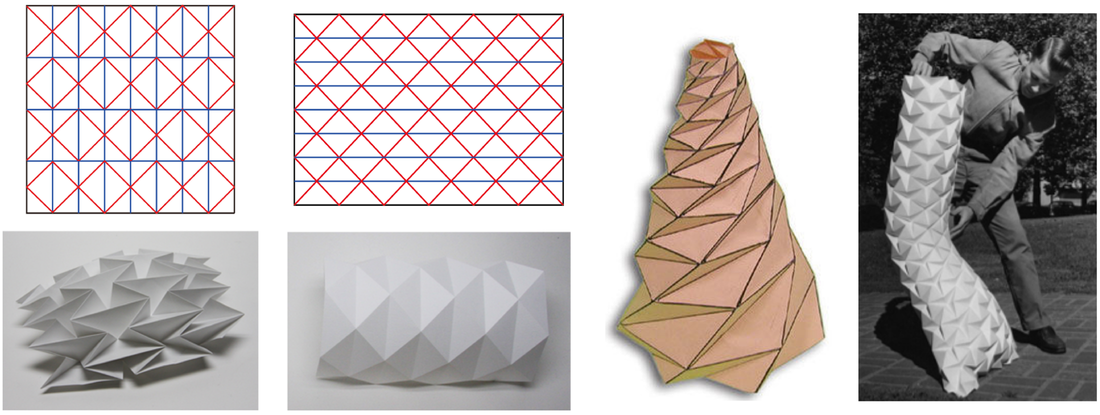

Figure 1.1: Examples of conventional triangle-based origami patterns. (a) A waterbomb tessellation, where the top shows a crease pattern and the bottom shows an origami piece. (b) A Yoshimura pattern, where the top shows a crease pattern and the bottom shows an origami piece. (c) A Nojima pattern. Image adopted from [75]. (d) A Resch's pattern. Image adopted from [70].

However, designing a triangle-based 3D origami is difficult, even if the planar constraint, which requires all vertices of a polygon lie on the same plane, is satisfied. Geometric constraints, e.g., developability, still limit its design space and make it hard to design. Several design methods exist for 3D origami, however, due to each origami has its own geometric constraints, and thus these existing methods cannot fully handle this kind of origami. Therefore, in this thesis, we focus on the triangle-based 3D origami and propose several design methods. The further advance of this type of origami not only contribute to the area of paper folding, but also to the related areas.

1.1 Motivation

Triangle-based origami can be found in the conventional origami patterns. Although planar constraint naturally satisfied, restricted design space limits its variations. On the application side, most studies are based on the conventional patterns, e.g., Yoshimura pattern and waterbomb tessellation. Therefore, variations of this kind of origami not only generates novel designs but also provide greater opportunities for applications.

In this thesis, the focus is drawn on the 3D origami consisting of triangular facets and several novel design methods are proposed. Fully explanations in terms of geometric definition, calculation, and simple folding simulation, will be described. In addition, several novel designs and potential usage will be illustrated. Several prototype systems will be provided. With the help of these systems, users can interactively design a 3D origami and quickly explore its variations. Finally, we hope these methods could inspire more and more novel designs and pave the way of applying.

1.2 Principal Contributions

We focus on the triangle-based 3D origami and proposed several design methods. First, we propose three design methods for the 3D origami with an axisymmetric structure. The axisymmetric origami can be widely noticed, because it is relatively easy to fabricate and more stable. Second, we focus on an inverse-origami-design problem, which uses origami to fit target 3D surfaces. Generalized waterbomb tessellations are used for approximating target surfaces represented as parametric surfaces.

In particular, we present the following methods:

1. Axisymmetric 3D origami based on rotationally-symmetric crease patterns [96]
2. Tucking axisymmetric 3D origami
3. Axisymmetric 3D origami with generic six-crease bases [97]
4. Approximating 3D surfaces using generalized waterbomb tessellations [95]

The detailed contributions to each method are described as follows:

Axisymmetric 3D origami based on rotationally-symmetric crease patterns: We propose a novel design method for axisymmetric 3D origami based on rotationally-symmetric crease patterns (Figure 1.2 (a)). Benefiting from the symmetry property, the developable constraint of the origami can be satisfied. Then, we describe the detailed calculation of the geometry (the left model shown in Figure 1.2 (b)). We implemented a prototype design system, using which users can interactively design the crease pattern and explore various shapes with real-time interaction. Furthermore, we simulate two one-parameter rigid motions. One motion shows a rigid transformation from one folded state to a flat state (Figure 1.2 (b)). The other shows a motion that can flat fold the shape about a common axis (Figure 1.2 (c)).

Tucking axisymmetric 3D origami: We focus on the kind of axisymmetric triangle-based 3D origami folded from the rotationally-symmetric crease patterns and propose a design method for tucking such origami. Our method can handle the crease pattern consisting of

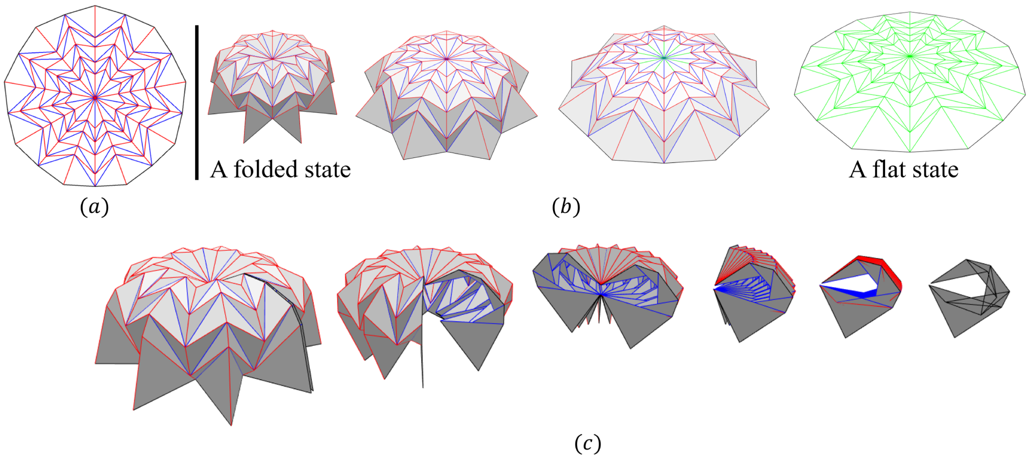

Figure 1.2: Contributions of the design method for axisymmetric 3D origami based on rotationally-symmetric crease patterns. (a) A rotationally-symmetric crease pattern. (b) A rigid motion from a folded state to a flat state. The 3D origami is folded from the crease pattern shown in (a). (c) A motion that can flat fold the shape about a common axis.

interior vertices having non-zero angle deficit (e.g., p_2 and p_4 in Figure 1.3 (a)) generated during the editing in 3D space. Editing the 3D origami while retaining each angle deficit of interior vertices equals zero, i.e., the sum of the angles around each interior vertex retains 360 degrees, is difficult. Those interior vertices with non-zero angle deficit could generate blank spaces (unfold areas shown in Figure 1.3 (a)), which hinder us from folding, or invalid crease pattern due to self-intersections. Here, we focus the former case and propose a computational procedure to handle blank spaces emerged in the crease pattern. We first divide such blank spaces into triangular facets by considering an edge symmetry. Then, we calculate the resultant 3D shape with flaps outside (Figure 1.3 (b)) or tucks inside, which are folded from such areas. By adding flaps or tucks, we make the origami realizable through tucking. Finally, on the application side, we describe a load-bearing experiment on a stool shape-like origami to demonstrate the potential usage.

Axisymmetric 3D origami with generic six-crease bases: We propose a method to design axisymmetric 3D origami with generic six-crease bases. Inspired by the conventional six-crease bases, i.e., waterbomb base or Yoshimura base, where six regular crease lines meet at an interior vertex, we generalize the base so that the lengths of the crease lines can be regular or irregular. The geometry of such a crease pattern ensures the satisfaction of the developability. The proposed method is based on designing a mirror-symmetric crease pattern (Figure 1.4 (a)) and then analytically calculates the axisymmetric shape (Figure 1.4 (b)). Furthermore, exploring various configurations, i.e., a set of input parameters, are demonstrated. Besides, this method presents a motion that can axisymmetrically deploy or flatten the shape by continually changing one parameter.

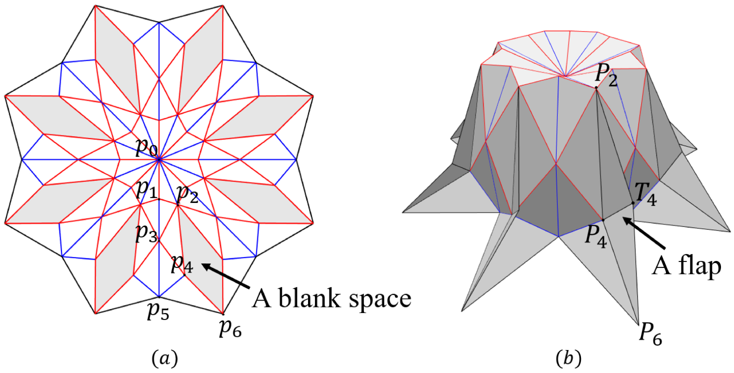

Figure 1.3: Contributions of the tucking axisymmetric 3D origami. (a) A crease pattern with blank spaces. (b) A calculated 3D origami with flaps outside.

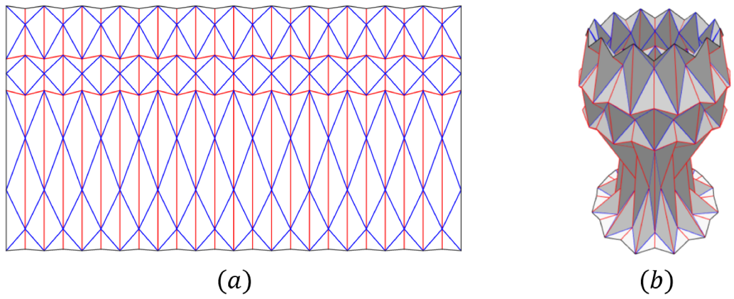

Figure 1.4: Contributions of the design method for axisymmetric 3D origami with generic six-crease bases. (a) A mirror-symmetric crease pattern with generic six-crease bases. (b) A calculated axisymmetric 3D origami.

Approximating 3D surfaces using generalized waterbomb tessellations: Origami could transform flat sheets of paper into complex geometries through folding crease patterns. Waterbomb tessellation has been used to create geometrically appealing 3D shapes and been widely studied. Here, we propose a method for approximating target surfaces, which are parametric surfaces of varying or constant curvatures, using generalized waterbomb tessellations. We first generate a base mesh by tiling the target surface using waterbomb bases. Then, by applying a simple numerical optimization algorithm to the base mesh, we achieve a developable waterbomb tessellation. We provide a prototype system using which the user can adjust the resolutions of the tessellation and modify waterbomb bases. It is the first work for approximating 3D surfaces using generalized waterbomb tessellations. Our work could extend the exploration of building developable 3D structures using origami.

1.3 Outline

This thesis begins by reviewing related work in Chapter 2. We introduce preliminaries knowledge on origami. Then, we introduce several fundamental mathematics, including operations on paper, developable constraint, and theorems on flat-foldability. Besides, we describe related studies in terms of designing 2D and 3D origami. Finally, we overview several origami-inspired applications.

In Chapter 3, a design method for axisymmetric 3D origami based on rotationally-symmetric crease patterns is proposed. The geometry of the 3D shape are defined. Then, detailed calculations are presented. Depending on the analysis of the geometry, two kinds of one-parameter rigid motion are described.

In Chapter 4, a computational procedure to handle the crease pattern with blank spaces, caused by interior vertices with non-zero angle deficit, is proposed. Flaps outside and tucks inside are calculated from such blank areas. By adding flaps or tucks, the shape becomes realizable through tucking without cutting.

In Chapter 5, a method to design axisymmetric 3D origami with generic six-crease bases is proposed. The generic base is inspired by the conventional six-crease bases. The geometry of the 3D origami is given and detailed calculations are presented. Furthermore, a design space is explored by enumerating configurations. Last, a one-parameter rigid motion is presented.

In Chapter 6, a method for approximating target surfaces using generalized waterbomb tessellations is described. A base mesh is generated by tiling the target surface using waterbomb bases. Then, a developable waterbomb tessellation is achieved by applying a simple numerical optimization algorithm. Several results of varying curvatures are demonstrated.

Chapter 7 summarizes the conclusions of this thesis and provides future research directions.

1.4 Publications and Awards

1.4.1 Reference papers

This thesis is based on the following publications:

Journal papers (with peer review)

1. Y. Zhao, Y. Kanamori, J. Mitani, "Geometry of Axisymmetric 3D Origami Consisting of Triangular Facets", *Journal for Geometry and Graphics, Vol. 21, No. 1*, pp. 107-118, 2017.

2. Y. Zhao, Y. Kanamori, J. Mitani, "Design and Motion Analysis of Axisymmetric 3D Origami with Generic Six-crease Bases", *Computer Aided Geometric Design, Vol.*

59, No. Supplement C, pp. 86-97, 2018.

3. Y. Zhao, Y. Endo, Y. Kanamori, J. Mitani, "Approximating 3D Surfaces using Generalized Waterbomb Tessellations", *Journal of Computational Design and Engineering*, 2018 (Accepted).

International poster (without peer review)

1. Y. Zhao, Y. Kanamori, J. Mitani, "Simulation of Triangle-based Axisymmetric Rigid Origami", *In International Conference on Mathematical Modeling and Applications*, Tokyo, Japan, November 2016.

Domestic conference papers (without peer review)

1. Y. Zhao, Y. Kanamori, J. Mitani, "A Computational Design Method for Tucking Axisymmetric 3D Origami Consisting of Triangle Facets", *The Japan Society for Industrial and Applied Mathematics Annual Conference 2016*, pp. 80-81, September 2016.

2. Y. Zhao, Y. Endo, Y. Kanamori, J. Mitani, "Triangle-based Axisymmetric 3D Origami Design", *The Japan Society for Industrial and Applied Mathematics Annual Conference 2017*, pp. 399-400, September 2017.

1.4.2 Other papers

The additional following papers were also published but not directly related to this thesis:

International conference paper (with peer review)

1. Y. Zhao, Y. Sugiura, M. Tada, J. Mitani, "InsTangible: A Tangible User Interface Combining Pop-up Cards with Conductive Ink Printing", *In International Conference on Entertainment Computing 2017*, pp. 72-80, Tsukuba, Japan, September 2017.

Domestic conference paper (with peer review)

1. Y. Zhao, K. Matsuyama, F. Chiba, K. Konno, "A Study of Inside Surface Shape Reconstruction from Refitted Flakes Based on Point Clouds Segmentation", *NICOGRAPH 2013*, pp. 49-52, CD-ROM, 2013 (in Japanese).

1.4.3 Grants and awards

1. March2017: Interactive presentation award, in Interaction 2016.

Chapter 2

Related Work

Origami, which is folding a piece of paper, can generate very complex 2D and 3D shapes. It is not only an activity belonging to human beings, but can be found and provide efficient solutions in nature, e.g., the flexible configuration of hornbeam leaves [42, 11] and foldable insect wings [31]. Furthermore, researches have learned from origami and applied its concepts in engineering. Before describing our design methods, we first introduce several preliminaries knowledge and fundamental mathematics. Then, we introduce several existing design methods for 2D and 3D origami and describe origami-inspired applications. Finally, we focus on triangle-based designs and applications.

2.1 Preliminaries

Traditionally, the piece of paper used in origami is often assumed to be a square [18]. We expand this assumption and allow our piece of paper could be planar polygon throughout this thesis.

For documenting an origami, origami diagrams and crease patterns are widely used. Origami diagrams, i.e., a sequence of step-by-step instruction depicting how to fold an origami, is used for illustrating the folding procedure (e.g., Figure 2.1 (a)). Benefiting from the notions, e.g., lines and arrows indicating the position of the folds and the movement of the paper, they are relatively easy to be followed. However, as the origami pieces became more and more detailed and complex, the number of instructions for folding are dramatically increased.

The crease pattern is another documentation for representing (e.g., Figure 2.1 (b)). Different from the origami diagrams, which require a number of figures depicting the instructions, the crease pattern is only one figure which contains the pattern of creases left on the paper after folding an origami piece. The crease pattern contains a set of creases, each of which is a line segment (or, in some cases, a curve) on a piece of paper. Creases may be folded as a mountain fold or as a valley fold. A mountain fold forms a convex crease at

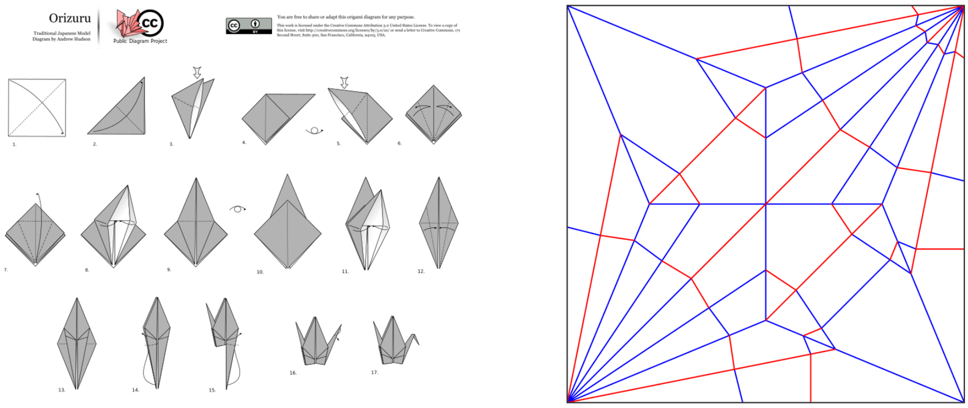

(a) (b)

Figure 2.1: Examples of origami diagrams and crease pattern for a paper crane. (a) Origami diagrams by Andrew Hudson. (b) A crease pattern exported by ORIPA [55].

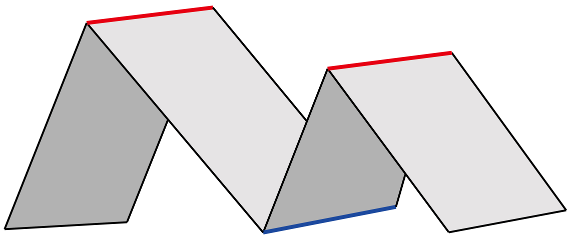

Figure 2.2: A crease pattern may be folded as a mountain (in red) or a valley (in blue).

top with the paper beside the crease folded down. On the other hand, a valley fold forms a concave crease with both sides folded up [90] (e.g., Figure 2.2). Actually, the mountain and valley assignments are interchanged when changing the point of view, i.e., the face of the paper, and thus two types of folds can be considered as dual to each other [21]. Using crease pattern for documenting origami is efficient, but it is difficult for nonexperts because it does not contain any procedural information. Representing an origami piece using crease pattern becomes important, because most of the recent techniques were developed for it. Besides, it is not appropriate to use origami diagrams to represent the origami, e.g., waterbomb tessellations and Yoshimura patterns, because such an origami is not folded step by step. Considering the above context, we use the crease pattern for representing an origami piece in this thesis.

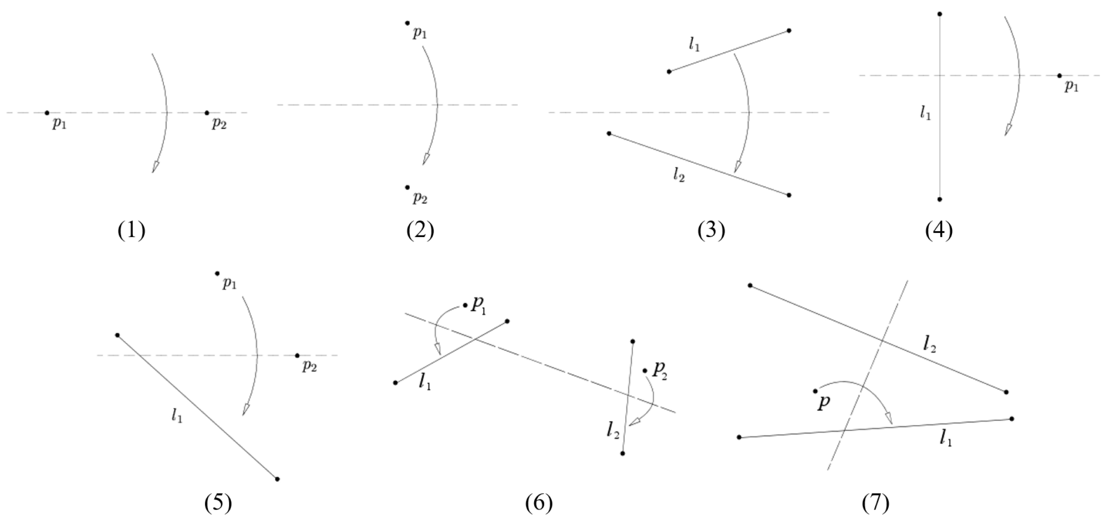

Figure 2.3: Huzita-Hatori (Huzita-Justin) axioms.

2.2 Mathematical principles of origami

Origami began as a trial-and-error art design. Benefiting from the developing mathematical understanding, more and more complex and detailed origami pieces emerged. Here, we introduce several fundamental mathematical principles, including Huzita-Hatori axioms, constraints of developability and flat-foldability.

2.2.1 Huzita-Hatori axioms

Huzita-Hatori (Huzita-Justin) axioms [28] which describe the operations that can be made for folding a piece of paper by referring to points and lines. Such axioms were firstly discovered by Jacques Justin in 1989, then improved by Humiaki Huzita in 1991, and finalized by Koshiro Hatori, Justin and Robert Lang in 2001 [13]. We depict the axioms in Figure 2.3 and describe them as follows:

- Given two distinct points p_1 and p_2, there is a unique fold that passes through both of them.
- Given two distinct points p_1 and p_2, there is a unique fold that places p_1 onto p_2.
- Given two distinct (straight) lines l_1 and l_2, there is a fold that places l_1 onto l_2.
- Given one line l_1 and one point p_1, there is a unique fold perpendicular to l_1 that passes through point p_1.

- Given one line l_1 and two distinct points p_1 and p_2, which are not on this line, there is a fold that places p_1 onto l_1 and passes through p_2.
- Given two distinct points p_1 and p_2 and two distinct lines l_1 and l_2, there is a fold that places p_1 onto l_1 and p_2 onto l_2.
- Given one point p and two lines l_1 and l_2, there is a fold that places p onto l_1 and is perpendicular to l_2.

Based on these axioms Tsuruta et al. [86, 87, 88] proposed several CAD systems for exploring the variations of the origami. In addition, Ida et al. [37] presented a computational system called Eos (E-Origami system), which provided the fold method based on such axioms.

2.2.2 Constraint of developability

The origami should satisfy the developable constraint, which requires an origami can be developable onto a flat plane without stretching. An angle constraint [78], defined in Eq. 2.1, is used for determining a developable vertex (Figure 2.4 left).

$$D_i = 360^\circ - \sum_{k=0}^{K_i - 1} \alpha_{i,k} = 0, \tag{2.1}$$

where K_i is the total number of sector angles around vertex i, and $\alpha_{i,k}$ is the k-th incident sector angle of vertex i. In our work, we classify vertices as interior and boundary vertices. For a developable surface, all the interior vertices should satisfy this angle constraint.

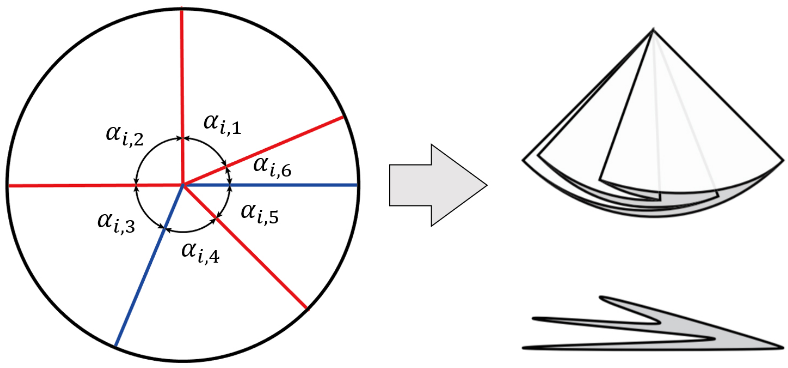

Figure 2.4: Flat-foldable vertex [78].

2.2.3 Constraint of flat-foldability

Most origami pieces can be found to be flat-foldable, although such a constraint is not a necessary for designing a 3D origami. However, this feature enables the origami to reach a compact folded state where all facets are parallel to each other, and thus can be applied to built large origami structures which can be folded into a much smaller space for specific applications, e.g., transportation.

There exist several local flat-foldable conditions, i.e., Kawasaki's theorem [40] and Maekawa's theorem [39], which are used to determine the flat-foldability of a single vertex with a surrounding crease pattern (e.g., Figure 2.4 left). Kawasaki's theorem is defined as follows:

$$\alpha_{i,1} - \alpha_{i,2} + \alpha_{i,3} - \alpha_{i,4} + \cdots + \alpha_{i,2n-1} - \alpha_{i,2n} = 0^\circ \tag{2.2}$$

or another way as follows:

$$\alpha_{i,1} + \alpha_{i,3} + \cdots + \alpha_{i,2n-1} = \alpha_{i,2} + \alpha_{i,4} + \cdots + \alpha_{i,2n} = 180^\circ \tag{2.3}$$

Maekawa's theorem is another criterion for one flat-foldable vertex, which defines as follows (Figure 2.4 left):

$$|M - V| = 2, \tag{2.4}$$

where M and V represent the number of mountain and valley creases, respectively. This theorem requires the numbers of mountains and valleys always differ by 2. Kawasaki's theorem alone is however sufficient to predict flat-foldability of a single vertex. A further explanation of these theorems can be referred to [5].

For determining a global flat-foldability of a given crease pattern consisting of multi-vertex, Kawasaki's theorem is a necessary but not sufficient condition. Such a problem is proven to be a problem of NP-complete [5].

2.3 Design methods of origami

We first introduce existing design methods for 2D origami. Then, we review several approaches for designing 3D origami.

2.3.1 Design methods for flat-foldable origami

The $tree\ method$ is a practical computational origami design method for achieving desired shapes. Its basic concept was first introduced by Meguro [54]. Then, Lang [45] fully described the theory of the tree method and implemented as an origami design software TreeMaker [44]. This software takes a weighted graph tree (Figure 2.5 (a)), which captures the essential features of a target object, as an input. Then, the software generates a crease pattern (Figure 2.5 (b)) based on the input graph tree. Even though the crease pattern is

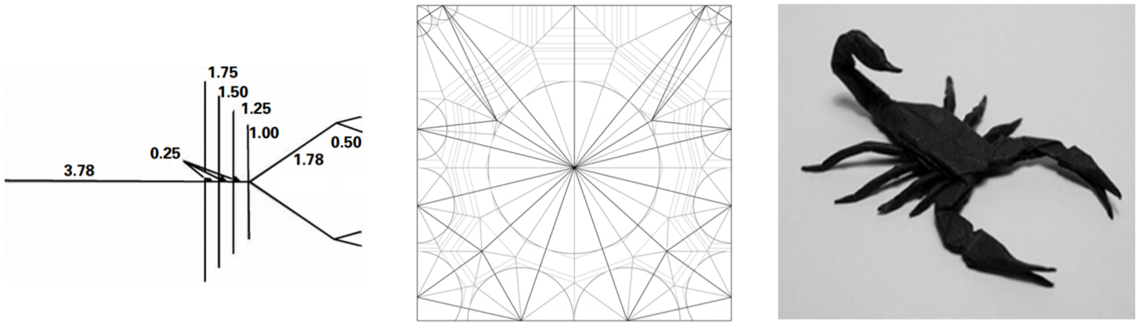

(a) (b) (c)

Figure 2.5: TreeMaker software sequence (Images adopted from [8]).

calculated, it requires an expert folder to achieve such a complex origami shape, which in this case is a scorpion (Figure 2.5 (c)).

Origami tessellation is generally a kind of flat origami. It became a specific area of origami originated by Shuzo Fujimoto [48]. Davis et al. [10] demonstrated many 3D tessellations investigated by David Huffman. Recently, Gjerde [30] provided an introduction to this folding techniques. The crease pattern of an origami tessellation is generated from a tiled plane. Bateman [4] developed a computer program $Tess$ for generating origami tessellations (Figure 2.6 (a)). The user can vary several key parameters and specify the symmetry pattern. The designed tessellations are theoretically easy to fold because the user only needs to twist one part of the paper over another. However, the actual fabrication work is hard considering the material of the paper could be crumpled. More recently, Yamamoto et al. proposed a method to express binary "pixel art" on the square grid pattern by the overlapping layers of the origami tessellation. They developed a system called as "ORI-RELIFE PIX" [91] is available on the Web.

Editing the crease pattern is a key issue of designing an origami. ORIPA is a dedicated crease pattern editor developed by Mitani [56, 55] (Figure 2.6 (b)). ORIPA enables the user to draw a crease pattern, but also illustrate the folded shape when the crease pattern is flat-foldable. Furthermore, it provides the rendering of a flat origami from its crease pattern, which is an NP-complete problem, by using a brute force to determine the ordering of the layers [57].

Enumerating the variations of the flat-foldable origami becomes possible benefiting from the growing computational power of the computer. Based on the Huzita-Hatori axioms introduced in the previous Section 2.2.1, Tsuruta et al. [87] proposed an interactive system for exploring simple origami models by random generation of folded pieces. The implemented system assists the user to recognize a folded shape as another object (e.g., an animal, insect, or flower) based on the color and physical appearance. Later, Tsuruta et al. [88] demonstrated various new folded pieces and considered symmetry property in their system called as $Origaminista$ (Figure 2.6 (c)). Matsukawa et al. [53] enumerated all

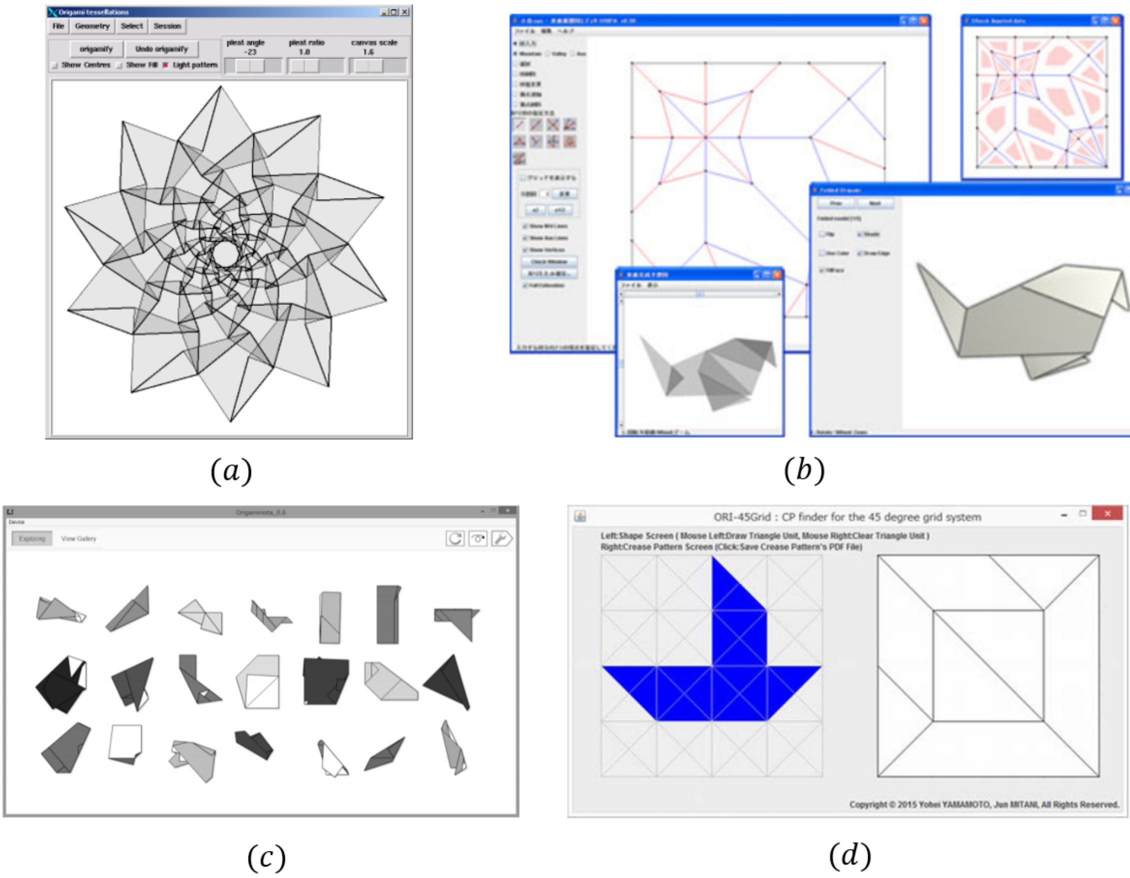

Figure 2.6: Examples of flat-foldable origami design systems. (a) Tess: origami tessellation software. (b) ORIPA: origami pattern editor. (c) Origaminista: a browser-based application which generates simple origami pieces. (d) CP finder.

possible shapes folded from the crease patterns based on a 45-degree grid system, i.e., the square/diagonal grid of a 4×4 size. They found 259,650,300 locally-flat-foldable crease patterns and 13,452 folded shapes. Furthermore, based on the enumerated results, they developed an application $CP\ finder$ to search the crease pattern which is folded into a user-specified shape (Figure 2.6 (d)).

2.3.2 Design methods for 3D Origami

Tachi proposed $Origamizer$ method [80] which is the first practical approach for obtaining a crease pattern which folds into a given polyhedral surface based on a topological disc condition, e.g., a 374-triangle Stanford bunny shown in Figure 2.7 (a). He implemented the algorithm as a computer software called as “Origamizer” [76]. The Origamizer soft-

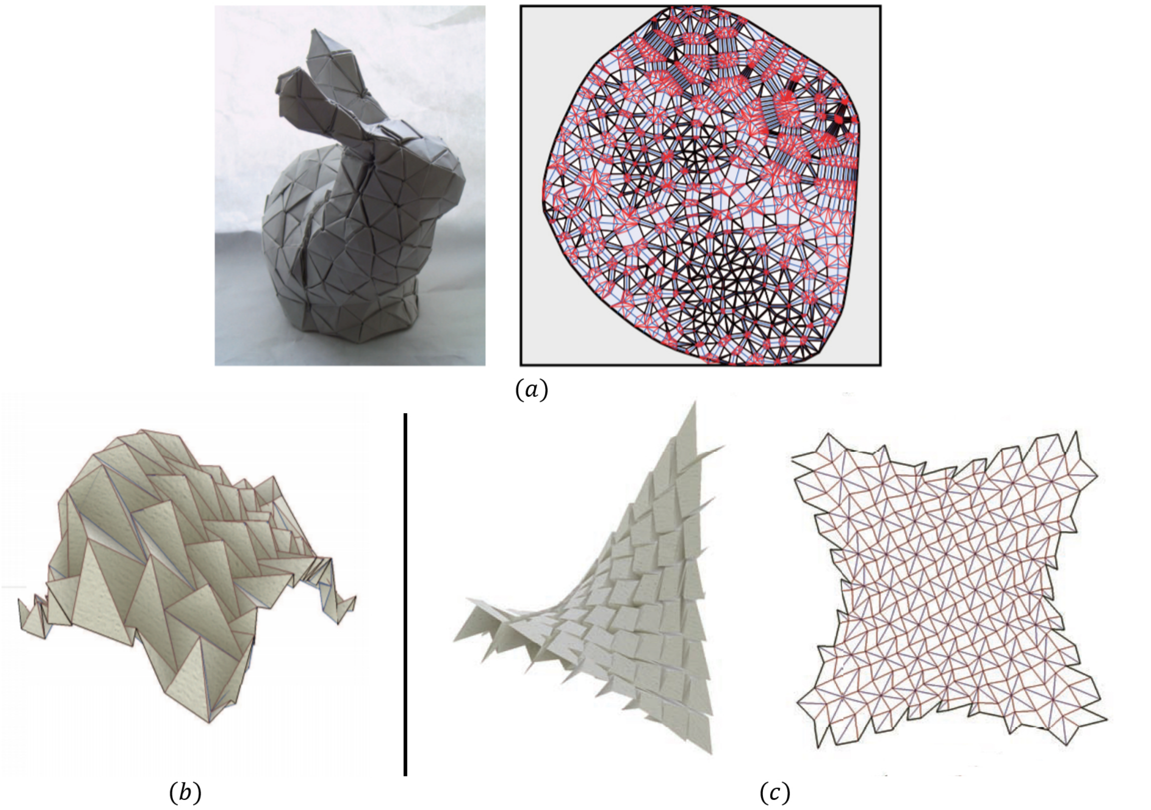

Figure 2.7: Examples of 3D origami design methods proposed by Tachi. (a) Origamizer software applied to Stanford bunny, where the real-world folding shown on the left and the computed crease pattern shown on the right. Images adopted from [19]. (b) Freeform origami used to edit a waterbomb tessellation in 3D. Image adopted from [78]. (c) Freeform origami tessellations by generalizing Resch′s patterns. Images adopted from [81].

ware, however, could sometimes fail to give a solution or generate highly inefficient crease patterns. More recently, Demaine and Tachi developed the $Origamizer\ algorithm$ that is guaranteed to find a feasible foldings for any orientable polyhedral manifold [19]. By using the $Origamizer$ software, although the appearance of the resulting origami becomes equivalent to the target shape, it might be thought that the crease pattern is too complicated even for a simple model [58].

$Freeform\ Origami$ [78] developed by Tachi allows the user to vary a known origami in 3D while preserving the developability and other optional conditions inherent in the crease pattern. The system can edit a given pattern into a freeform through dragging the vertices in 3D (Figure 2.7 (b)). Then, he proposed a system [81] for generating a target shape by using a subset of generalized Resch patterns. This method inserts a tuck structure in the 3D form and numerically solves the geometric constraints of the developability and local collision (Figure 2.7 (c)).

Most origami uses straight creases and this type of origami is also referred to as prismatic origami [17] due to straight creases surround planar facets and compose a polyhedral surface. A more general class of folding are based on curved creases. Comparing to the prismatic origami, the curved-crease origami can achieve an elegant curved 3D structure using a small number of creases. Designing a curved-crease origami is difficult due to its mathematical foundation have not been fully developed. Although the designing curved-crease origami is beyond the scope of this thesis, we briefly introduce several methods in this challenging area.

Bauhaus model [32] is the earliest known curved-crease sculpture from a students work at the Bauhaus. This model is made of concentric circles with alternating mountain and valley folds (Figure 2.8 (a)). Huffman described the local behavior of a crease by introducing spherical trigonometry on the Gauss sphere [35]. Based on his theory, a design of lens tessellations [16] and a number of masterpieces, e.g., hexagonal column with cusps [14] shown in Figure 2.8 (b), were proposed. LeKlint company proposes a lamp design [38], which is almost the same way Huffman did in his approach (Figure 2.8 (c)). Kilian et al. proposed a curved folding approach [41] which can reconstruct a car model based on the design of Gregory Epps (Figure 2.8 (d)). Their approach applied planar quadrangle meshes (PQ-meshes) and used an optimization process.

(a) (b) (c) (d)

Figure 2.8: Examples of curved-crease origami. (a) The Bauhaus model [32]. (b) David Huffman and his "hexagonal column with cusps" [14]. (c) A lamp design [38]. (d) Reconstruction of the car model designed by Gregory Epps [41].

Handling curved folds is still a difficult problem. However, by limiting the curve to be planar, the problem becomes drastically simple [62]. In particular, Mitani [58] proposed a design method based on rotational sweeping a 2D polyline around a common axis. To ensure the shape is folded from a single sheet of paper, this method adds appropriate flaps between the polygonal faces which constitute the final shape. When the input polyline is smooth curved, this method can generate 3D curved origami (Figure 2.9 (a)). The implemented system $ORI-REVO$ is available at [60]. More recently, he proposed a variant of this method where the flaps are replaced by "triangular prism protrusions" [59]. Mitani and

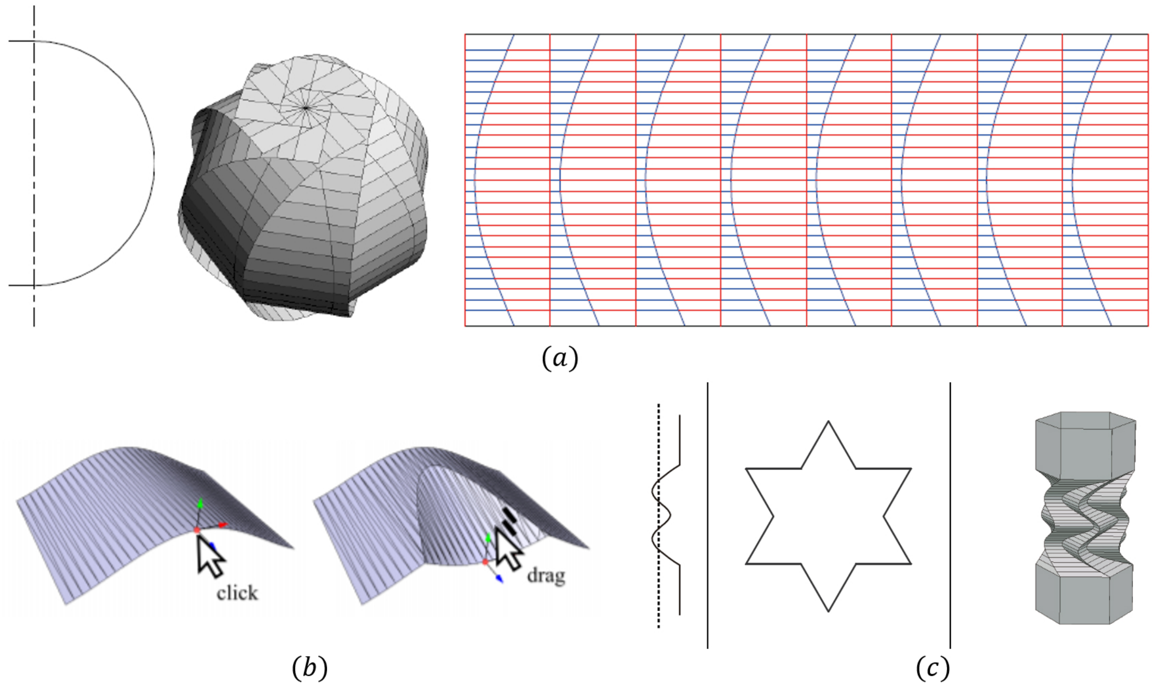

Figure 2.9: Examples of 3D origami design methods proposed by Mitani. (a) A design method for 3D origami based on rotational sweep. Images adopted from [58], where the left shows a smooth curved polyline as an input, the middle shows the calculated 3D shape, and the right shows its crease pattern. (b) An interactive design of planar curved folding by reflection. Images adopted from [62]. (c) A column-shaped origami design based on mirror reflections. Images adopted from [61], where the left shows profile polyline, the middle shows the trajectory polyline, and the right shows the resulting shape.

Igarashi [62] proposed an interactive user interface for designing curved-crease origami. This method is based on the fact that when a part of a developable surface is reflected with a mirror operation, the resulting shape retains developable. In their implemented system, the user can interactively click and drag a point on a surface and see the changing of the shape (Figure 2.9 (b)). Later, Mitani [61] proposed a new method, which combines the reflection and sweep operations, to design column-shaped origami. The method determines a 3D shape by a profile polyline and a trajectory polyline. When sweeping a smooth profile curve, this method can generate curved-crease origami (Figure 2.9 (c)).

Inverse origami design aims to fit a target 3D surface using predefined crease pattern. It is another research direction of designing 3D origami. The *Origamizer* algorithm [77, 80] fit 3D triangle mesh models with a topological disc condition. His another method [81] apply a subset of generalized Resch patterns to approximate a target shape. The above approaches require to insert tuck structures in the 3D form. By dragging the vertices in

3D, the *Freeform Origami* [78] system enables the user to edit a given pattern into a freeform. However, the method cannot fully support approximating target 3D surfaces. In addition, several approximating approaches based on modified Miura-ori have been proposed. Zhou et al. [98] developed the "vertex method" to inversely calculate a developable crease pattern of a given 3D geometry. Song et al. [74] proposed a mathematical framework for the generation of rigid-foldable 3D origami based on the crease pattern that can simultaneously fit two doubly curved surfaces with rotational symmetry about a common axis. Dudte et al. [20] used modified Miura cells to approximate orientable 3D surfaces with positive, zero, negative, and mixed Gauss curvatures (Figure 2.10).

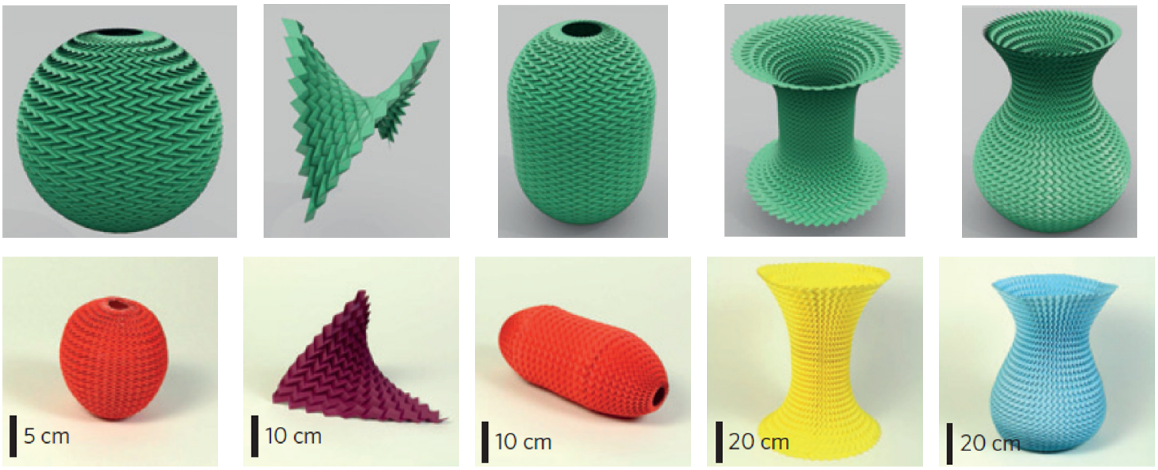

Figure 2.10: Generalized Miura-ori tessellations fitting target surfaces. The top row depicts calculated 3D surfaces, while the bottom row shows physical models. Images adopted from [20].

2.4 Origami-inspired applications

Origami has not only aroused considerable research interest in mathematics but provide effective solutions in engineering. The developable feature of origami inspired the designs, e.g., airbags design [9, 34] and shelters design[12, 84, 52, 68, 6]. Flat-foldable feature inspired the applications, such as crash boxes [50, 51], origami tubes [27]. The scale-independent feature leads to apply origami concepts at centimeter scale, e.g., self-folding robots [33, 49, 25, 26, 65], or meter scale, e.g., foldable solar panels [64, 99, 100] and telescope [22, 47, 89]. Besides, origami have also been applied on DNA folding [71, 85, 66, 23] and drug delivery [94].

In addition, the advances in material science and robotics engineering accelerate the development of $self-folding\ origami$. In this area, origami becomes more active by reacting to various stimuli. In particular, Ahmed et al. [2] introduced a concept of multi-field responsive origami, which actively folds in response to electric and magnetic. Ryu et al. [72] proposed photo-origami, which can be folded with light. Furthermore, An et al. [3] build a single self-folding sheet by using folding actuators.

2.5 Triangle-based origami designs and applications

Designing a 3D origami constructed by triangular facets is convenient due to the planar constraint does not need to be considered. Triangular meshes are simple and provide more freedom of movement than quadrilateral meshes [79]. Benefiting from its high freedom, Francis et al. [29] proposed a backpack design (Figure 2.11 (a)). Tachi et al. [82] achieved adaptive freeform surfaces, which could be applied in architecture (Figure 2.11 (b)). Furthermore, inspired by this kind of origami, Kuribayashi and You [43, 93] proposed an origami stent graft for biomedical application (Figure 2.11 (c)). Lee et al. [49] proposed a deformable wheel robot (Figure 2.11 (d)).

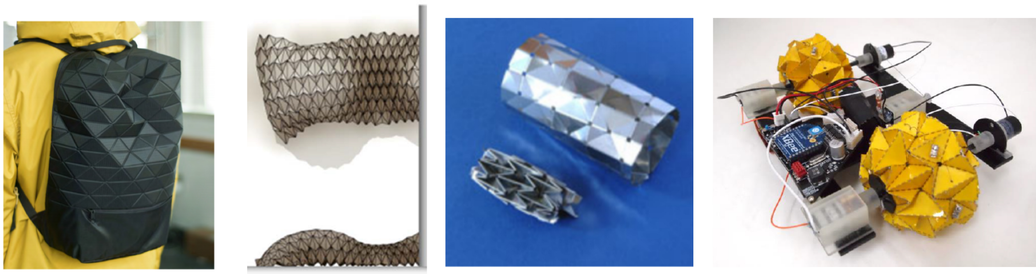

(a) (b) (c) (d)

Figure 2.11: Triangle-based origami designs and applications. (a) A backpack design. Image adopted from [29]. (b) An adaptive freeform surface. Image adopted from [82]. (c) An origami stent graft made from a semi-rigid sheet. Image adopted from [93]. (d) A deformable wheel robot. Image adopted from [49].

Chapter 3

Axisymmetric 3D origami based on rotationally-symmetric crease patterns

Designing 3D origami is a new challenging area comparing to the designing 2D origami. Axisymmetric 3D origami is preferred by origami designers due to such an origami is relatively easy to be fabricated. In addition, the folded axisymmetric 3D origami could be more stable than non-axisymmetric one when fabricated. Using a set of triangular facets to construct an axisymmetric 3D origami do not need to consider the planar constraint, however the developable constraint limits the design space, and thus the user cannot freely design.

In this chapter, we focus on a category of axisymmetric triangle-based 3D origami folded from rotationally-symmetric crease patterns. We first define the geometry of the rotationally-symmetric crease pattern. Based on such a crease pattern, developable constraint can be satisfied. Then, we analytically calculate the axisymmetric 3D shape.

In particular, Figure 3.1 shows an overview of our method. We first design the right of the $1/N$ part ($N = 8$ for this example) of the whole crease pattern (Figure 3.1 (a)), where N indicates the order of rotational symmetry ($N > 2$) and the angle θ is determined by N, i.e., $\theta = 180°/N$. After the $1/N$ part has been specified, we generate the rotationally-symmetric crease pattern (Figure 3.1 (b)) by repeating such part $N - 1$ times around the origin. Next, we calculate the 3D origami (Figure 3.1 (c)) from its crease pattern. Here, we first calculate the $1/N$ part of the 3D origami from its crease pattern together with the user-specified angle φ between edge P_0P_1 and the z axis. Note that P_i and P_i' (with even indices) has a planar symmetry with respect to a plane through the z axis and P_i (with odd indices). Then, the axisymmetric structure of the 3D origami can be achieved by iteratively rotating its $1/N$ part about the z axis. Finally, based on the generated 3D model, we determine the mountain and valley assignments on the crease pattern, which are used to fold an origami piece (Figure 3.1 (d)). We also implemented a prototype system, using which the user can interactively design a 3D origami by editing its crease pattern with real-time human interaction.

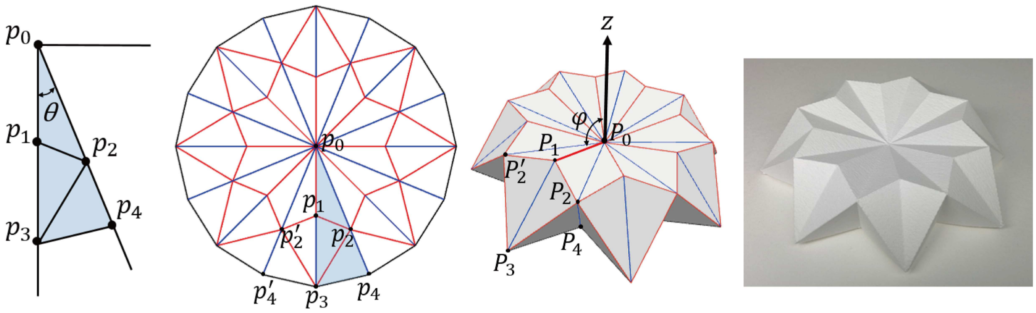

(a) (b) (c) (d)

Figure 3.1: An overview of our method.

3.1 Designing crease pattern

Our method is based on designing the crease pattern. In this section, we describe the rotationally-symmetric crease pattern consisting of triangular facets. Figure 3.2 (a) shows a $1/N$ part of the crease pattern, and Figure 3.2 (b) shows the shape in 3D space. The symbols in Figure 3.2 are defined as follows:

- Planes Π_1 and Π_2 are vertical planes whose intersecting lines with the horizontal plane (i.e., the $x - y$ plane) are lines l_1 and l_2, respectively.
- P_0 is located at the origin in 3D space and expressed as p_0, indicating the intersection point of lines l_1 and l_2 on the horizontal plane.
- θ is the angle between lines l_1 and l_2, which equals $180°/N$, and expressed as Θ in 3D space, indicating the angle between planes Π_1 and Π_2.
- P_1 and P_3 (with odd indices) lie on the plane Π_1 and represent p_1 and p_3 along line l_1 in the crease pattern, respectively.
- P_2 and P_4 (with even indices) lie on the plane Π_2 and represent p_2 and p_4 along line l_2 in the crease pattern, respectively.
- P_2' and P_4' (denoted as p_2' and p_4' in the crease pattern) are the symmetric points of P_2 and P_4 with respect to plane Π_1, respectively.

Note that p_i and p_i' (with even indices) has a symmetry with respect to the line l_1.

The rotationally-symmetric crease pattern can be interactively designed. Specifically, as shown in Figure 3.2 (a), the θ in the crease pattern can be changed by $N(N > 2)$. $p_i(i > 0)$ can be added or deleted along lines l_1 and l_2. Furthermore, $p_i(i > 0)$ can be moved along lines l_1 or l_2. After the right part is specified, the symmetric points with respect to line l_1

are calculated. Finally, as shown in Figure 3.2 (c), the whole crease pattern is generated by repeating the $1/N$ part around the origin $N-1$ times by 2θ. The mountain and valley assignments are not determined until the 3D model is generated (Section 3.2.2).

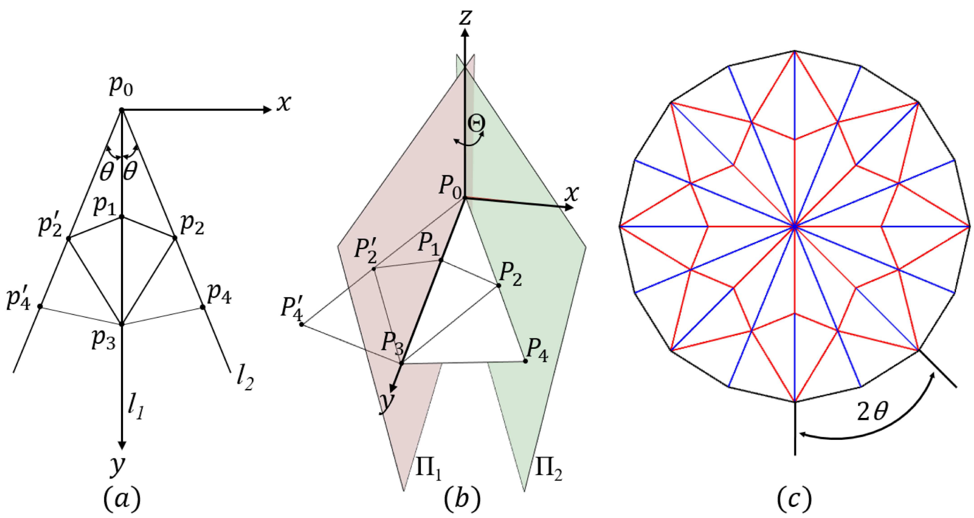

Figure 3.2: Designing rotationally-symmetric crease pattern consisting of triangular facets.

3.2 Calculation of 3D origami

In this section, we describe a method to calculate each point on the 3D origami based on its crease pattern (using the example shown in Figure 3.1). P_0 is located at the origin in 3D space. Each 3D $P_i(i > 0)$ is calculated sequentially in the order of its index. In Section 3.2.1, we describe the calculation of P_1 separately because a user-specified angle φ is needed. In Section 3.2.2, the calculation of $P_i(i > 1)$ is described. In Section 3.2.3, a special case during calculation is given.

3.2.1 Calculation of $\mathrm{P_1}$

To calculate the 3D coordinates of P_1, the following constraints should be satisfied:

1. The distance between P_1 and P_0 should be the same as the length of edge p_1p_0 in the crease pattern.

2. P_1 should lie on the plane Π_1.

3. Angle φ ($0° \leq \varphi \leq 180°$) between line P_0P_1 and the z axis should be the same as the user-specified value.

Figure 3.3 shows the process for calculating P_1. Firstly, considering constraint 1), the possible solutions for P_1 in 3D space lie on the red sphere (Figure 3.3 (a)) whose center is P_0 and radius equals the length of edge p_1p_0, which is measured from the crease pattern (Figure 3.1 (a)). Secondly, considering constraint 2), the possible solutions are shown as a red solution circle (Figure 3.3 (b) and (c)), which is the intersection between the red sphere and plane Π_1. Finally, by specifying the angle φ between line P_0P_1 and the z axis, the 3D coordinates of P_1 are determined. Figure 3.3 (b) and (c) show the solution of P_1 with $\varphi = 66°$ and $\varphi = 140°$, respectively. The angle φ is set to $66°$ and fixed throughout the subsequent calculation of the remaining 3D points.

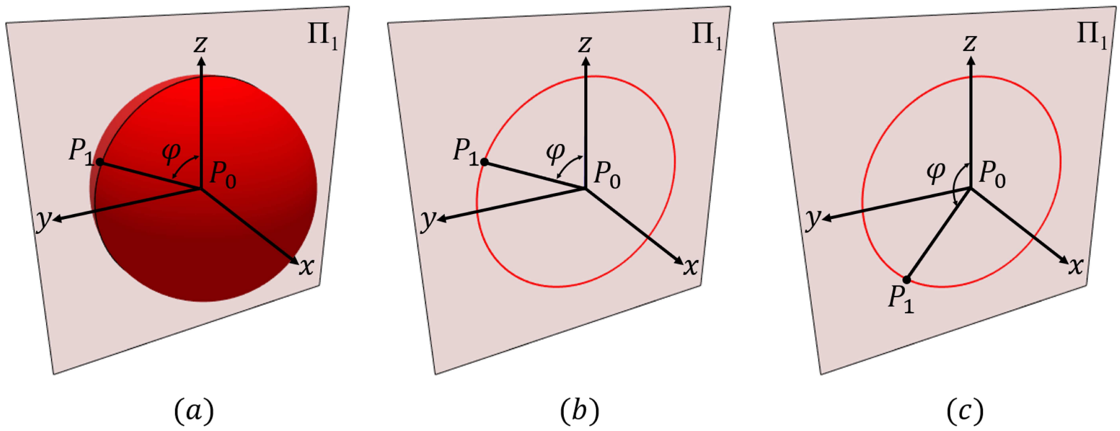

Figure 3.3: Calculation of P_1.

3.2.2 Calculation of $\mathbf{P}_i(i > 1)$

In the sequential calculation of P_i, the 3D coordinates of P_{i-1} and P_{i-2} are required. For calculating $P_i(i > 1)$, the following three constraints should be satisfied:

1. The distance between P_i and P_{i-1} should be the same as the length of edge p_ip_{i-1} in the crease pattern.

2. The distance between P_i and P_{i-2} should be the same as the length of edge p_ip_{i-2} in the crease pattern.

3. P_i should lie on the plane Π_1 (for odd index) or Π_2 (for even index).

For generating $P_i(i = 2)$ (Figure 3.4), the 3D coordinates of P_1 and P_0 are required. In Figure 3.4 (a) and (c), we first consider constraint 1) between P_i and P_{i-1} (i.e., P_2 and P_1 in this example). The possible solutions for P_2 in 3D space lie on a sphere, called a solution sphere, whose center is P_1 and radius equals the length of edge p_2p_1. Then, by

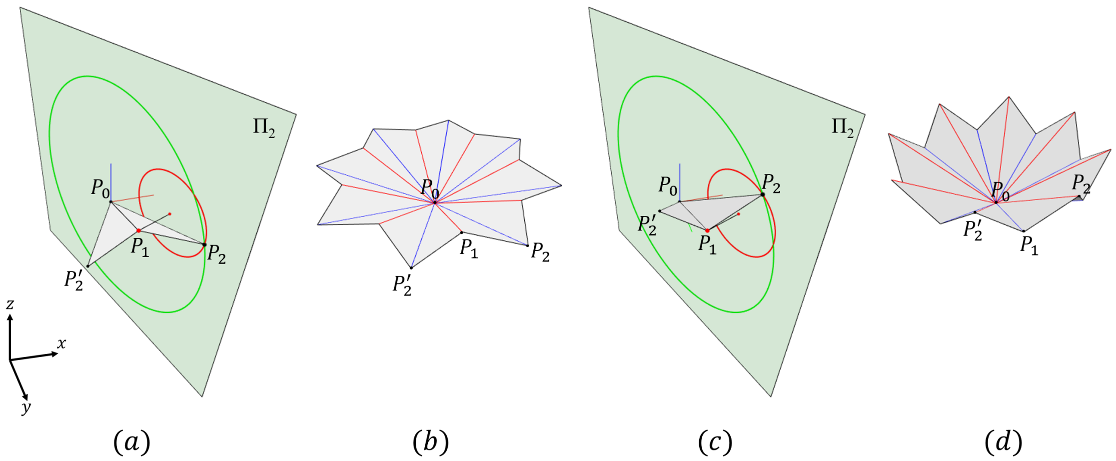

Figure 3.4: Calculation of $P_i(i = 2)$.

considering constraint 3), the solution circle shown in red is obtained from the previous solution sphere intersected by plane Π_2. Next, by considering constraint 2) between P_i and P_{i-2} (i.e., P_2 and P_0) and constraint 3), we obtain the solution circle shown in green on plane Π_2 whose center is P_0 and radius equals the length of edge p_2p_0. Finally, the two intersection points between the two solution circles (the red one and the green one) that satisfy all the constraints at the same time are selected as two candidate solutions for $P_i(i = 2)$. For the solution of P_2 (with even index), the symmetric point P_2' with respect to plane Π_1 is calculated. After the $1/N$ part of the 3D origami is specified, the axisymmetric 3D origami is generated by iteratively rotating its $1/N$ part about the z axis through 2Θ, as shown in Figure 3.4 (b) and (d), respectively.

The calculation process of $P_i(i = 3)$, which lies on plane Π_1, is shown in Figure 3.5. By satisfying all the constraints, the two intersection points of the two solution circles on plane Π_1 are selected as candidate solutions for $P_i(i = 3)$ (Figure 3.5 (a) and (c)). For

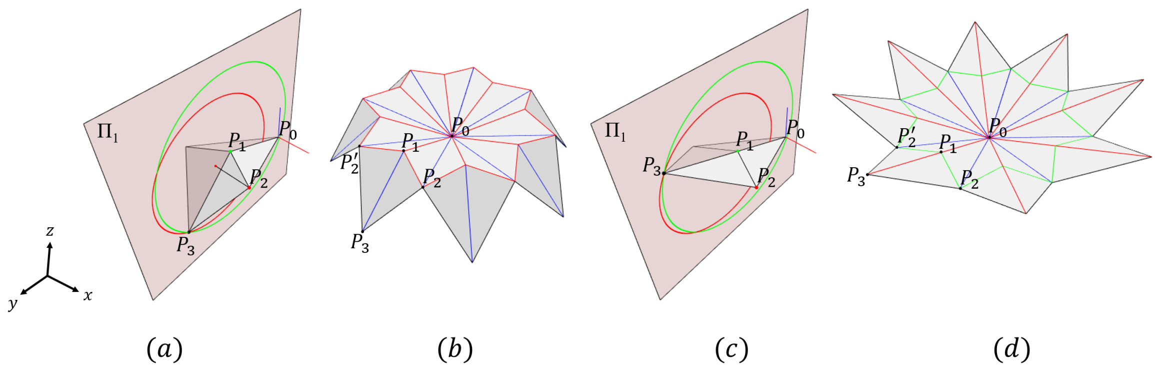

Figure 3.5: Calculation of $P_i(i = 3)$.

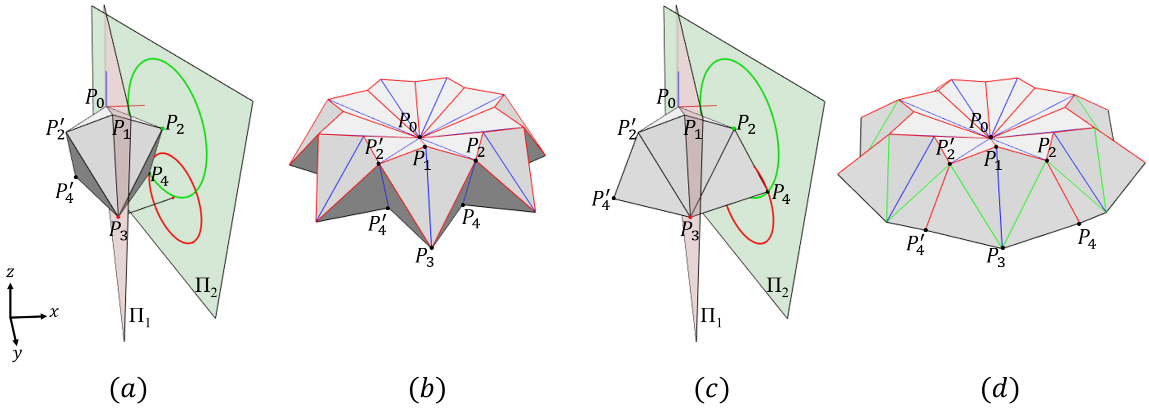

Figure 3.6: Calculation of $P_i(i = 4)$

designing various shapes of 3D origami, either candidate can be selected as the solution of P_3 (Figure 3.5 (b) and (d)). However, one solution could flatten two connected facets (Figure 3.5 (d)); thus, the crease lines between such flattened facets are rendered in green.

We also show the calculation for $P_i(i = 4)$, which lies on plane Π_2, with the constraints from P_3 and P_2 (Figure 3.6). The shape (Figure 3.6 (b)) is the 3D model introduced in Figure 3.1 (c). We then determine the mountain and valley assignments on a 3D model and then translate them to the crease pattern (Figure 3.1 (b)) to fold the origami piece (Figure 3.1 (d)).

3.2.3 Special Case in Calculation of $\mathbf{P}_i(i > 1)$

The candidate solutions for each $P_i(i > 1)$ are two intersection points of the two solution circles as described in Section 3.2.2. A special case occurs when the two solution circles are identical. Then, the candidate solutions for $P_i(i > 1)$ are not just two points but all the points along the solution circle.

Figure 3.7 shows one example of the special case for calculating P_3, where $\varphi = 90°$ and line P_2P_1 is vertical to plane Π_1. In such a case, the solution circle shown in red is constructed by points that satisfy constraints 1) and 3). The other solution circle shown in green is constructed by the points that satisfy constraint 2) and 3). Both circles share the same center P_1 and have the same radius, which is the length of edge p_3p_1. As a result, the candidate solutions for P_3 in this case are not just two points but all the points along the solution circle. In Figure 3.7, P_3 can be selected arbitrarily on the solution circle to design various 3D origami.

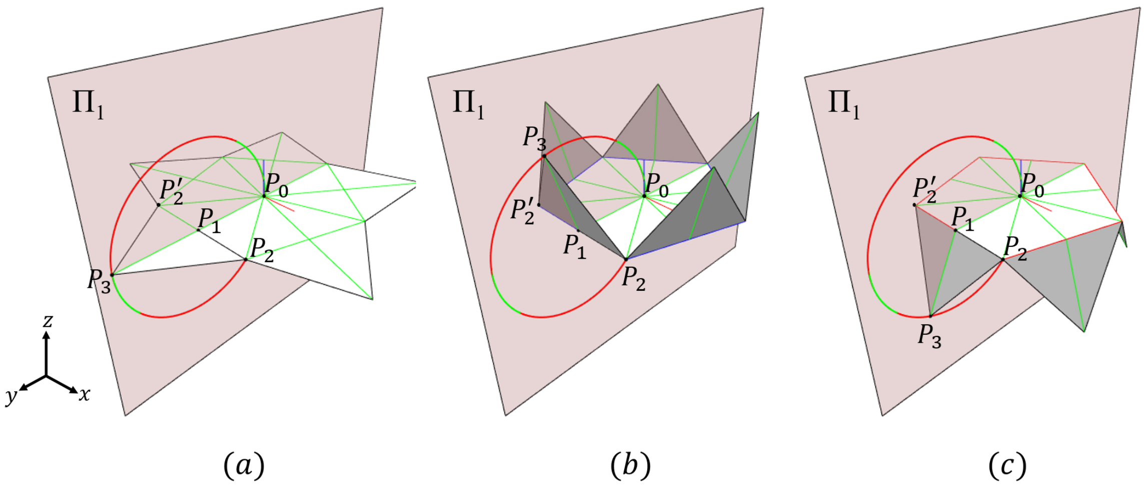

Figure 3.7: Special case in calculation.

3.3 Effects on geometry

In this section, we analyze the effects of variations by changing the parameters including angle φ (Section 3.3.1) and angle Θ (Section 3.3.2).

3.3.1 Changing angle φ

The 3D origami is a developable surface, which means that it is isometric to a planar shape, i.e., the distance within the surface between any two points is equal to the distance between the corresponding points in the plane. When angle φ is changed continuously, the shape of our 3D origami is also changed correspondingly while retaining its developability. We can recalculate the shape efficiently due to the following reasons:

1. The change in angle φ only affects P_1 directly.
2. Each subsequent $P_i (i > 1)$ is to be recalculated sequentially, which means P_i is not recalculated until the previous P_{i-1} and P_{i-2} have been recalculated.
3. Each $P_i (i > 1)$ is recalculated based on P_{i-1} and P_{i-2}, which have already been recalculated.

The user can explore various origami models by only changing angle φ. Figure 3.8 shows some possible origami models. We set φ to $66°$ (Figure 3.8 (b)) to obtain the shape we introduced in Figure 3.1 (c). Figure 3.8 (d) shows that the 3D origami can be completely unfolded just the same as the 2D crease pattern. With angle φ set from $66°$ to $90°$, we can figure out a continuous folding motion that shows the change from the fold-state to

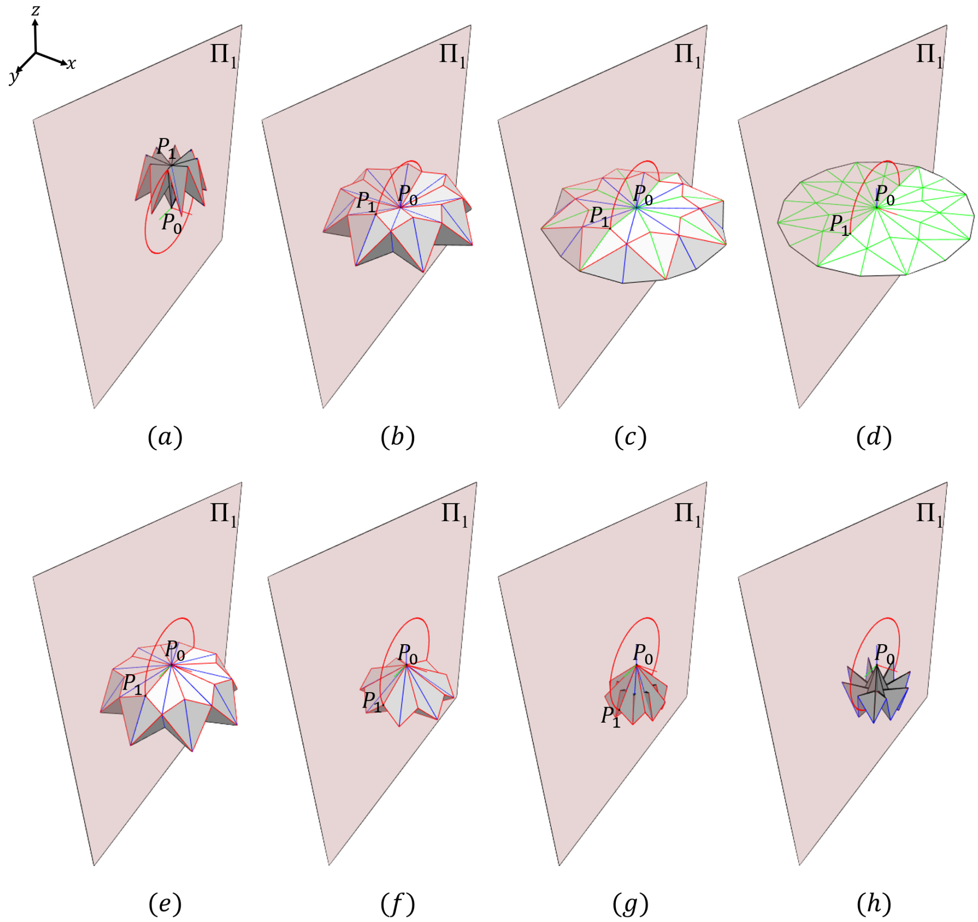

Figure 3.8: Various origami designs obtained by changing φ from $0°$ to $180°$: (a) $\varphi = 0°$, (b) $\varphi = 66°$, (c) $\varphi = 83°$, (d) $\varphi = 90°$, (e) $\varphi = 97°$, (f) $\varphi = 115°$, (g) $\varphi = 135°$, (h) $\varphi = 180°$.

the unfold-state of such a 3D origami. Although φ can theoretically be from $0°$ to $180°$, penetration between triangular facets could happen at some values of φ (Figure 3.8 (a), (f), (g) and (h)). We leave it up to the user in the designing process to avoid such illegal values of φ to generate real-world origami pieces.

3.3.2 Changing angle Θ

Θ denotes the angle between planes Π_1 and Π_2 in 3D space, which equals $180°/N$. After the $1/N$ part of the origami model is calculated, the axisymmetric origami model is generated by iteratively rotating its $1/N$ part about the z axis $N-1$ times through 2Θ.

Here, we decrease Θ, expressed as Θ', from $180°/N$ to $0°$. By inserting an extra boundary line in the crease pattern, we keep the developability of the 3D model. Then, we verify the flat-foldability of each interior vertex on the crease pattern by Kawasaki's theorem and Maekawa's theorem, leading to a way of folding called "along-arc flat-folding".

Specifically, we first decrease Θ to Θ' and then use Θ' to generate the $1/N$ part of the origami model. Note that such a $1/N$ part still maintains a developable surface as each 3D edge is equivalent to the corresponding edge on the flat plane (crease pattern). Then, we

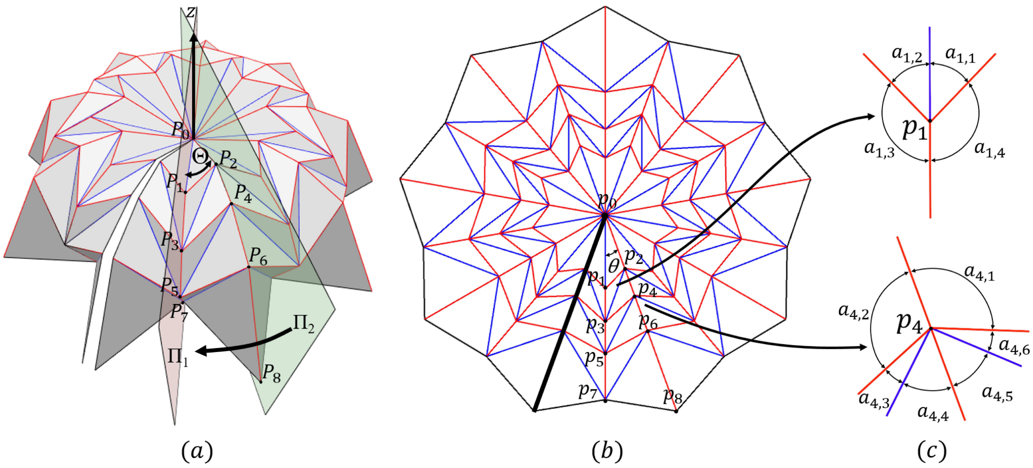

Figure 3.9: Preparation for along-arc flat-folding.

iteratively rotate the $1/N$ part about the z axis $N-1$ times through $2\Theta'$ to generate the whole origami model (Figure 3.9 (a)). Note that the last $1/N$ part is separated from the first $1/N$ part, which breaks the developable property. In this situation, we insert a boundary line in the crease pattern (Figure 3.9 (b)) to maintain the developability of the whole 3D model.

The process of decreasing angle Θ' makes P_i (with even indices) on plane Π_2 together with the symmetric P_i' fall towards plane Π_1. For the whole 3D model, such a process compresses the 3D origami towards plane Π_1. Here, we check the flat-foldability of the 3D origami by verifying the flat-foldability of each interior point using Kawasaki's theorem and Maekawa's theorem.

In Figure 3.9 (c), without loss of generality, we verify the flat-foldability of the interior points by showing the details of the crease pattern around P_1 and P_4, which lie on the planes Π_1 and Π_2, respectively. Angle $\alpha_{i,k}$ denotes the $k-$th incident sector angle of p_i. For P_1, since $\alpha_{1,1} = \alpha_{1,2}$ and $\alpha_{1,3} = \alpha_{1,4}$ and thus $\alpha_{1,1} + \alpha_{1,3} = \alpha_{1,2} + \alpha_{1,4} = 180°$, which satisfies Kawasaki's theorem. Also, since the number of mountain lines (3) minus the number of valley lines (1) equals 2, Maekawa's theorem is satisfied. Similarly, for P_4, since $\alpha_{4,1} = \alpha_{4,2}$, $\alpha_{4,3} = \alpha_{4,6}$ and $\alpha_{4,4} = \alpha_{4,5}$, and thus $\alpha_{4,1} + \alpha_{4,3} + \alpha_{4,5} = \alpha_{4,2} + \alpha_{4,4} + \alpha_{4,6} = 180°$, which satisfies Kawasaki's theorem. Also, since the number of mountain lines (4) minus the number of valley lines (2) equals 2, Maekawa's theorem is satisfied. If all interior points satisfy Kawasaki's theorem and Maekawa's theorem, we can decrease Θ' to $0°$ to fold the whole 3D model around the z axis (Figure 3.14 (b)), which is a way of folding called "along-arc flat-folding". In general, benefiting from the mirror symmetry in each $1/N$ part crease pattern and the rotational symmetry of the whole crease pattern, local flat-foldable conditions can be satisfied.

3.4 Results

We developed a prototype system, using which the user can interactively design a 3D shape by editing its crease pattern. The system contains three windows as shown in Figure 3.10 (a), (b), and (c), where (a) is used to design the part of the crease pattern, (b) renders the 3D shape, and (c) shows the whole crease pattern. For designing an origami, the user can edit the crease pattern by adding, deleting, and dragging vertices in the crease pattern editor window (Figure 3.10 (a)). In particular, p_4 is dragged as shown in Figure 3.10 (d). At the same time, the 3D shape and the crease pattern will be changed as shown in Figure 3.10 (e) and (f), respectively. The user can also switch the candidates of p_4 by double-clicking p_4 on the crease pattern editor window (Figure 3.10 (d)) to achieve different shape shown in Figure 3.10 (g).

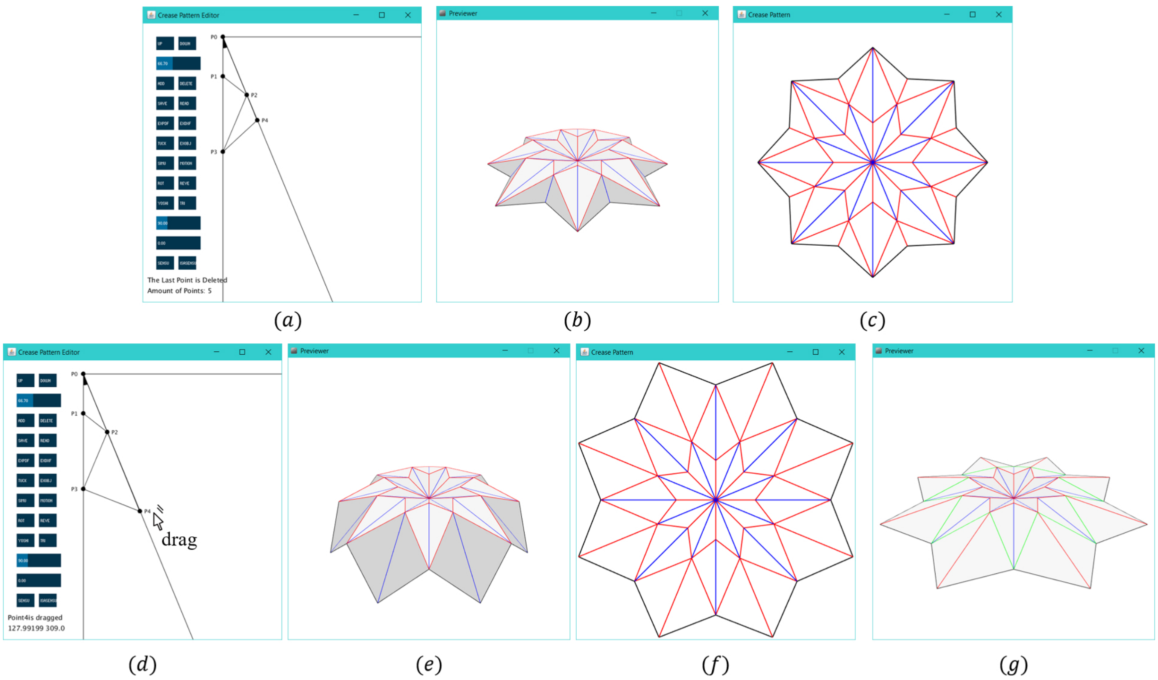

Figure 3.10: A prototype system implemented our algorithm.

We show several resulting origami pieces in Figure 3.11 and Figure 3.13, where the first column is the crease pattern, the second column is the 3D model, and the third column is the photo of the origami piece. Figure 3.11 shows the 3D origami pieces constructed with triangular facets. In Figure 3.12, we show the folding motion of the origami (Figure 3.11) from the fold-state to the flat-state by changing parameter φ.

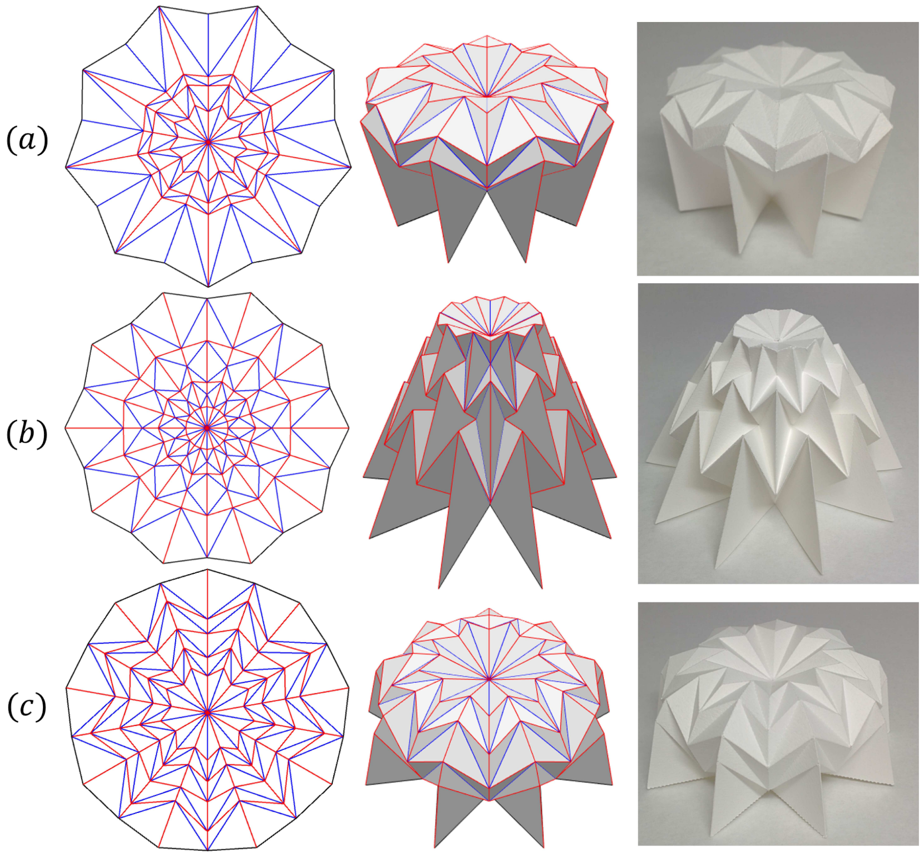

Figure 3.11: Resulting origami pieces with triangular facets.

By applying the special case, we design origami pieces that have both a flat center area and triangular facets, as shown in Figure 3.13. Figure 3.14 shows the “along-arc flat-folding” of the 3D origami shown in Figure 3.11 (b) and (c). The photo of the real origami pieces and the folded shapes are shown in Figure 3.15.

3.5 Summary

We described a design method for a category of axisymmetric triangle-based 3D origami folded from rotationally-symmetric crease patterns. We introduced a rotationally-symmetric crease pattern and then described the details of the calculation. For the calculation of

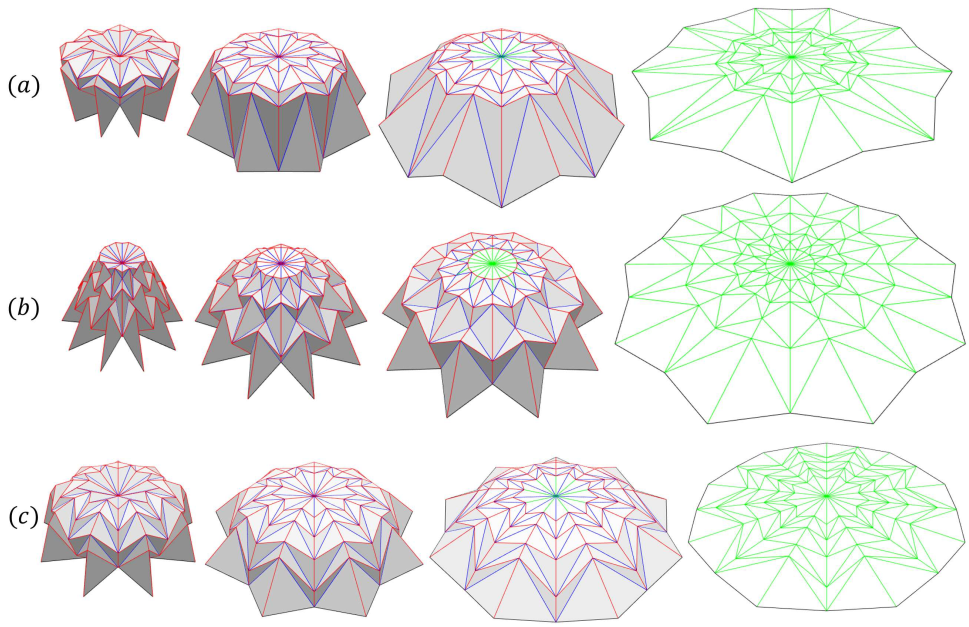

Figure 3.12: Flat-folding motion.

$P_i(i > 1)$, the two intersection points of the solution circles were selected as solution candidates. Each of them was used to create different 3D models. During the calculation, we found a special case where the two solution circles are identical; thus, the candidate solutions are not two points but all the points on the solution circle. We have applied the special case in designing origami pieces with a flat center.

We demonstrated the variations of the geometry by changing two parameters: angle φ and Θ. First, we changed φ, which is the angle between the edge P_0P_1 and the z axis. The benefit of the process of generating the 3D origami is, for each updated φ, the updated model remains developability. This enables us to explore various origami designs and figure out a folding motion from the fold-state to the flat-state of such a 3D origami. Next, we introduced a way of folding called "along-arc flat-folding" by changing the value of Θ, which is the angle between planes Π_1 and Π_2, from $180°/N$ to $0°$. To keep consistency between the crease pattern and the 3D model, we inserted a cut line in the crease pattern. Then, we checked the flat-foldability of the 3D origami by verifying the flat-foldability of each interior point using Kawasaki's theorem and Maekawa's theorem. We showed the "along-arc flat-folding" sequences and practiced such folding in real origami pieces.

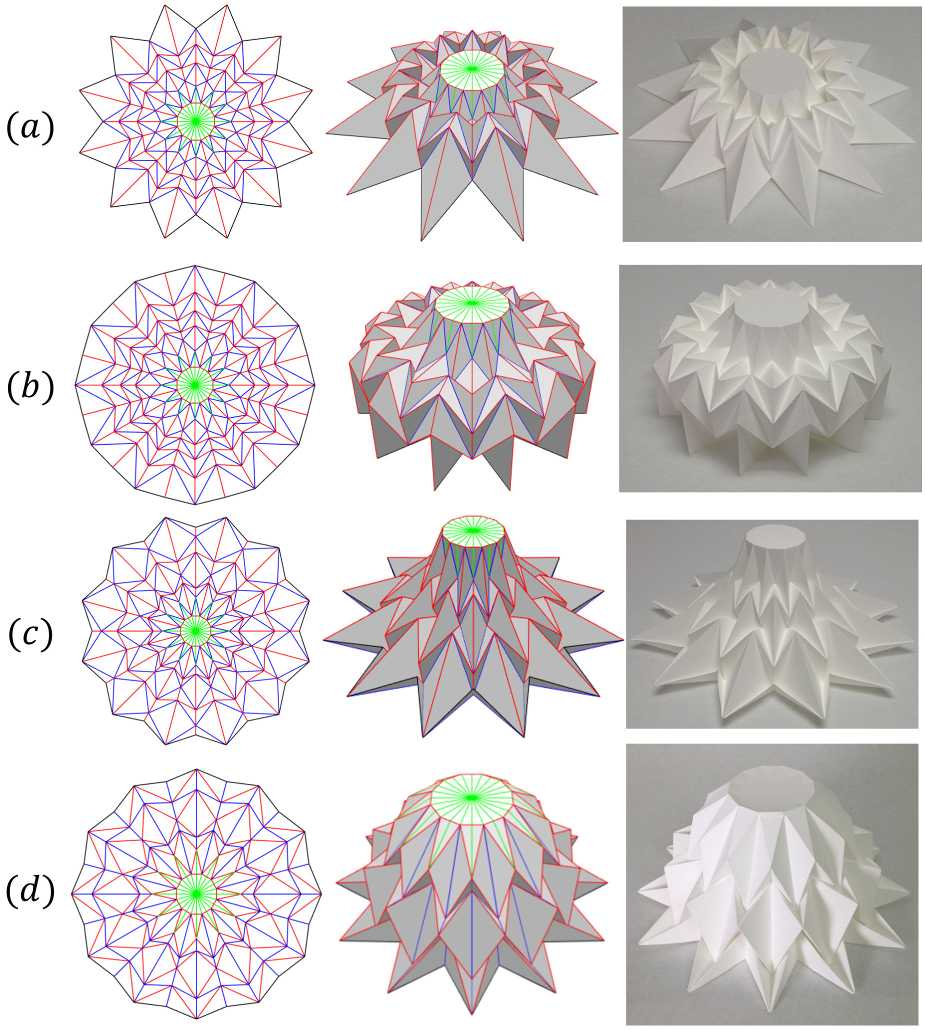

Figure 3.13: Resulting origami pieces with flat center area and triangular facets.

(a)

(b)

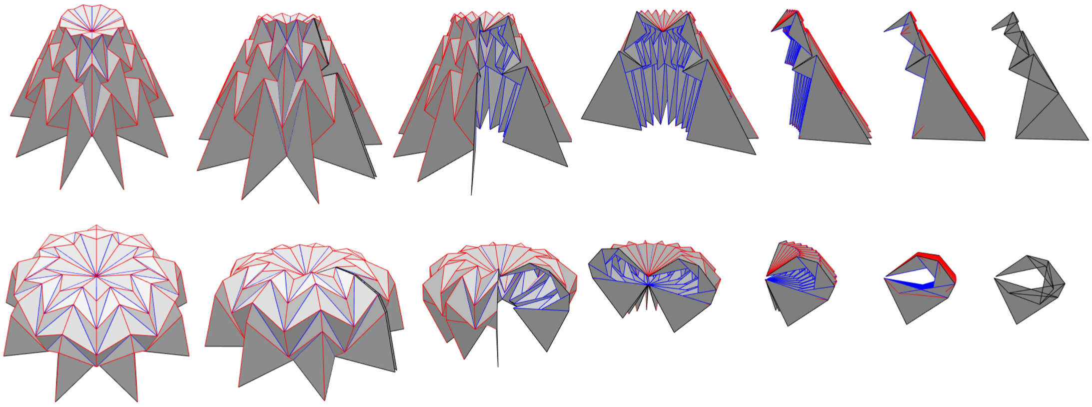

Figure 3.14: Along-arc flat-folding sequences.

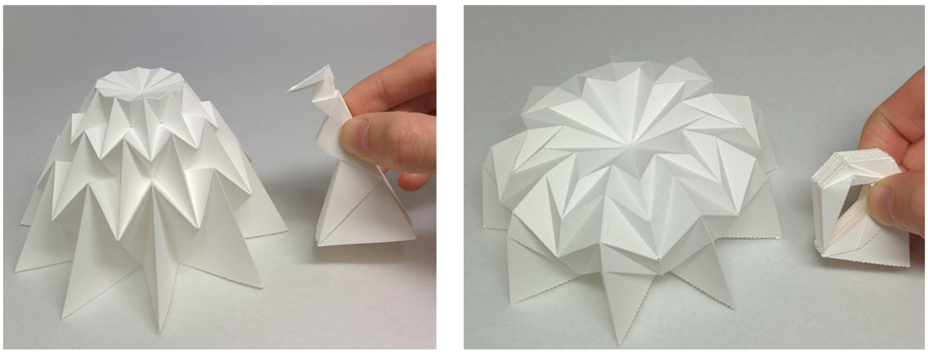

(a) (b)

Figure 3.15: Along-arc flat-folding of real origami pieces.

Chapter 4

Tucking axisymmetric 3D origami

The method [96] described in the previous chapter can only handle the crease pattern containing interior vertices having zero angle deficit, which indicates that the sum of the angles around each interior vertex is equal to 360 degrees. However, such a crease pattern is hard to be generated when editing the origami in 3D space.Those interior vertices with non-zero angle deficit become an obstacle to achieve a realizable 3D origami. In this chapter, we focus on the kind of axisymmetric triangle-based 3D origami folded from rotationally-symmetric crease patterns [96] and propose a design method for handling interior vertices with non-zero angle deficit generated during the 3D editing. As a result, the edited 3D shape becomes realizable through tucking a piece of paper without cutting.

An overview of our method is shown in Figure 4.1. First, we take one 3D origami (e.g., Figure 4.1 (a)) as an input and then edit the 3D shape by moving its $P_i(i > 1)$. Mountain and valley folded lines are rendered in red and blue, respectively. We render the crease lines connected by two almost flat facets in green. P_i (with odd indices) can be moved along plane Π_1 and P_i (with even indices) can be moved along plane Π_2.

Hereafter, we set i as four and move P_4 along plane Π_2 (Figure 4.1 (b)). During the 3D editing process, the crease pattern is updated by recalculating the location of p_4 with considering the distance constraints between P_iP_{i-1} and P_iP_{i-2} (Figure 4.1 (c)). The sum of the angles around interior vertex could be larger than or less than 360 degrees in the updated crease pattern. Intersections occur between crease lines when such a value is larger than 360 degrees. We call these patterns invalid. On the other hand, blank spaces (unfolded areas), colored in gray in Figure 4.1 (c), emerge in the crease pattern when the sum of the angles around interior vertices p_2 and p_4 are less than 360 degrees. Blank spaces hinder us from folding the resulting 3D origami.

Editing 3D origami while retaining angle deficit for each interior vertex equals zero is difficult. Here, we propose a computational procedure to handle blank spaces by adding crease lines (Figure 4.1 (c)) and calculate flaps outside (Figure 4.1 (d)) or tucks inside, which are folded from such areas. By adding flaps or tucks on the edited 3D shapes, we make such shapes realizable by tucking its crease pattern.

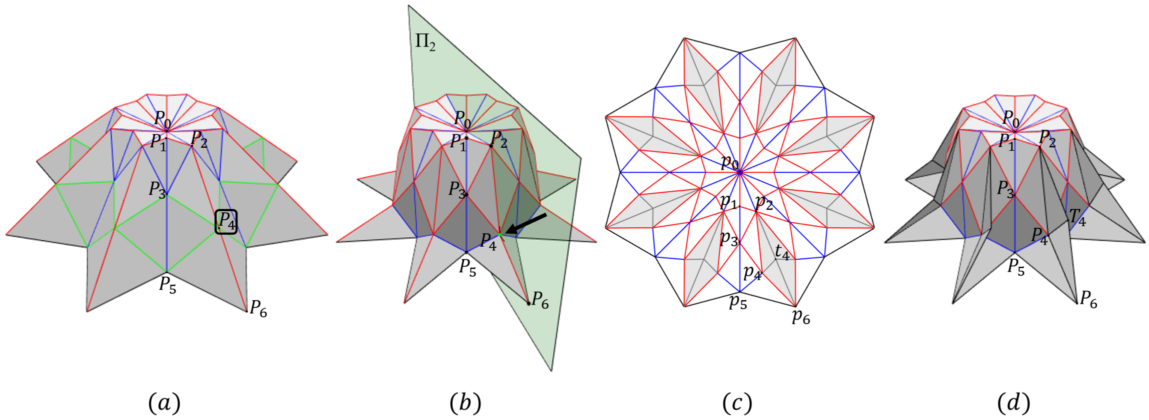

Figure 4.1: An overview of our method.

4.1 Methodology

4.1.1 Calculating 3D Origami with flaps or tucks

First, we introduce our user interface for 3D editing. Second, we describe a calculation of 3D flaps folded from quadrilateral blank spaces. Last, we describe a general case for calculating 3D flaps that are folded by polygonal blank spaces.

The origami is edited by moving its P_i (with odd indices) along plane Π_1 and P_i (with even indices) along plane Π_2. Figure 4.2 (a) shows the origami be edited by moving P_4 along plane Π_2. P_4 can be moved along the u direction (Figure 4.2 (b) or (c)) and the v direction (Figure 4.2 (d) or (e)) on the plane Π_2. Because the u and v directions are orthogonal, P_4 can be flexibly moved on plane Π_2 by moving along such two directions repeatedly.

During the design process, the system recalculates its crease pattern to keep it congruent with the newly edited 3D shape. Specifically, for the shape shown in Figure 4.2 (e), we calculate the new position of p_4 (Figure 4.3 (a)) that makes the distance between p_4p_3 and p_4p_2 the same as the distance between P_4P_3 and P_4P_2, respectively. Although p_4'' also satisfies such distance constraints, we leave such selection because it generates an invalid crease pattern with intersections. The updated crease pattern is shown in Figure 4.3 (b) and the detail around interior vertex p_2 is shown in Figure 4.3 (c) where the angle $a_{i,k}$ denotes the $k-$th incident sector angle of p_i. Note that the sum of the angles around interior vertex p_2 is less than 360 degrees, and thus the blank spaces shown in gray emerge (Figure 4.3 (b)).

Editing an origami in 3D space can hardly retain zero angle deficit for each interior vertex. Figure 4.4 shows the updated crease patterns corresponding to the 3D shapes shown in Figure 4.2, respectively. The new position of p_4 (Figure 4.4 (b) and (d)) makes the sum of the angles around p_2 larger than 360 degrees, thereby leading to invalid crease patterns

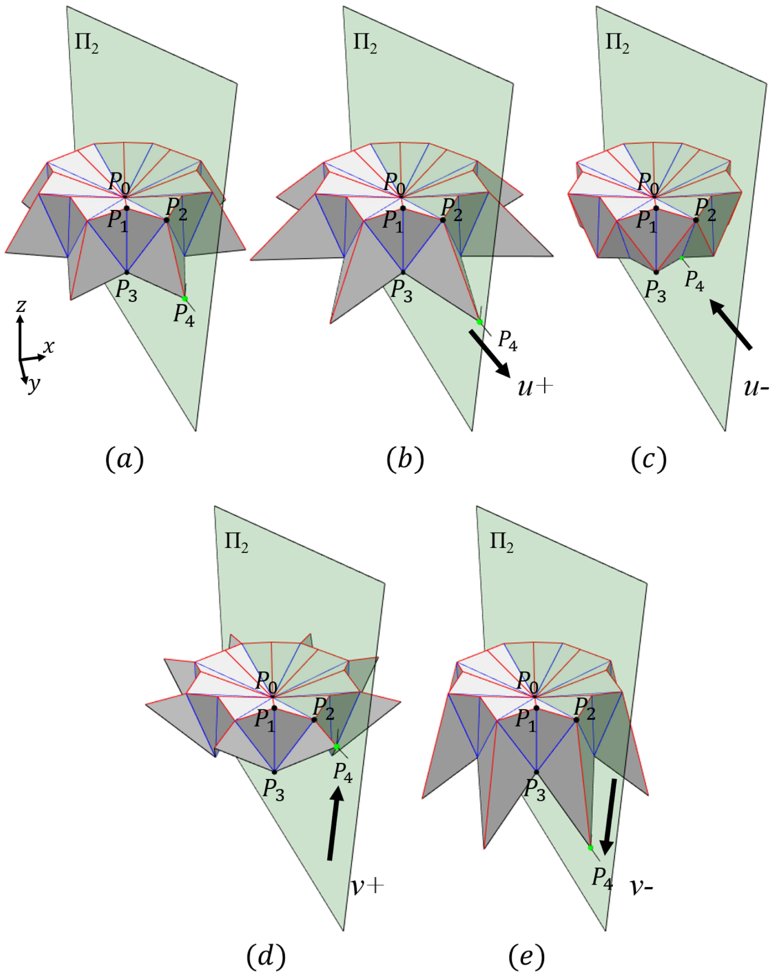

Figure 4.2: Designing origami in 3D space.

due to intersections. By checking the sum of the angles around an interior point, our system can give feedback to the user when an invalid crease pattern is generated. When the sum of the angles around p_2 is less than 360 degrees, blank spaces without crease lines are emerged in the crease pattern (Figure 4.4 (c) and (e)) hindering us from folding.

For tucking the 3D origami with blank spaces, we add crease lines in the blank space under symmetry property. Consider the crease pattern in Figure 4.5 (a) and its part shown in (b), where the blank space is quadrilateral. To make the edges $p_2p_4^{'}$ and $p_4^{'}p_6$ coincide with p_2p_4 and p_4p_6, respectively, by folds, we first add a crease line between p_2 and p_6 to divide the blank space $p_2p_4{'}p_6p_4$ equally. Then, we add a new point t_4 along segment p_2p_6 with two crease lines t_4p_4 and $t_4p_4^{'}$ to fold the blank space. Note that t_4 takes any position on the segment p_2p_6. Next, we calculate the shape of a flap or tuck in 3D space by calculating the coordinates of T_4, whose distances to P_2, P_4, and P_6 are $|p_2t_4|$, $|p_4t_4|$,

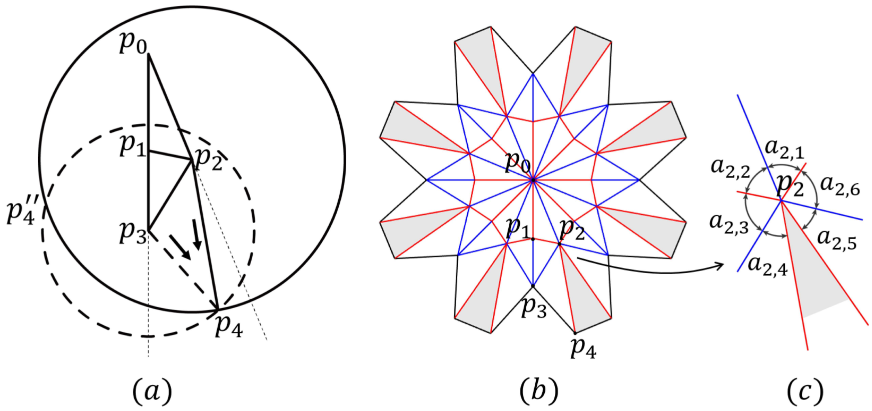

Figure 4.3: Recalculating crease pattern.

and $|p_6t_4|$, respectively. Therefore, T_4 lies on the intersection points of three spheres whose centers are P_2, P_4, and P_6 and radius equal $|p_2t_4|$, $|p_4t_4|$, and $|p_6t_4|$, respectively. If two intersection points exist, our system allows the user to choose either of them as the solution of T_4 to obtain different result (Figure 4.5 (c) and (d)).

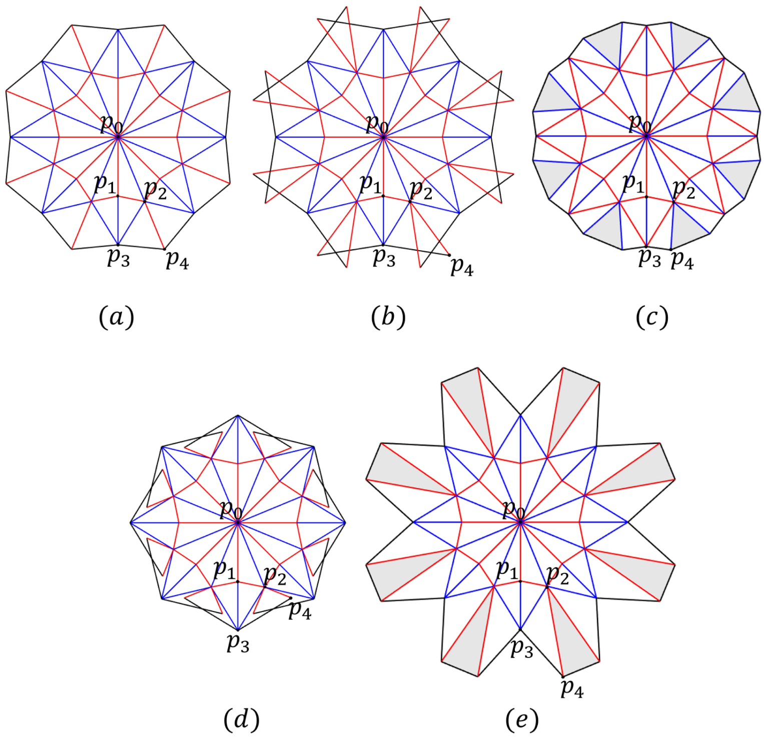

Figure 4.4: Updated crease patterns corresponding to the operations shown in Figure 4.2.

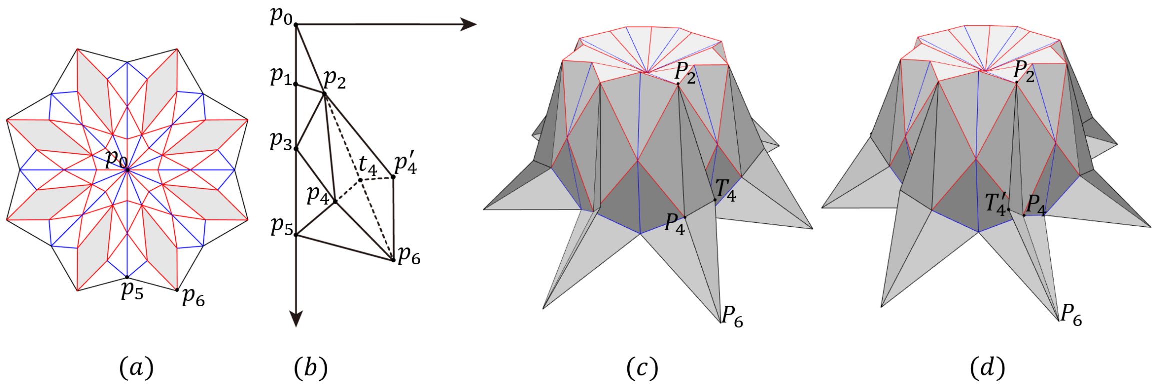

Figure 4.5: Calculate 3D shape of flap.

We can also explore various 3D flaps by moving t_4 along the segment p_2p_6. Figure 4.6 (a) shows one scenario where three choices of t_4, i.e., $t_{4,1}, t_{4,2}, t_{4,3}$ and the resulting 3D origami are shown in Figure 4.6 (b), (c), and (d), respectively. Some location of t_4 could make the generated 3D flaps penetrate facets in the resulting 3D origami (Figure 4.6 (b)). In such a situation, the user changes t_4 to another location (e.g., $t_{4,2}$ or $t_{4,3}$) until no penetration occurs (if such a location exists). By interactively editing possible 3D flaps, the user can find and revise the invalid location of t_4 in the design process. Using a computational way to add crease lines without causing penetrations is left as future work.

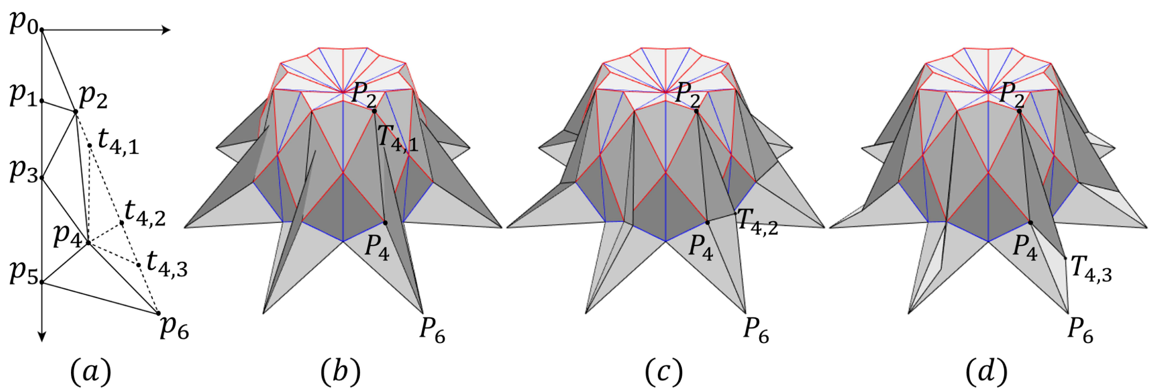

Figure 4.6: Variation of 3D flaps.

Last, we describe a general case for calculating 3D flaps that are folded by polygonal blank spaces. As shown in Figure 4.7, (a) shows a 3D origami and (b) shows its crease pattern whose blank spaces are polygons. Edges p_3p_5', $p_5'p_7'$, and $p_7'p_9$ should coincide with p_3p_5, p_5p_7, and p_7p_9, respectively, by folds. We first equally divide the polygonal area by adding a crease line p_3p_9. Then, we divide such area into triangles by adding t_5 and t_7 along segment p_3p_9 as shown in (c). Finally, we calculate the 3D coordinates of T_5 with the distance constraints from P_3, P_5, and P_7. In the same way, T_7 is calculated by considering the distance constraints from T_5, P_7, and P_9. Because the points are positioned inside of the shape, the blank space area is folded inside as a tuck, as shown in (d). This process is also applicable for general polygons that have more than six vertices.

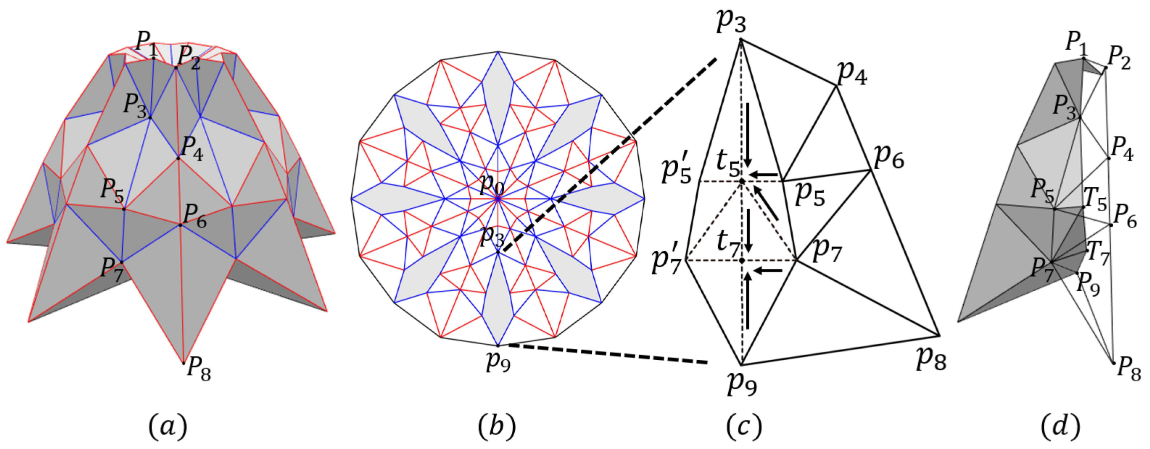

Figure 4.7: Calculating 3D flaps folded from polygonal blank spaces.

4.1.2 Special case of 3D flaps

On the basis of the aforementioned explanation, the system adds flaps outside or tucks inside of the 3D origami. In this section, we describe a special case where 3D flaps lie exactly on the surface of the 3D origami. Figure 4.8 shows one example of such a special case.

P_5, the middle point of P_4 and P_4', is on the plane Π_1 because P_4 and P_4' are symmetric to the plane Π_1. In addition, P_5 makes $P_3P_5P_4$ a 90-degree angle. P_7, which is another middle point of P_6 and P_6', makes $P_5P_7P_6$ a 90-degree angle. P_5, P_4, P_6, and P_7 are coplanar because line P_4P_4' is parallel to line P_6P_6'. Next, we add appropriate crease lines in the blank space as shown in Figure 4.8 (b) and the part shown in (c). Angles $p_3p_5t_5$ and $p_5p_7t_7$ should equal 90 degrees to let flaps lie exactly on the surface. Therefore, we specify t_5 by extending line p_4p_5 and line $p_4'p_5'$. Similarly, t_7 is specified by extending line p_6p_7 and line $p_6'p_7'$. Under such a configuration, the calculated flaps lie exactly on the surface of 3D origami (Figure 4.8 (a)). As a result, the 3D flaps become a part of the origami whatever they are viewed from inside or outside.

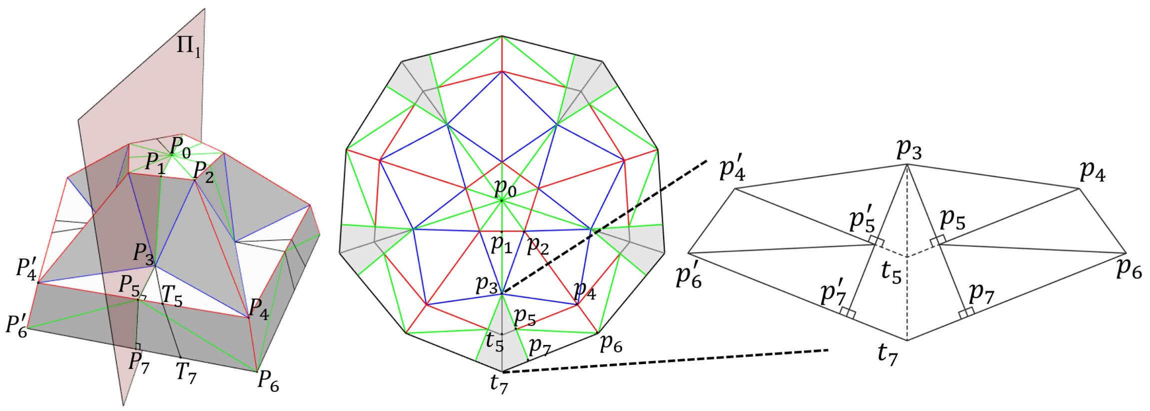

Figure 4.8: Special case of 3D flaps.

4.2 Results

We updated the prototype system, introduced in the previous chapter, for supporting 3D editing. Figure 4.9 shows such a process, where (a) is an input 3D origami. Here, the user can select one vertex, e.g., P_4, by clicking. The system also shows a plane which the selected vertex can be moved (Figure 4.9 (b)). Then, the user can move P_4 along v and u directions by dragging as shown in Figure 4.9 (c) and (d), respectively. After adding P_5 (Figure 4.9 (e)) and P_6 (Figure 4.9 (f)), the user can achieve a 3D shape. Finally, by adding flags outside (Figure 4.9 (g)), the shape shown in Figure 4.9 (f) can be achieved by folding. Note that our system allows the user to change the shape of the flap (Figure 4.9 (h)).

We show several resulting 3D origami pieces in this section. In Figure 4.10: (a) shows the flaps lie outside of the 3D origami and (b) shows a similar shape but with a flat center area; (c) shows the tucks inside of the 3D origami; (d) shows the 3D origami piece whose flaps lie exactly on itself. Figure 4.11 illustrates the 3D origami pieces with two types of flaps, where (a) has a flat center area and (b) is consisting of triangular facets.

Figure 4.12 shows two 3D origami pieces with the shape of a stool. Such origami pieces are locked by tucks and thus do not easily open at the bottom when we put pressure on their top surfaces. Such a feature could be potentially used as a stool for sitting. Therefore, we fabricated the origami piece (Figure 4.12 (a)) using polypropylene with 0.75 mm thickness to demonstrate its potential usage. The length and width of the material used in this experiment were about 50 cm. We made all crease lines on the top surface of the material using a cutting plotter. Then, to valley fold smoothly, we manually made valley lines on the other side of the material. We took almost two hours to fold the material. As a result, we obtained an origami stool (Figure 4.13 (a)) with 22 cm length and width and 15 cm height without gluing. Furthermore, we found that a two-year-old boy of 13 kg could sit on it (Figure 4.13 (b)).

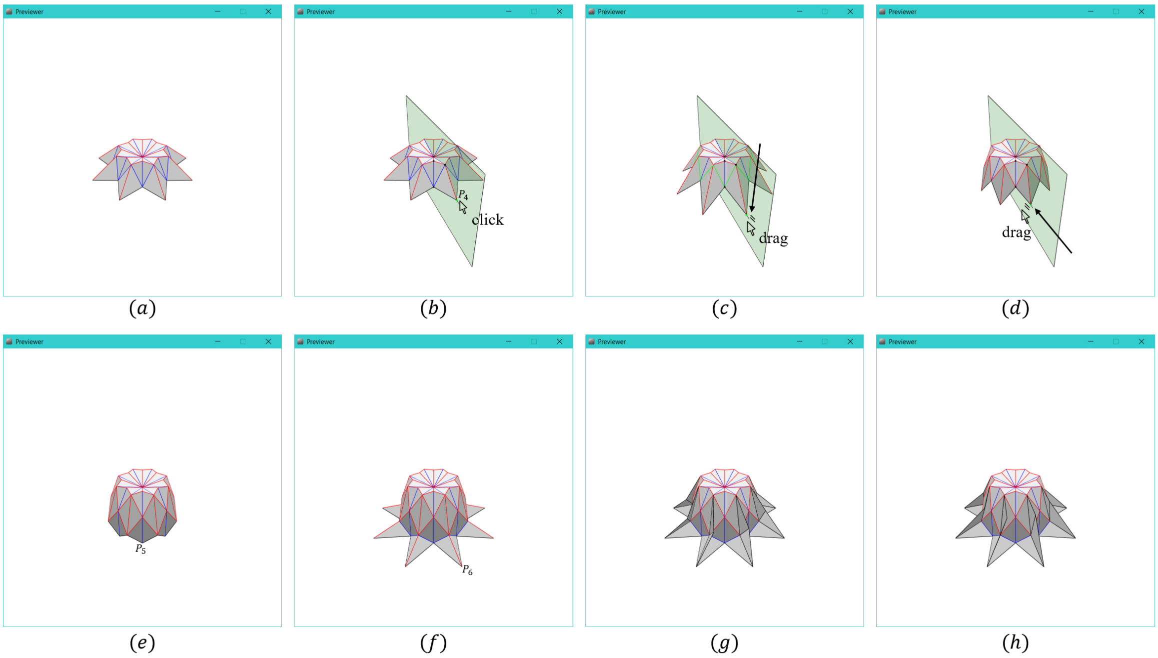

Figure 4.9: A graphical user interface for supporting 3D editing.

Beyond observation of this experiment, we found that bending and distortions occurred in some facet of the origami stool. The main reason could be that we did not consider designing an origami piece with material thickness. Revising crease patterns to adapt for thick material is left as future work.

4.3 Summary

We focused on a family of axisymmetric triangle-based 3D origami folded from the rotationally-symmetric crease patterns and proposed a computational design method for tucking such origami. We described the procedure for handling blank spaces caused by non-zero angle deficit of interior vertices and the calculation of the flaps outside or tucks inside folded from such areas. We demonstrated several new 3D origami pieces with flaps or tucks. Finally, we did a load-bearing experiment on a stool shape-like origami to demonstrate the potential usage of our origami piece.

The *Origamizer* algorithm by Tachi [80, 76, 19] is a general approach based on the tucking technique, a technique to hide the unnecessary areas of a sheet of paper inside the shape. The algorithm places the triangles on the plane with some margins that are "tucked" inside. Our approach is similar to this. Tachi utilizes a numerical optimization, while our approach is based on a simple analytical formula because of the symmetric property of the target shape. Although the Origamizer can handle our target shapes, the generated pattern

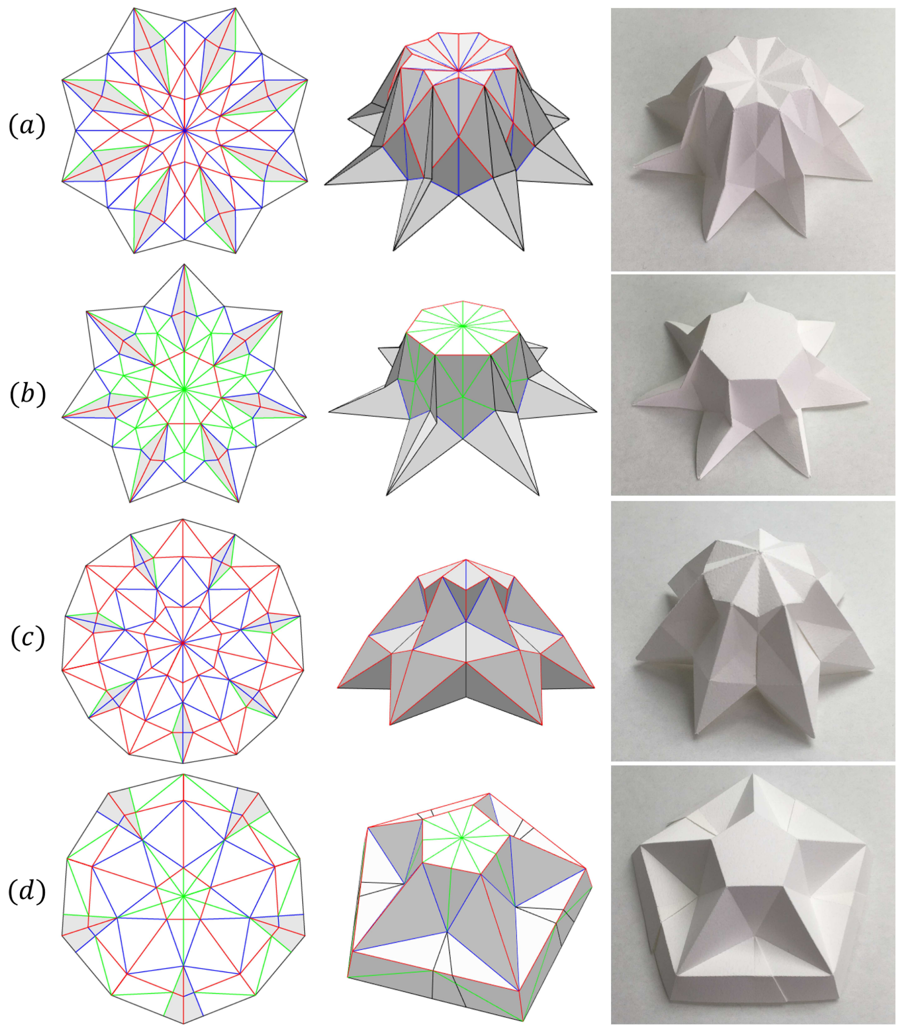

Figure 4.10: Resulting origami pieces with 3D flaps or tucks.

tends to be overly complicated because adding tucks *inside* is the one and only solution. However, our system adds tucks *outside* (we call them “flaps”) if adding tucks inside is not a simple solution.

As future work, four aspects of this study can be improved: (i) using a computational way to add crease lines in the blank spaces without causing penetrations, (ii) revising crease patterns with considering the thickness of material, (iii) exploring an optimal shape of tucks or flaps to increase the strength of the origami structure, (iv) analysing physical changes of paper during the process of tucking flaps or tucks.

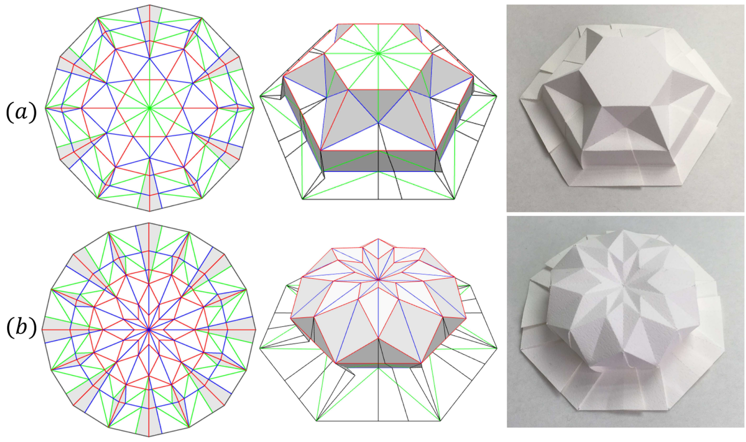

Figure 4.11: Resulting origami pieces with two types of 3D flaps.

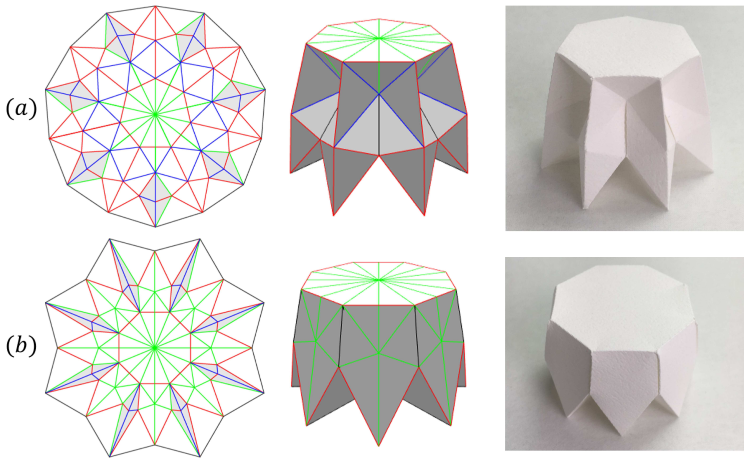

Figure 4.12: Resulting origami pieces with shape of stool.

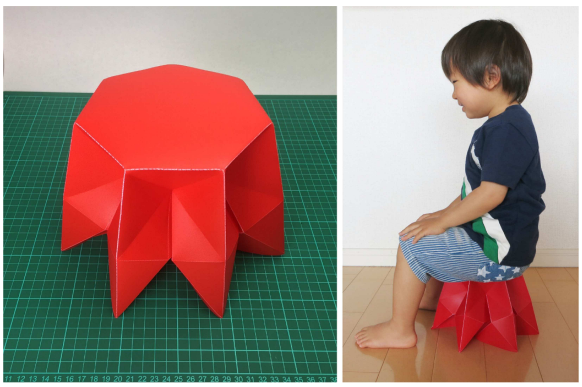

Figure 4.13: Load bearing experiment on stool shape-like origami with tucks inside.

Chapter 5

Axisymmetric 3D Origami with Generic Six-crease Bases

Among the crease patterns, the waterbomb tessellation (Figure 1.1 (a)) and Yoshimura pattern (Figure 1.1 (b)) with interior vertices having six-crease lines are widely used and have been widely researched. The interior vertex surrounded by six creases is referred to as a six-crease base. When the length of the symmetric creases is equal, such a base is referred to as a regular six-crease base. Besides, origami patterns, e.g., Miura-ori [63] and its generalization (Figure 5.1), can be noted that they are consisting of four-crease bases. Comparing to the four-crease-base origami, origami constructed by six-crease bases is simple and provide more freedom of movement.

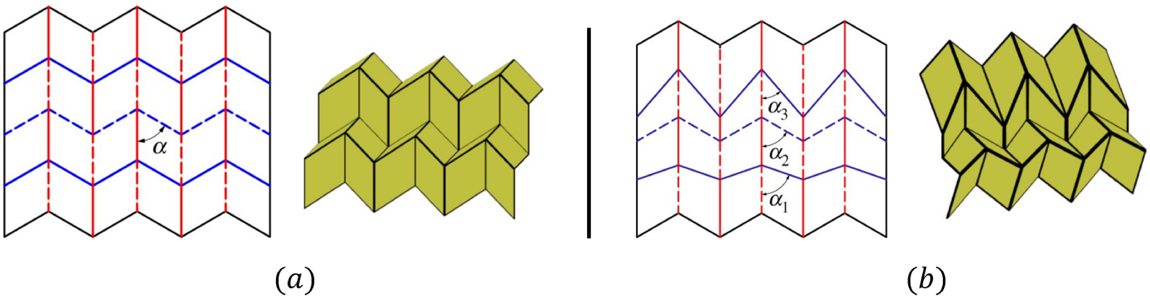

Figure 5.1: Origami consisting of four-crease bases. (a) Miura-ori. (b) Generalized Miura-ori pattern. For each origami, the left shows the crease pattern and the right shows a partially folded state. In the crease pattern, mountain creases are indicated by solid lines and valley folds by dashed lines. Fold lines of the same colour have the same fold angle. Images adopted from [24].

Most existing studies based on the six-crease patterns are focused on the regular bases. In this chapter, inspired by the regular six-crease base, we present our generalization of the base, enabling the lengths of the crease lines to be regular or irregular. By using such generic bases, variations of this kind of origami can be increased. Furthermore, the 3D origami constructed by generic bases could be more flexible than the origami based on regular bases for specific applications. First, we interactively generate a crease pattern consisting of such generic bases (Figure 5.2 (a)). Then, our method analytically calculates the 3D origami shape with an axisymmetric structure (Figure 5.2 (b)). Finally, while referring to the shape of the 3D origami, the user can fabricate the 3D origami piece (Figure 5.2 (d)). The 3D origami consisting of triangular facets has multiple DOFs, but by continually changing one parameter, we present a motion that can axisymmetrically deploy or flatten the shape around the z axis (Figure 5.2 (c)).

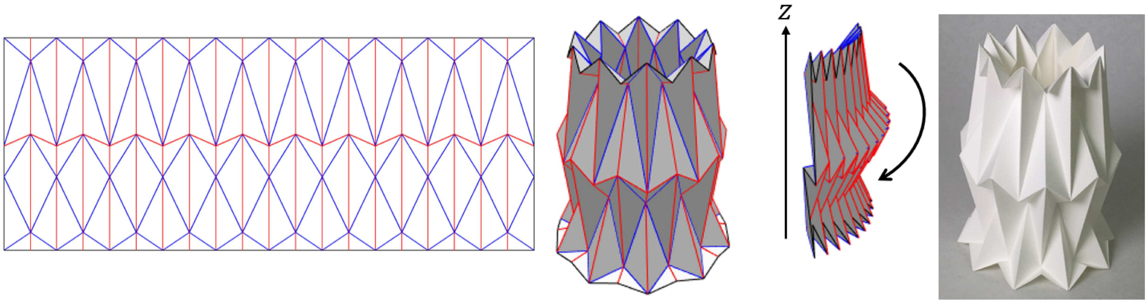

(a) (b) (c) (d)

Figure 5.2: An overview of our method.

5.1 Designing 3D origami

5.1.1 Designing crease pattern

We describe the crease pattern made using generic six-crease bases. Figure 5.3 (a) shows a $1/N$ part of the crease pattern (where N indicates the order of rotational symmetry and equals 10 in this example), (b) shows the corresponding part in 3D space. $p_i(i = 1, 2, 3, ...)$ denote the points in the 2D crease pattern, and $P_i(i = 1, 2, 3, ...)$ indicate the corresponding points in 3D space. l_1 and l_2 are two parallel lines. p_i (with odd indices) lie on line l_1 and p_i (with even indices) lie on line l_2. $p_i^{'}$ (with even indices) are the symmetric points of p_i with respect to line l_1. The crease pattern can be interactively designed. Specifically, we can adjust the space between lines l_1 and l_2. We can also move, add, and delete p_i along lines l_1 or l_2. For a newly added $p_i(i > 2)$, we place crease lines p_ip_{i-1} and p_ip_{i-2}, to guarantee that all interior points have valence six. After the $1/N$ part of the crease pattern is specified, we generate the whole crease pattern by repeating the $1/N$ part N times (Figure 5.3 (c)).

Figure 5.3 (b) illustrates the overall layout of the pattern in 3D space. O is the origin of a Cartesian coordinate system. Π_1 is a vertical plane passing through the z axis and y

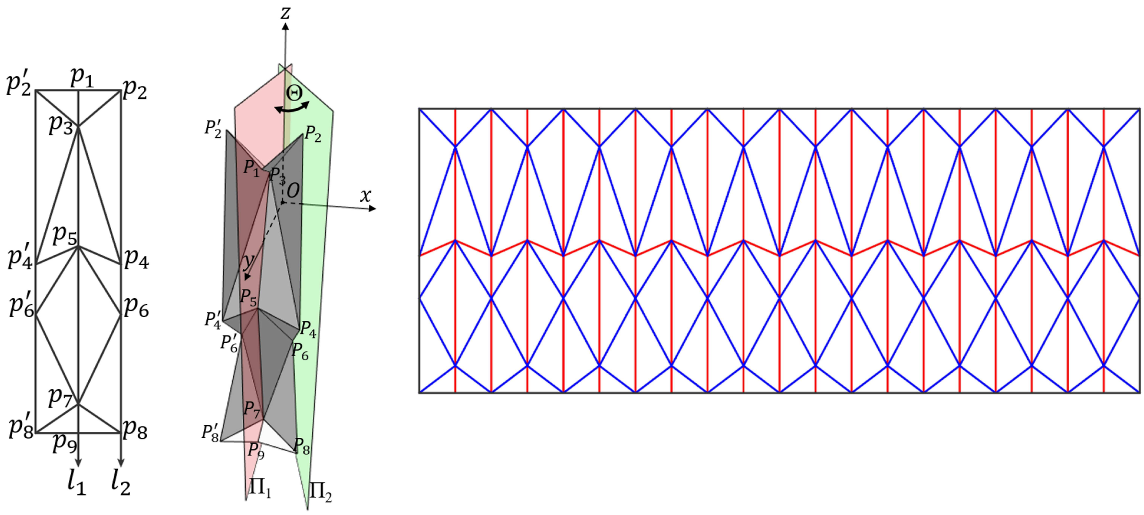

(a) (b) (c)

Figure 5.3: Designing crease pattern.

axis. Π_2 is another vertical plane passing through the z axis. Θ, which equals $180°/N$, is an angle between such two vertical planes. P_i (with odd indices) lie on the plane Π_1 and P_i (with even indices) lie on the plane Π_2. P_i' and P_i (with even indices) are symmetric with respect to plane Π_1. After the $1/N$ part of the 3D origami is calculated, we achieve the axisymmetric 3D shape by iteratively rotating its $1/N$ part about the z axis.

We also introduce a parameter T to represent the number of editable points in the 1/N part of the crease pattern (e.g., $T = 9$ in Figure 5.3 (a)). Note that every interior vertex having six crease lines has a mirror-symmetric property. We can make the six crease lines of the interior vertex irregular (e.g., $|p_3p_1| \neq |p_3p_5|$ and $|p_3p_2| \neq |p_3p_4|$ at p_3) because p_i are interactively moved in the crease pattern. Using such a crease pattern consisting of regular or irregular six-crease bases, we can generate novel 3D origami (e.g., the origami pieces shown in Figure 5.13).

5.1.2 Calculation of each 3D point

We take the generated $1/N$ part of the crease pattern (shown in Figure 5.3(a)) as an input and describe a method to calculate each point on 3D origami. P_i is calculated sequentially in the order of its index. First, we use Eq. 5.1 to define P_1 on the plane Π_1 (Figure 5.4 (b)).

$$P_1 = (0, L\sin(\varphi), L\cos(\varphi)), \tag{5.1}$$

where L indicates the length of $|OP_1|$ and φ represents the angle between OP_1 and the z axis. As shown in Figure 5.4, φ is set as $58°$ for generating (a). V is the foot of the perpendicular from P_1 to the z axis.

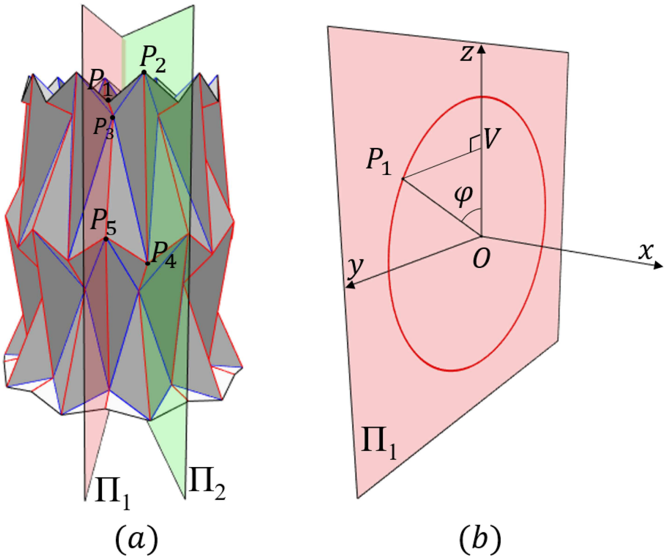

Figure 5.4: Determination of P_1.

Next, we calculate the 3D coordinates of P_2 based on the following constraints: (i) the distance between P_2 and P_1 should be the same as $|p_2p_1|$ in the crease pattern, (ii) P_2 should lie on the plane Π_2. To satisfy these two constraints, we achieve candidates for P_2, which are gathered on the solution circle shown in red, the center of which is represented as C_2 (Figure 5.5 (a) and (b)). To achieve one solution of P_2, we introduce a parameter denoting as β, which is the angle between C_2P_2 and the z axis. By specifying the angle β ranging from $0°$ to $360°$, we can achieve various P_2, as examples shown in Figure 5.5 (a) and (b), where β equals $0°$ and $90°$, respectively. The solution circle shown in red is an intersection of plane Π_2 and a sphere, the center of which is P_1 and the radius of which equals $|p_1p_2|$. Here, we introduce an upper bound of L as L_b, when the solution circle degenerates to one point C_2 (Figure 5.5 (c)). L_b can be defined as Eq. 5.2 in right triangle OVP_1.

$$L_b = \frac{|VP_1|}{\sin(\varphi)}. \tag{5.2}$$

Meanwhile, $|VP_1|$ is defined as Eq. 5.3 in right triangle VP_2P_1.

$$|VP_1| = \frac{|P_1P_2|}{\sin(\Theta)}. \tag{5.3}$$

By substituting Eq. 5.3 for Eq. 5.2, we can achieve L_b in Eq. 5.4:

$$L_b = \frac{|P_1P_2|}{\sin(\Theta)\sin(\varphi)} = \frac{|p_1p_2|}{\sin(180°/N)\sin(\varphi)}. \tag{5.4}$$

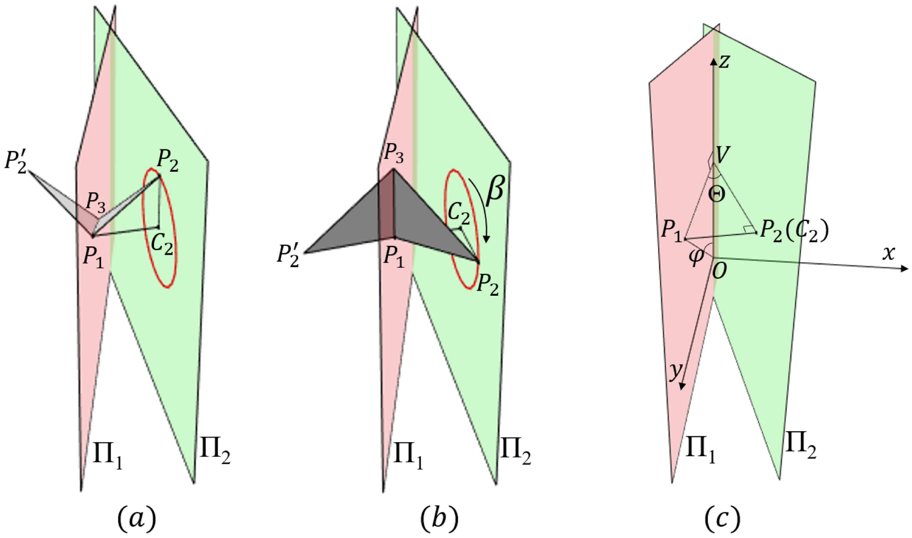

Figure 5.5: Calculation of P_2.

Note that $|p_1p_2|$ and N are given by the crease pattern, and thus for a given crease pattern L_b is related to another input φ.

Next, we calculate the 3D coordinates of P_i ($i > 2$) based on the following constraints: (i) the distance between P_i and P_{i-1} should be the same as $|p_ip_{i-1}|$ in the crease pattern, (ii) the distance between P_i and P_{i-2} should be the same as $|p_ip_{i-2}|$ in the crease pattern, (iii) P_i should lie on the plane Π_1 (for an odd index) or Π_2 (for an even index). We set $i = 5$ and describe the calculation of P_5 (Figure 5.6). P_5 lies on the plane Π_1 and is connected to P_4 and P_3. First, by considering the distance constraint between P_5 and P_4, we achieve the candidates that are gathered on the circle shown in green. Second, by considering the distance constraint between P_5 and P_3, we achieve the candidates that are gathered on the circle shown in red. Finally, two intersection points between the two circles (the red one and the green one) that satisfy all the constraints at the same time are selected as two candidates for P_5 (if they exist). Our system gives feedback when no candidates achieved and allows us to select when two candidates exist. By selecting either of them, we can achieve different shapes of 3D origami (Figure 5.6 (a) and (b)). After all P_i and P_i' (with even indices) are calculated, we achieve the $1/N$ part of the 3D origami. Then, by iteratively rotating such 3D part about the z axis, we can achieve the resultant shape of 3D origami (Figure 5.4 (a)). Finally, based on the generated 3D model, we determine the mountain and valley assignments on its crease pattern (Figure 5.3 (c)).

The space of 3D origami consisting of triangular facets could be very rich. For a calculated 3D origami (whose crease pattern and choices for selecting 3D candidates are determined), we explore its variations by changing parameters φ, L, and β in the discrete domain. We refer to a set of φ, L, and β as a configuration. We set a range of φ from $0°$ to

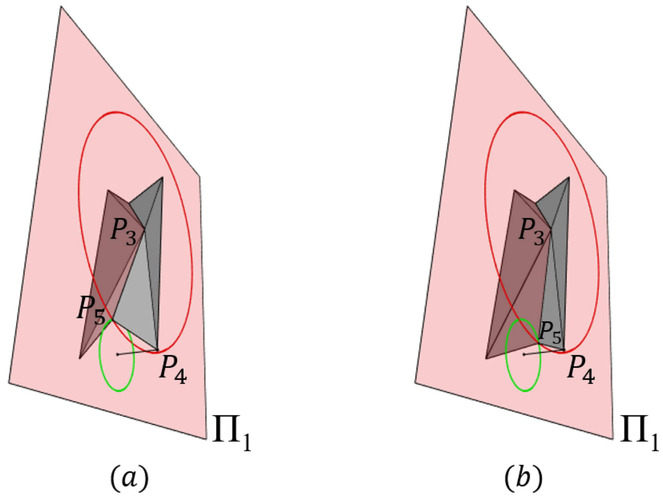

Figure 5.6: Calculation of $P_i (i > 2)$, where $i = 5$.

$180°$ without $0°$ and $180°$, because we cannot achieve L_b when φ equals such two values. L ranges from 0 to L_b for a given φ (Eq. 5.4). The value of β ranges from $0°$ to $360°$.

Hereafter, for the 3D origami shown in Figure 5.13 (a), we demonstrate various configurations as points (Figure 5.7 (a)) that represent 3D origami pieces achievable without self-intersections. The crease pattern and choices for selecting 3D candidates are remained during the exploration. To normalize L, we introduce L_{max}, found in the experiment, which indicates the maximum of L that exists at least one configuration for generating achievable 3D origami. Specifically, we demonstrate 18 samples (Figure 5.7 (b), (c), and (d)) and their corresponding 3D shapes (Figure 5.7 (e)). We achieve 3D shapes from #1 to #6 by increasing φ from $21°$ to $86°$ while keeping L and β remained as 2.56e-2 L_{max} and $36°$, respectively. By increasing L from 0.95e-2 L_{max} to 3.34e-2 L_{max}, we achieve 3D shapes from #7 to #12, where φ and β are fixed as $106°$ and $36°$, respectively. We can also achieve 3D shapes from #13 to #18, by increasing β from $157°$ to $167°$ while keeping φ and L remained as $61°$ and 2.59e-2 L_{max}, respectively. As a result, we demonstrate that different 3D shapes can be achieved based on the same crease pattern.

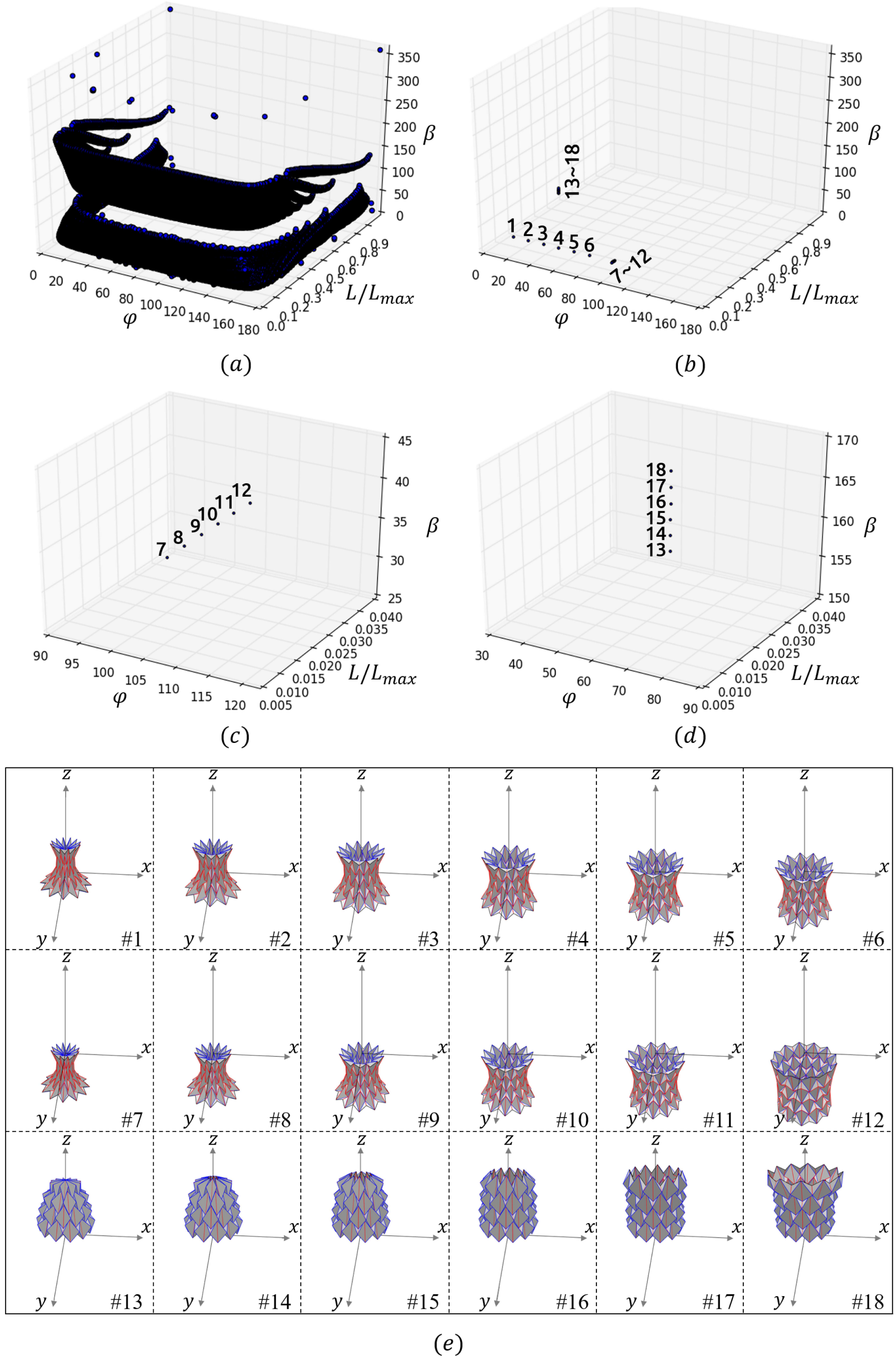

Figure 5.7: Variations in 3D origami by changing configuration.

5.2 Motion analysis

We describe an along-arc flat-folding, which is triggered by parameter Θ, the angle between planes Π_1 and Π_2.

5.2.1 Calculation of degree of freedom

The degrees of freedom of a triangular mesh are represented as Eq. 5.5

$$DOF = N_{Eo} - 3N_L - 3, \tag{5.5}$$

where N_{Eo} is the number of edges on the boundary, and N_L is the number of holes [79]. In our work, N_{Eo} is represented by Eq. 5.6

$$N_{Eo} = 4N + 2(\left\lfloor \frac{T}{2} \right\rfloor - 1), \tag{5.6}$$

where N indicates the order of rotational symmetry, and T represents the number of editable points in the $1/N$ part of the crease pattern. In addition, N_L equals zero, thus the degrees of freedom in our work are represented as

$$DOF = 4N + 2(\left\lfloor \frac{T}{2} \right\rfloor - 1) - 3. \tag{5.7}$$

According to Eq. 5.7, the 3D origami in Figure 5.8 (a) has 43 DOFs ($N = 10$ and $T = 9$).

Within those DOFs, we can axisymmetrically flat fold the 3D origami with decreasing angle Θ. Specifically, P_i (with even indices) on plane Π_2 together with the symmetric $P_i^{'}$ fall towards plane Π_1 with decreasing Θ (represented as $\Theta^{'}$, $0° \leq \Theta^{'} \leq \Theta$, in Figure 5.8 (a)).

For the whole origami, such a process compresses the 3D shape towards plane Π_1. Meanwhile, the 3D origami is locally flat-foldable based on the satisfaction of Kawasaki's theorem.Here, we show the interior vertices p_5 and p_6 (Figure 5.8 (b) and (c)), for which the 3D points P_5 and P_6 are convex and concave, respectively. Angle $\alpha_{i,k}$ denotes the $k-$th incident sector angle of p_i. For p_5, because $\alpha_{5,1} = \alpha_{5,6}$, $\alpha_{5,2} = \alpha_{5,5}$, and $\alpha_{5,3} = \alpha_{5,4}$, $\alpha_{5,1} + \alpha_{5,3} + \alpha_{5,5} = \alpha_{5,2} + \alpha_{5,4} + \alpha_{5,6} = 180°$, satisfying Kawasaki's theorem. Similarly, we can show that p_6 also satisfies Kawasaki's theorem (Figure 5.8 (c)). In general, interior vertices satisfy Kawasaki's theorem because they have a mirror-symmetric property.

To intuitively describe the folding state due to angle $\Theta^{'}$, we introduce a folding rate:

$$FR = 100(1 - \frac{\Theta^{'}}{\Theta})\%. \tag{5.8}$$

Figure 5.9 shows the along-arc flat-folding where the folding rate equals 0%, 20%, 40%, 60%, 80%, and 100% corresponding to (a), (b), (c), (d), and (f), respectively. The origami

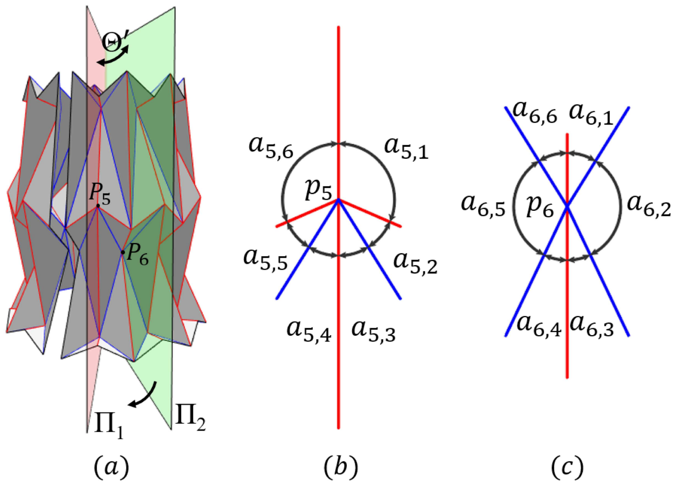

Figure 5.8: Satisfaction of Kawasaki's theorem for each interior vertex.

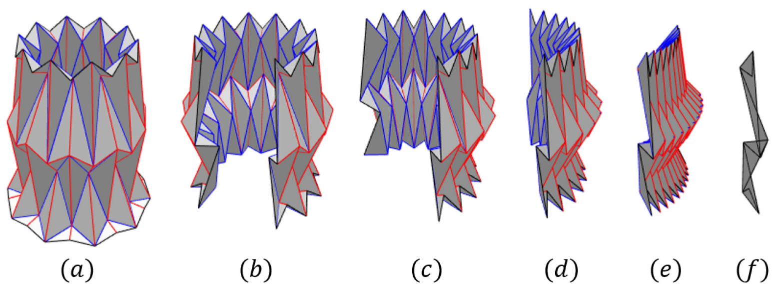

Figure 5.9: Along-arc flat-folding with self-intersection-free test.

remains rigid in this folding sequence, which is triggered by continually changing $\Theta^{'}$. Self-intersections could occur during the motion. Here, we enumerate the folded 3D shapes based on $\Theta^{'}$, ranging from Θ to 0° in the discrete domain with dense sampling. The folding sequence is considered as self-intersection-free when none of the enumerated 3D shapes has self-intersections.

5.2.2 Kinematic behavior

We analyzed the kinematic behavior of the vertices in a designed 3D origami during motion. For the origami shown in Figure 5.8 (a), without loss of generality, we selected a convex P_5 that has four mountain and two valley folded lines and a concave P_6 that has two mountain and four valley folded lines for analysis. We introduced angle $\phi_{i,k}$ indicating the $k-$th dihedral angle at vertex P_i, and k is started from one and assigned clockwise (Figure 5.10 (a) and Figure 5.11 (a)). The relationship between the folding rate and dihedral angles at selected vertices P_5 and P_6 during motion are illustrated in Figure 5.10 (b) and Figure 5.11 (b), respectively.

The maximum dihedral angles at P_5 are $119°$, $104°$, $111°$, and $76°$ corresponding to $\phi_{5,1}$, $\phi_{5,2}$, $\phi_{5,3}$, and $\phi_{5,4}$, respectively. For P_6, the maximum dihedral angles are $129°$, $111°$, $98°$, and $94°$ corresponding to $\phi_{6,1}$, $\phi_{6,2}$, $\phi_{6,3}$, and $\phi_{6,4}$, respectively. The knowledge of these maximum dihedral angles helped us to build a rigid origami structure with double layered thick composite panels because it is a factor to avoid collision between panels [79]. In addition, based on the kinematic analysis during motion, we could control the dihedral angles by setting actuators to build self-folding tessellations or deployable architectures.

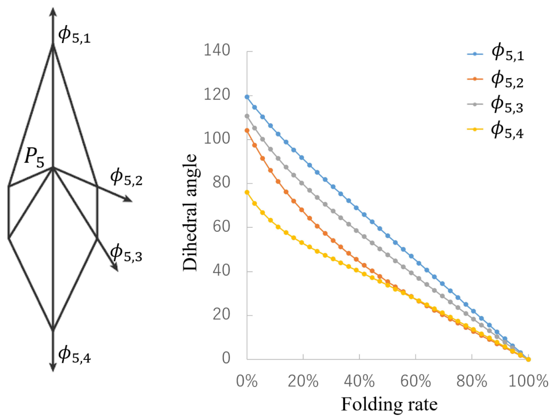

(a) (b)

Figure 5.10: Kinematic behavior of P_5.

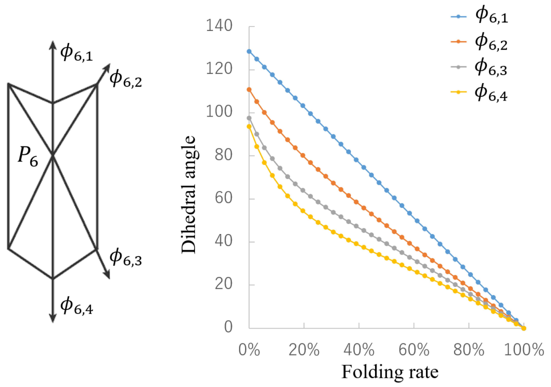

(a) (b)

Figure 5.11: Kinematic behavior of P_6.

5.3 Results

We developed a prototype system for implementing our algorithm as shown in Figure 5.12, where (a) is used to interactively design the crease pattern, (b) renders the 3D shape, and (c) shows the whole crease pattern.

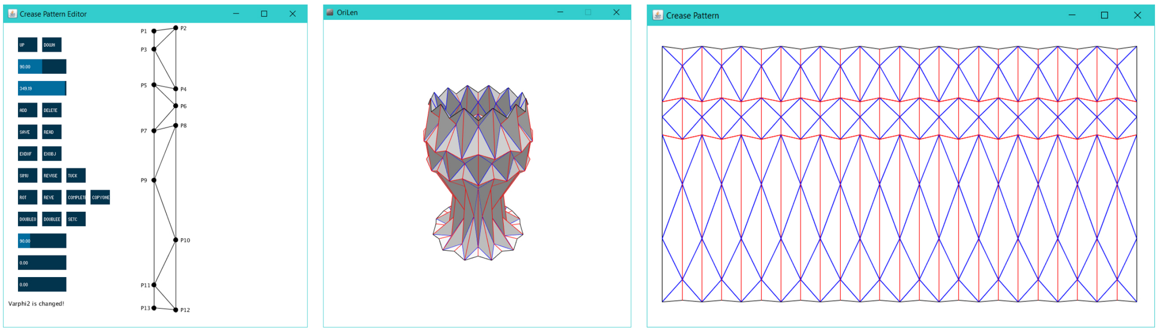

(a) (b) (c)

Figure 5.12: A prototype system implemented our algorithm.

We show several resulting origami pieces in Figures 5.13 and 5.14. Figure 5.13 shows (a) a candlestick with a negative global Gaussian curvature, (b) a rugby ball with a positive global Gaussian curvature, and (c) a vase with a curved base having a positive global Gaussian curvature and a curved neck having a negative global Gaussian curvature. Here, our interest lies in the macroscopic behavior of the sheets, and thus we consider the global Gaussian curvature [73] of an equivalent mid-surface of the folded sheet.

Figure 5.14 shows (a) a lampshade and (b) a bud. P_1 in both of them lie on the symmetric axis. (c) shows another bud, and (d) and (e) show a ball and a cup, respectively. We achieved the folding sequences shown in Figure 5.15. Note that P_1 stays on the symmetric axis during motion in Figure 5.15 (a).

For the 3D origami having self-intersections during the motion, we manually modified the design. Here, we take the shape shown in Figure 5.16 (a) as an example. We can see that the facets shown in red penetrated each other (Figure 5.16 (b)). In addition, from Figure 5.16 (c) showing the relationship between the folding rate and dihedral angles at vertex P_5, we note that the folding motion is interrupted by self-intersections when folding rate is larger than 46%. For the origami shown in Figure 5.16 (a), we adjust its vertices in crease pattern to achieve the shape shown in Figure 5.17 (a). The modified one can be flat folded without self-intersections (Figure 5.17 (b) and (c)).

(a)

(b)

(c)

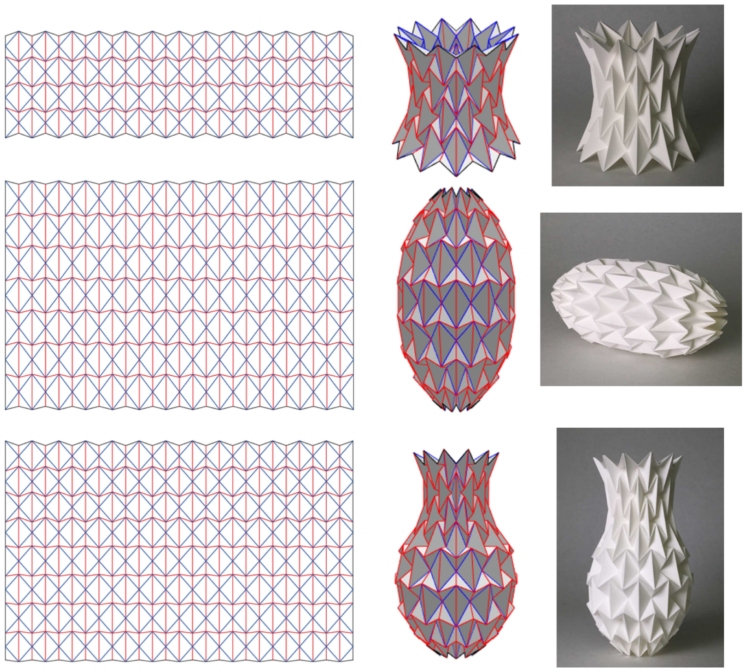

Figure 5.13: Resulting origami pieces with different ‘global’ Gaussian curvature.

5.4 Summary

We described a design method for a class of axisymmetric 3D origami with generic six-crease bases, for which the lengths of the crease lines can be regular or irregular. First, we interactively generate a crease pattern consisting of such generic bases. Then, our method analytically calculates the geometry with an axisymmetric structure. We demonstrated various configurations to explore the variations of the calculated 3D origami.

We described an along-arc flat-folding to flat fold the 3D origami axisymmetrically by continually changing parameter Θ. First, we described the calculation of DOF and the folding process triggered by changing Θ. We also showed that the 3D origami is locally flat-foldable based on the satisfaction of Kawasaki’s theorem for each interior vertex p_i. Finally, we analyzed the kinematic behavior by illustrating the relationship between the folding rate and dihedral angles at selected vertices. Several origami pieces and folding sequences are presented to demonstrate the validity.

The method described in this chapter have shown several resulting shapes of varying curvature. It indicates that origami has the potential to fit target surfaces. In the next chapter, we introduce an inverse-origami-design problem and provide a solution by using generalized waterbomb tessellations for approximating target 3D surfaces.

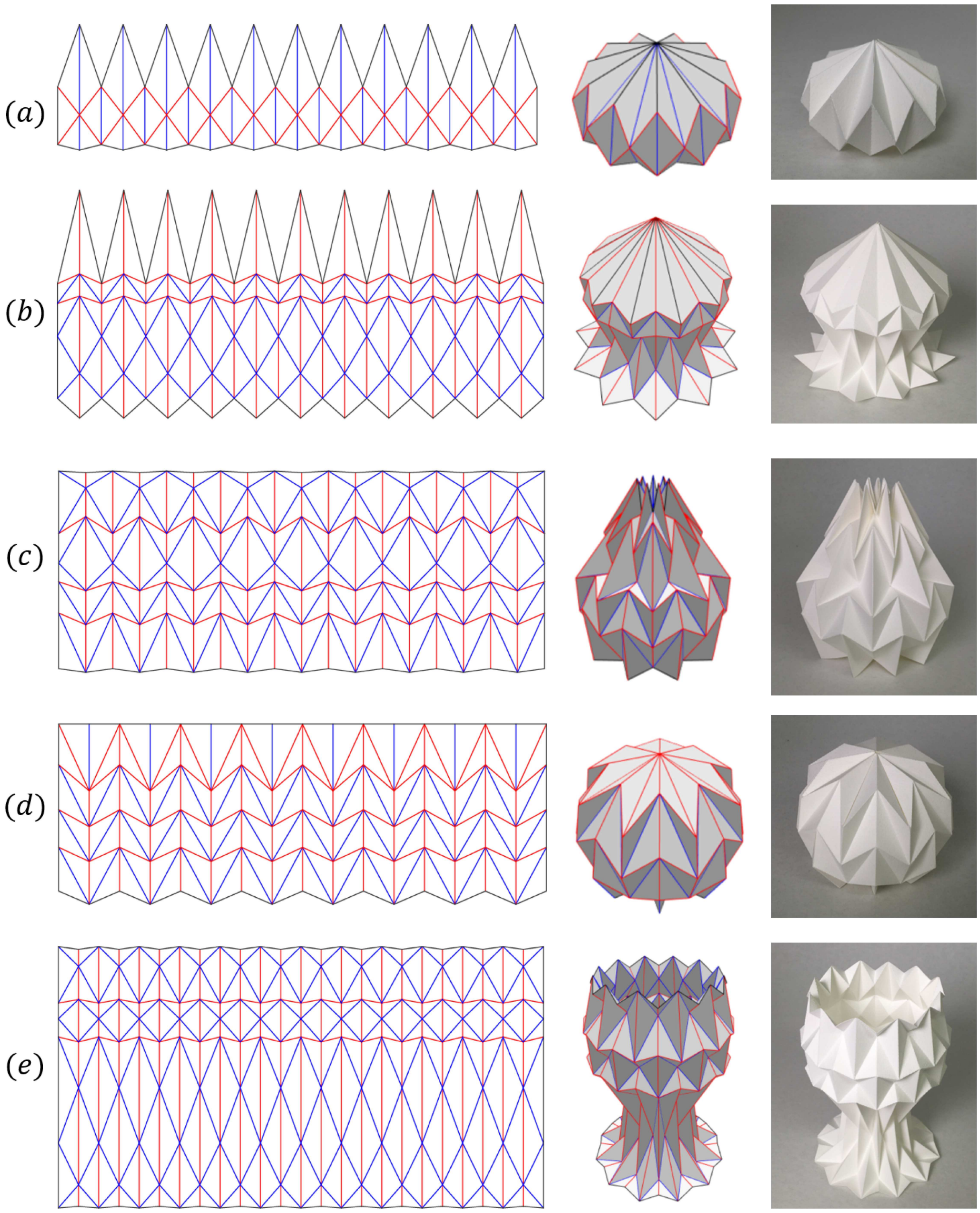

Figure 5.14: Resulting origami pieces.

(a)

(b)

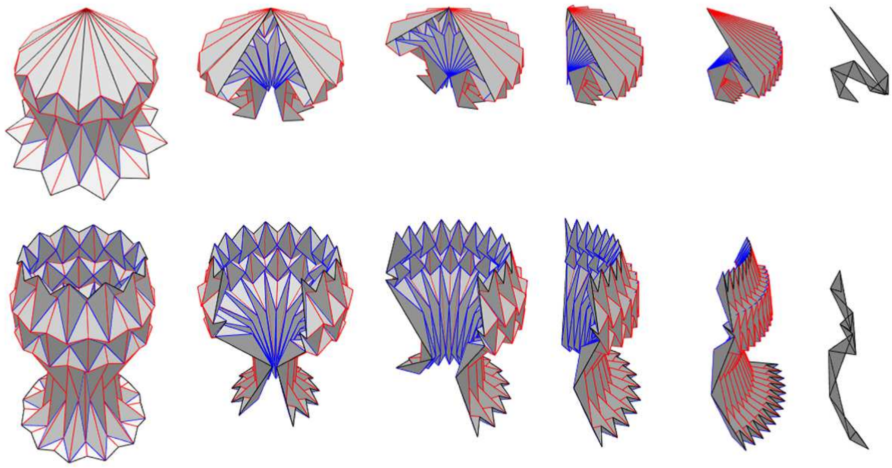

Figure 5.15: Folding sequences with self-intersection-free test.

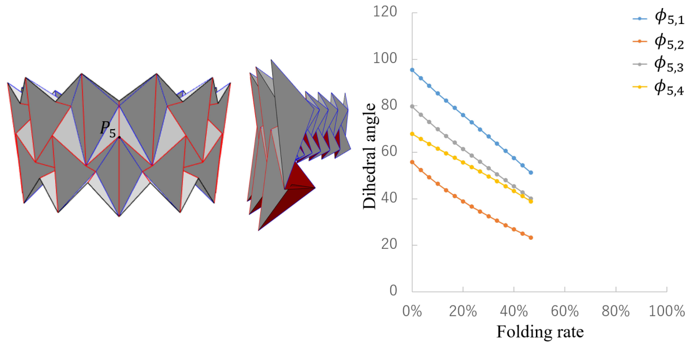

(a) (b) (c)

Figure 5.16: Self-intersections occur during folding motion.

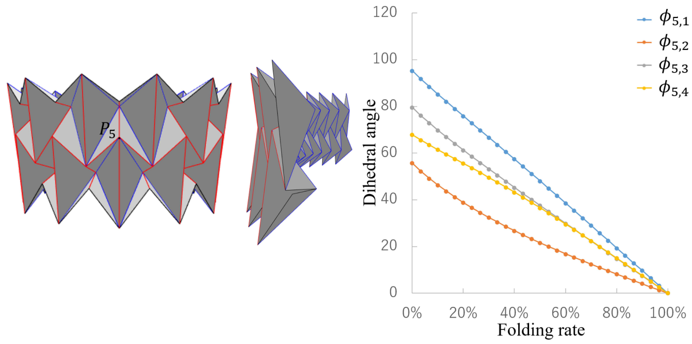

(a) (b) (c)

Figure 5.17: Modification to enable the origami be flat folded.

Chapter 6

Approximating 3D Surfaces using Generalized Waterbomb Tessellations

Origami has the potential to construct 3D shapes of varying curvature by folding thin sheets of paper along predefined creases. Inverse origami design is another research direction of designing origami. Comparing to the approaches based on designing the crease pattern, the inverse-origami-design approach fits a target 3D surface using a calculated crease pattern. Among the types of origami, waterbomb tessellation is a traditional one that can be used to create geometrically appealing 3D shapes, e.g., the model shown in Figure 6.1 (a). As shown in Figure 6.1, a 3D waterbomb origami (a) is defined by its crease pattern (b), which contains a set of waterbomb bases (c). Such origami pieces are developable, which is guaranteed by the fact that the sum of the sector angles around each interior vertex equals $360°$. The waterbomb base, which is also referred to as a regular base, has a mirror-symmetric property. The base has the geometric feature containing four valley and

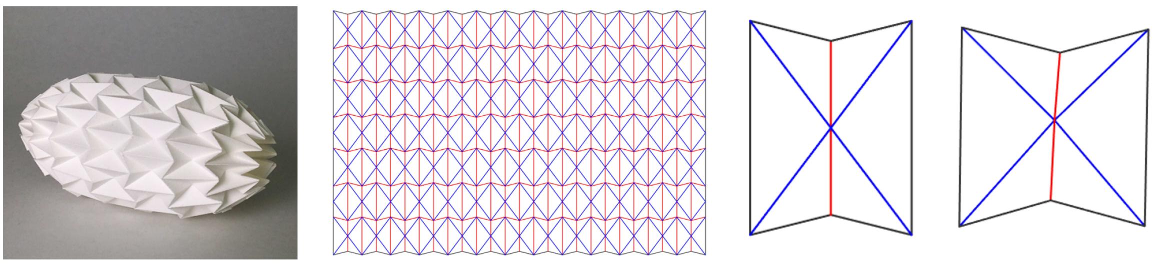

(a) (b) (c) (d)

Figure 6.1: Geometry of generalized waterbomb origami

two mountain folded lines meeting at the center vertex. Here, we introduce a generalized waterbomb base (Figure 6.1 (d)) that inherits this geometric feature but could omit the mirror-symmetric property. Furthermore, we introduce a generalized waterbomb tessellation that contains generalized waterbomb bases. The generalized waterbomb tessellations have the potential to be used for approximating target 3D surfaces due to its high degree of freedom.

In this chapter, we approximate target surfaces, which are parametric surfaces of varying or constant curvatures, using generalized waterbomb tessellations. An overview of our method is shown in Figure 6.2. We take a 3D parametric surface, e.g., Figure 6.2 (a), as an input. Then, we sample u and v coordinates in the parametric uv-plane to achieve a quad approximation (Figure 6.2 (b)). Next, we generate a base mesh (Figure 6.2 (c)) by creating waterbomb bases in the quads. Here, our prototype system enables us to generate base meshes with variable resolutions and modify waterbomb bases interactively. Then, by applying a simple numerical optimization algorithm to the base mesh, we achieve a developable waterbomb tessellation (Figure 6.2 (d)). Finally, the user can fold the crease pattern (Figure 6.2 (e)) to achieve the origami piece (Figure 6.2 (f)). We demonstrate several resulting approximations, which extend the exploration of building developable structures.

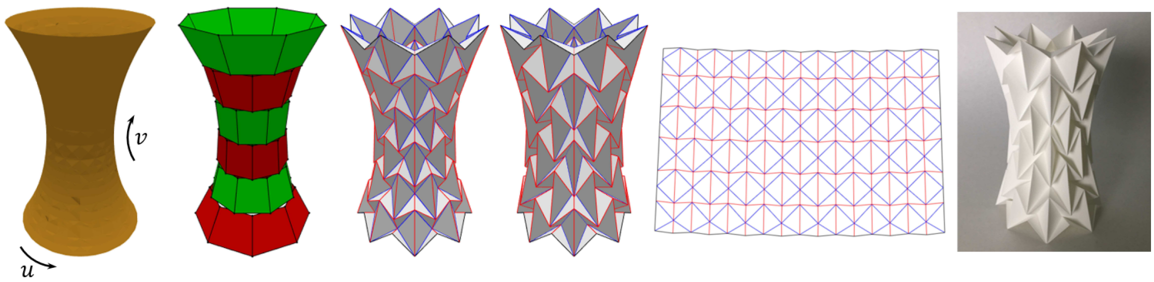

(a) (b) (c) (d) (e) (f)

Figure 6.2: An overview of our method.

6.1 Approximating target surfaces

We demonstrate the generation of a base mesh in Section 6.1.1. Optimizing the base mesh to achieve a developable approximation is discussed in Section 6.1.2.

6.1.1 Generation of base mesh

The generation of the base meshes on parametric surfaces is versatile. In particular, we can generate base meshes on axisymmetric or non-axisymmetric target surfaces. Besides, owing to the high degree of freedom of the waterbomb tessellation, orientable or non-orientable target surfaces can be handled. Here, we tile a given surface using quads for the initial approximation. Parametric surfaces are taken as input in this work. Therefore, we can easily achieve a set of quads by isometrically sampling u and v coordinates, which vary within a certain domain D in the parametric $uv-$plane, of the input parametric surface.

Hereafter, we explain the case of a catenoid surface as an example. A catenoid surface (Figure 6.2 (a)) is defined with $u,\ v$ parameters as:

$$P(x, y, z) = (\cosh\frac{v}{c}\cos u, \cosh\frac{v}{c}\sin u, v), \tag{6.1}$$

where $u \in [0, 2\pi]$, $v \in [-\pi, \pi]$, and c is a non-zero real constant that is set as 2.5 in this case. As shown in Figure 6.3 (a) and (b), we isometrically sample u and v coordinates to achieve sampling points. The steps of u and v for sampling are denoted as Δu and Δv, which equal $2\pi/N_u$ and $2\pi/N_v$, respectively. N_u indicates the number of quads in one strip, which is shown in red and green. N_v means the number of strips used for constructing the approximation. Both N_u and N_v are integers and set as 10 in this case.

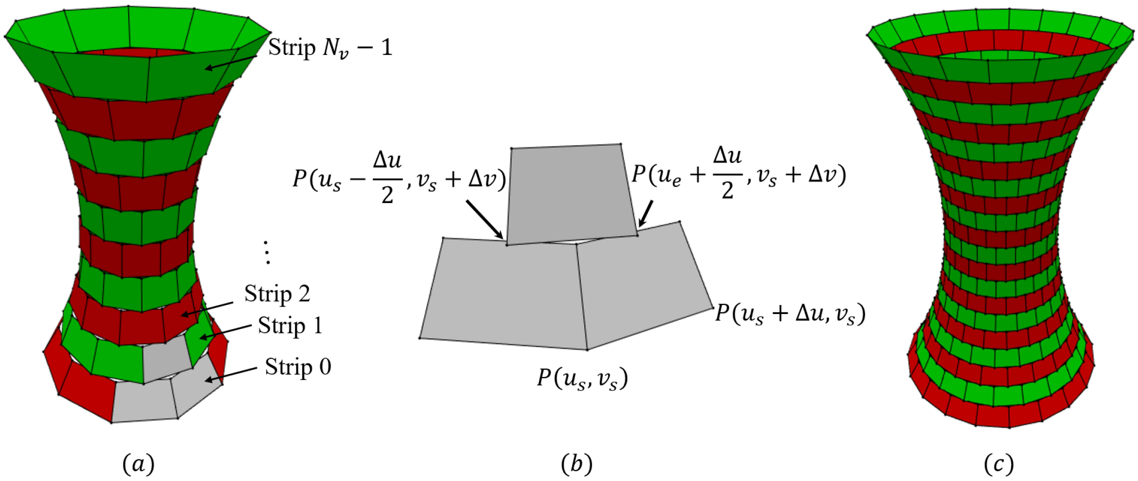

Figure 6.3: Initial approximation using quads

As can be observed from waterbomb tessellations, adjacent strips are shifted against each other by $\Delta u/2$ in the u direction in the $uv-$plane. A naïve way of doing this is to shift only odd strips by $-\Delta u/2$. However, this works with axisymmetric shapes but fails with non-axisymmetric ones because quads along boundaries become jagged and cannot cover the target surfaces. To handle both axisymmetric and non-axisymmetric shapes, we first temporarily generate $N_u + 1$ quads for odd strips in the range from $u_s - \Delta u/2$ to $u_e + \Delta u/2$, where we suppose that the parameter u ranges from u_s to u_e in the given parameter surfaces. In particular, the first quad's u ranges from $u_s - \Delta u/2$ to $u_s + \Delta u/2$, and the last quad's u ranges from $u_e - \Delta u/2$ to $u_e + \Delta u/2$ (Figure 6.3 (b)). In the case of axisymmetric shapes, the first and the last quads are identical because parameter u is periodic. We then generate a waterbomb base in each quad and select only a half of the first and the last waterbomb bases to ensure N_u waterbomb bases in each strip (shown in Figure 6.5 and discussed below).

During the initial approximation using quads, we allow the user to adjust the density of quads by changing N_u and N_v interactively. Figure 6.3 (c) is an approximation created by double density sampling both in the u and v directions, and thus, it has four times more quads than that in Figure 6.3 (a) to represent the target surface. The more quads we use, the more accurately we can approximate the target surface. Considering fabrication by paper-folding, however, we also have to consider the increase of labor. Balancing the approximation accuracy and fabrication labor is an interesting problem, which is left as future work.

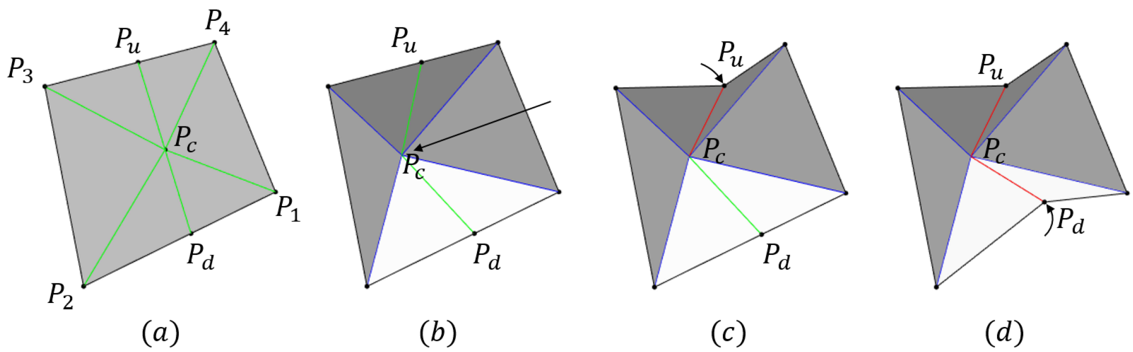

Figure 6.4: Modification of waterbomb base

Finally, we merge adjacent bases to achieve a base mesh (Figure 6.5 (c)). Figure 6.5 (a) is an approximation with gaps. By averaging the positions of adjacent vertices (b), we achieve a base mesh without gaps as shown in (c). Note that there are $N_u + 1$ bases for odd strips. Here, we select only the right part of the first base and the left part of the last base to ensure N_u bases in the odd strips.

6.1.2 Numerical optimization

We apply a simple numerical optimization to base meshes to produce developable surfaces. We use an angle constraint Eq. 2.1 to define a developable vertex. In our work, we classify vertices as interior vertices having six adjacent facets and boundary vertices having less than six adjacent facets. For a developable surface, all the interior vertices should satisfy the angle constraint.

We implemented the Levenberg-Marquardt algorithm to solve such an optimization problem. Boundary/interior vertices are viewed as fixed/free nodes, respectively. For each iteration of the Levenberg-Marquardt algorithm, we evaluate the maximum α_{max}, minimum α_{min}, and average α_{ave} of the sum of angles around each interior vertex for a termination criterion. Correspondingly, we introduce the errors of e_{max}, e_{min}, and e_{ave} represented

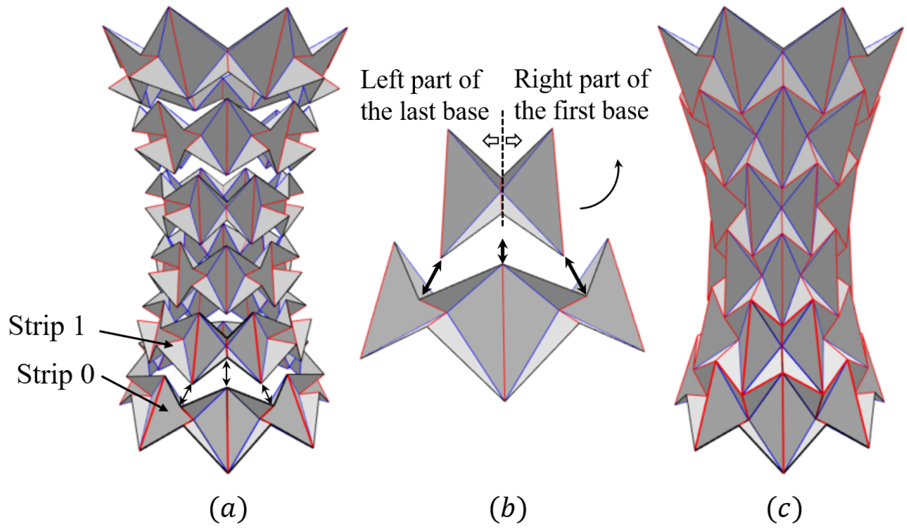

Figure 6.5: Merging waterbomb bases to achieve base mesh

as:

$$\begin{aligned} e_{max} &= |360° - \alpha_{max}|. \\ e_{min} &= |360° - \alpha_{min}|. \\ e_{ave} &= |360° - \alpha_{ave}|. \end{aligned} \tag{6.2}$$

Moreover, we introduce e_{total} as the maximum among e_{max}, e_{min}, and e_{ave}. The procedure is terminated when e_{total} is less than e_d. In our experiment, we set e_d as $1e$-5 to produce a developable surface.

Figure 6.6 shows graphs of convergence created during optimization on the base mesh (Figure 6.2 (c)), where Figure 6.6 (a) shows the relationship between the numbers of iterations and values of α_{max}, α_{min}, and α_{ave}. Correspondingly, Figure 6.6 (b) demonstrates the values of e_{max}, e_{min}, and e_{ave} that calculated during the iterations. In this case, e_{total} becomes less than $1e$-5 when the number of iterations is 198.

6.2 Results

We developed a prototype system using Java to implement our method. We ran our system on an Intel(R) Core(TM) i7-4770 CPU with an 8-GB-RAM PC. For a given target surface, our method allows the user to generate base meshes with variable resolutions and then produces developable approximations. As shown in Figure 6.7, we show four results, each of which contains a base mesh, its corresponding approximation, and the approximation with the target surface, as shown in Figure 6.2 (a).

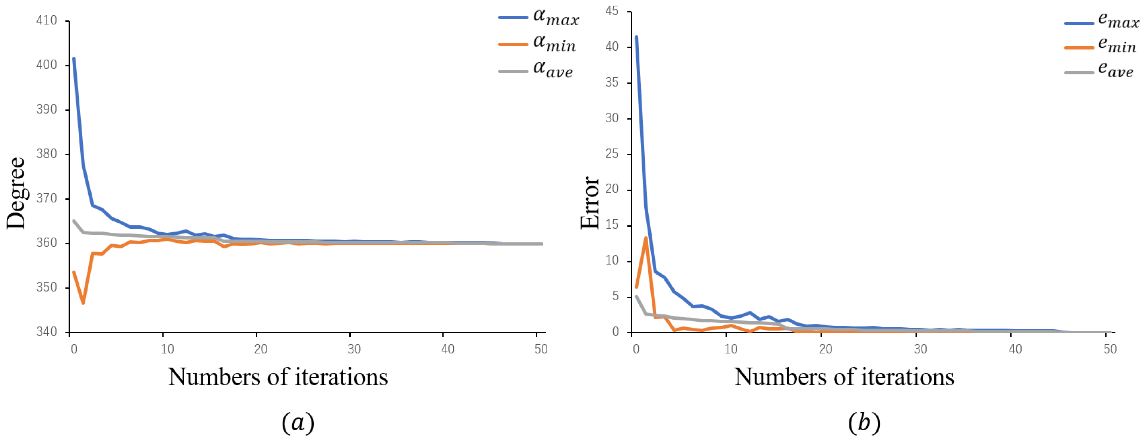

Figure 6.6: Graphs of convergence created during optimization for producing developable surface

Table 6.1 shows the parameters in detail and the results of the models shown in Figure 6.7. e_{total} of each approximation was less than $1e$-5 after optimization, with which we consider the approximation to be developable. To evaluate the difference between the resultant approximation A and the target surface T, we define distance $d(A, T)$ as:

$$
\begin{aligned}
d(A,T) &= \text{mean}\left[d(x,T)\right], x \in A, \\
d(x,T) &= \min\left[d(x,y)\right], y \in T,
\end{aligned}
\tag{6.3}
$$

where x and y denote vertices of the approximation A and the target surface T, respectively. $d(x, y)$ denotes the Euclid distance between x and y. $d(x, T)$ is the shortest distance between x and a set of y from T. $d(A, T)$ is similar in spirit to the Hausdorff distance, which is used to measure the difference between two surfaces. To compute $d(x, T)$, we sample all vertices from the approximation A for x by considering A is a discrete tessellation. When the target surface T is continuous, Dudte et al. [20] use an optimization procedure to find the optimized u and v coordinates, which let the distance between y and x become shortest. Here, we densely sample a set of y by subdividing T, and then find the closest y for x. $d(A, T)$ is normalized by the diagonal length of the bounding box of the target surface T. Note that we are only concerned about the difference from A to T and do not measure the inverse distance $d(T, A)$; $d(A, T)$ and $d(T, A)$ are different because they are not symmetric. In Table 6.1, we note that as the number of waterbomb bases increased, $d(A, T)$ decreased, which means that the result became closer to the target surface at the cost of more computational time.

We fabricated several approximations, shown in Figure 6.8, where (a) shows a catenoid and (b) shows a cylinder. Both approximations contained 48 waterbomb bases. (c) shows a sphere containing 75 waterbomb bases, and (d) shows a vase containing 112 waterbomb bases. For each result shown in Figure 6.8, we demonstrate a 3D model of the approxima-

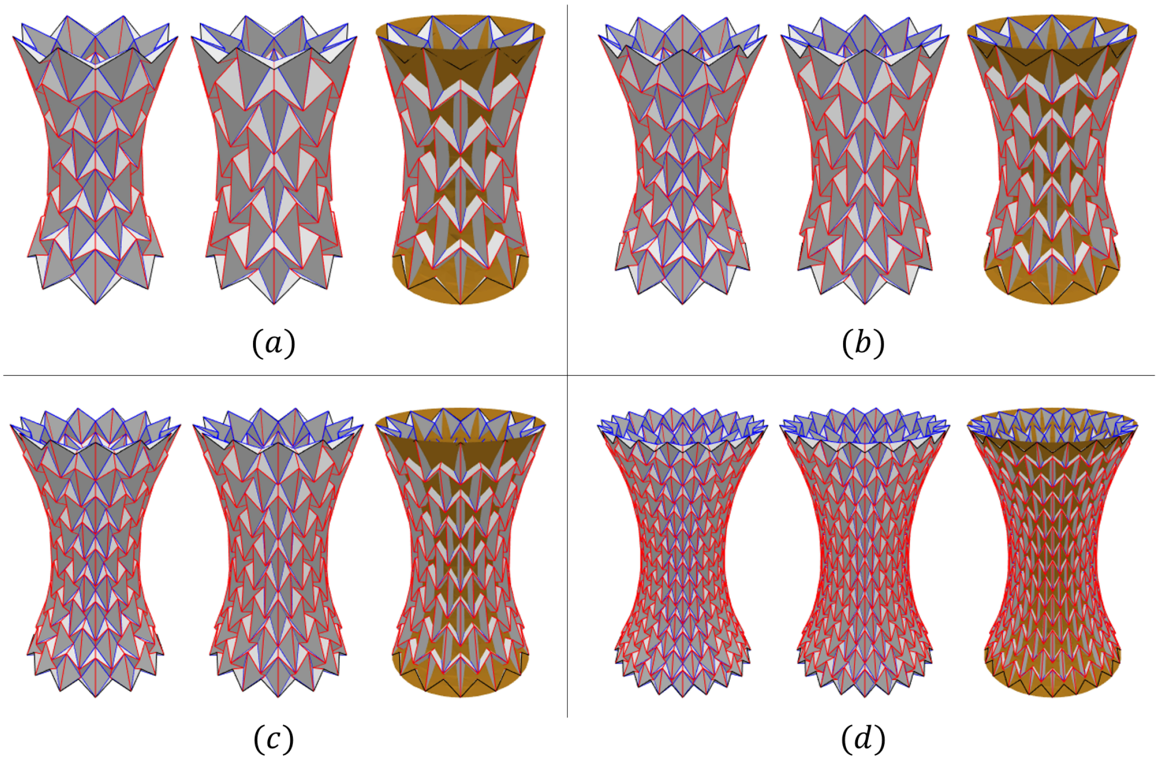

Figure 6.7: Approximations with variable resolutions for same target surface

tion, a crease pattern, and an origami piece.

We also approximated several 3D surfaces and show its crease pattern and rendered 3D model in Figure 6.9, where (a) shows an approximation of a catenoid, (b) a sphere, (c) a cylinder, (d) a vase, (e) a torus, (f) a hyperbolic paraboloid, (g) a möbius strip. Details of the target surfaces are demonstrated in Table 6.2.

Each surface ((a) to (e)) has an axisymmetric structure, and thus the boundary vertices along the left and right parts of the crease pattern are located at identical 3D positions to form the resulting approximation. Note that these vertices, which are used to connect the left and right parts of the crease pattern, have six adjacent facets in the 3D model. Therefore, we also applied our optimization process to these vertices in order to make them developable. For approximating torus, we not only connect the left and right parts of the crease pattern, but also the top and bottom parts (when N_v is even). As a result, we can generate a seamless approximation of torus (Figure 6.9 (e)). Additionally, we show an approximation of a hyperbolic paraboloid, which is the non-axisymmetric surface in Figure 6.9 (f), and an approximation of a Möbius strip, which is the non-orientable surface in Figure 6.9 (g). The Möbius strip approximation is not connected because the waterbomb bases at the start and end parts of the approximation had different orientations. Meanwhile, we demonstrate the

Table 6.1: Parameters in detail and statistics of models shown in Figure 6.7

Approximations	N_u	N_v	Bases	e_{total}	$d(A,T)$	Time
(a)	8	6	48	9.68e-6	3.29e-2	0.31 min
(b)	10	7	70	6.54e-6	2.95e-2	0.85 min
(c)	13	9	117	9.80e-6	2.41e-2	9.35 min
(d)	20	14	280	9.94e-6	1.61e-2	158.60 min

Table 6.2: Target surfaces used for generating developable approximations shown in Figure 6.9

Targets	Equations (x, y, z)
(a)	$(\cosh \frac{v}{2.5} \cos u, \cosh \frac{v}{2.5} \sin u, v), u \in [0, 2\pi], v \in [-\pi, \pi]$
(b)	$(\cos v \cos u, \cos v \sin u, \sin v), u \in [0, 2\pi], v \in \left[\frac{-\pi}{2.2}, \frac{\pi}{2.2}\right]$
(c)	$(\cos u, \sin u, v), u \in [0, 2\pi], v \in [-\pi, \pi]$
(d)	$((2 + \sin v) \cos u, (2 + \sin v) \sin u, -v), u \in [0, 2\pi], v \in [-3, 4]$
(e)	$((3 + \cos v) \sin u, (3 + \cos v) \cos u, \sin v), u \in [0, 2\pi], v \in [-\pi, \pi]$
(f)	$(u, v, uv), u \in [-1, 1], v \in [-1, 1]$
(g)	$((1 + \frac{v}{2} \cos \frac{u}{2}) \cos u, (1 + \frac{v}{2} \cos \frac{u}{2}) \sin u, \frac{v}{2} \sin \frac{u}{2}), u \in [0, 2\pi], v \in [-1, 1]$

detail results of the approximations (Figure 6.9) in Table 6.3 correspondingly.

In terms of fabrication, folding a waterbomb tessellation is not an easy task because it requires multi-fold simultaneous actuation. The folding process becomes more difficult when the waterbomb tessellation contains more waterbomb bases. Pre-folding crease lines on a sheet of paper can alleviate this problem. However, for a paper containing high density of creases, the material could become crumpled and the crease lines could become fuzzy after several pre-foldings. Therefore, we showed only crease patterns and rendered 3D models (Figure 6.9) instead of results with folded paper. A more effective way for fabricating complex approximations with many waterbomb bases would be printing the crease patterns on a textile using polymers because a textile can be folded many times without obvious fatigue.

Table 6.3: Details of statistics of models shown in Figure 6.9

Approximations	N_u	N_v	Bases	e_{total}	$d(A, T)$	Time
(a)	10	10	100	9.43e-6	2.60e-2	4.79 min
(b)	25	10	250	9.96e-6	1.44e-2	152.27 min
(c)	10	10	100	9.53e-6	1.59e-2	2.58 min
(d)	21	10	210	9.80e-6	1.59e-2	74.09 min
(e)	55	10	550	9.96e-6	8.97e-3	853.18 min
(f)	10	10	100	6.22e-6	1.35e-2	2.35 min
(g)	22	3	66	9.29e-6	1.40e-2	0.44 min

6.3 Summary

We proposed a method for approximating target surfaces, which are parametric surfaces of varying or constant curvatures, using generalized waterbomb tessellations. First, we described the generation of a base mesh by tiling the target surface using waterbomb bases. Then, we applied a simple numerical optimization algorithm to the base mesh to produce a developable approximation. Several developable approximations were presented to demonstrate the validity of our method. We provided a prototype system which enables us to interactively generate base meshes with variable resolutions and modify waterbomb bases.

Our work is different from $Origamizer$ [77, 80] and the system [81], because ours is not based on the tucking technique, which hides unnecessary areas of a sheet of paper inside the shape. Our method is also differs from $Freeform\ Origami$ [78], which generates a freeform surface by dragging the vertices of an origami in 3D. In addition, several existing approximating works were based on modified Miura-ori [98, 74, 20], while we focus on the waterbomb tessellation, another basic origami tessellation, to fit on target surfaces. We have demonstrated that our method can tile waterbomb bases on target surfaces, which can be axisymmetric or non-axisymmetric as well as orientable or non-orientable.

As future work, three aspects of our study can be improved: (i) finding an optimal density to balance the approximation accuracy and amount of fabrication labor when generating a base mesh, (ii) achieving a developable approximation while restricting $d(A, T)$, that is, the distance between the resultant approximation A and target surface T, and (iii) generating flat-foldable and self-intersection-free approximations. Furthermore, we hope this work can be extended to approximate complex 3D models which can be parameterized into $uv-$plane and pave the way of fully solving the inverse-origami-design problem.

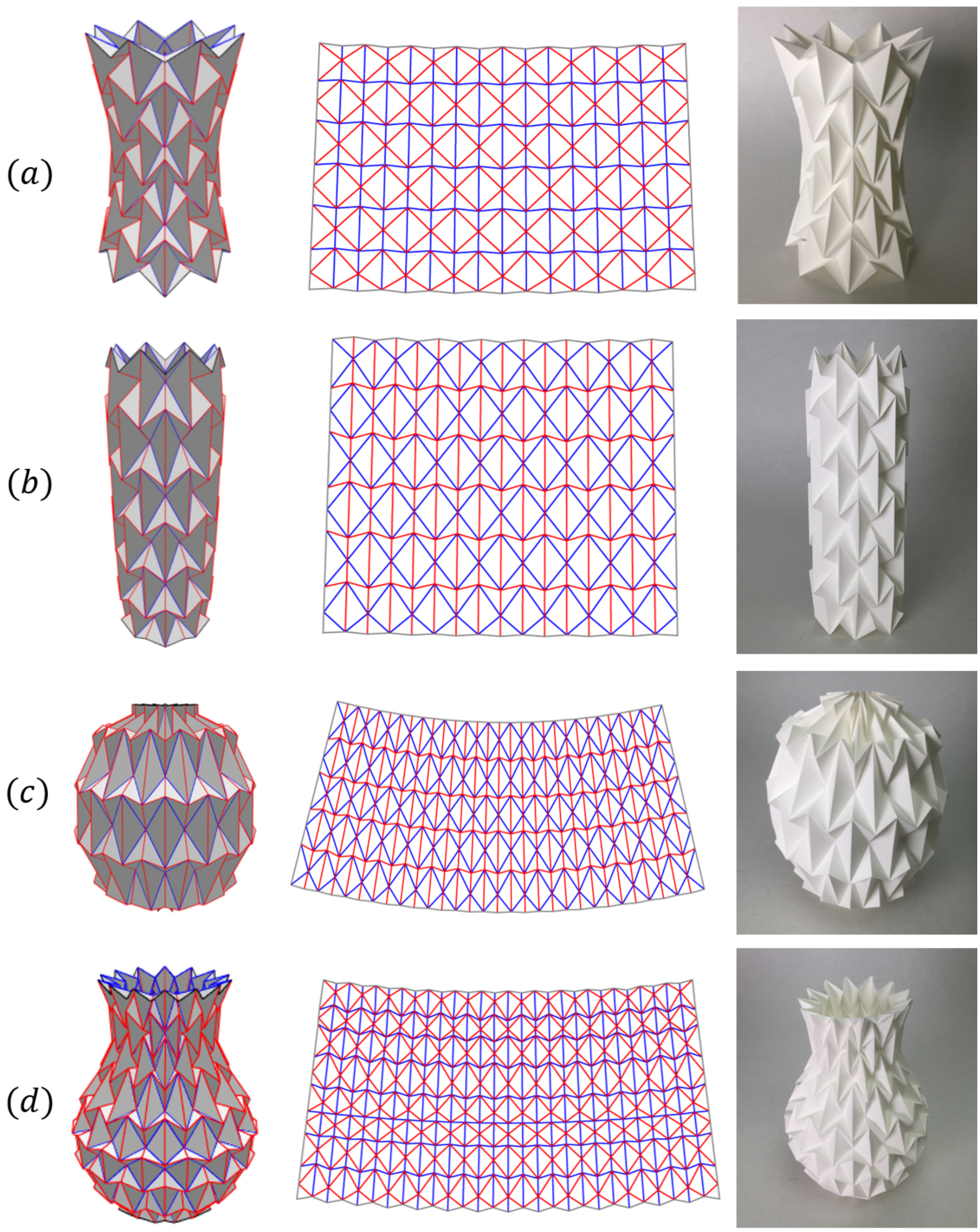

Figure 6.8: Fabricated origami pieces

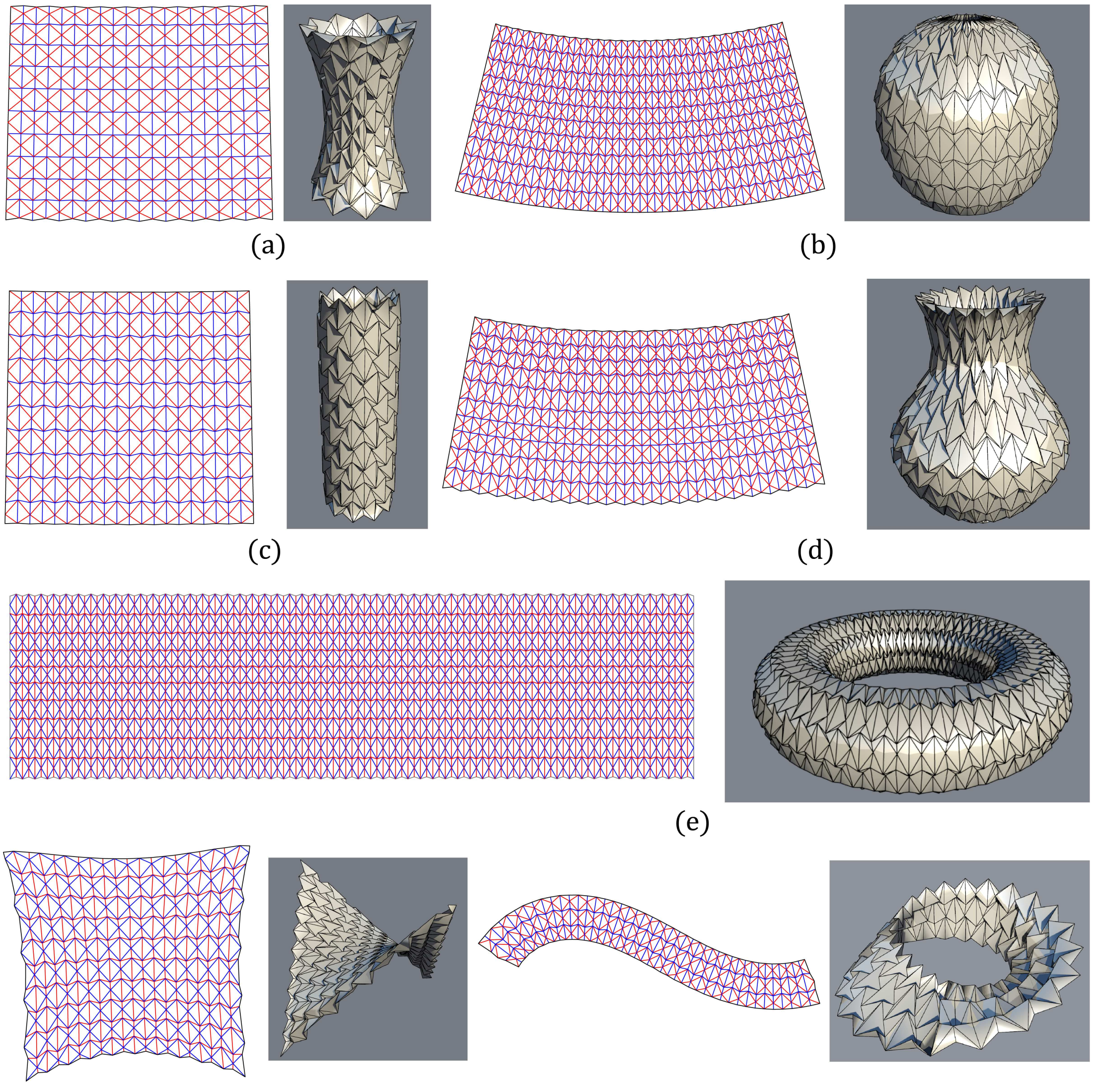
(a) (b) (c) (d) (e) (f) (g)

Figure 6.9: Developable approximations consisting of generalized waterbomb tessellations

Chapter 7

Conclusion and Future work

In this thesis, we focused on the goal of designing novel triangle-based 3D origami. First, we proposed three methods for designing axisymmetric 3D origami. In particular, we proposed a design method based on rotationally-symmetric crease patterns. Then, we tuck such a kind of 3D origami. Last, we proposed a design method for axisymmetric 3D origami with generic six-crease bases. By using these methods, users can create 3D origami that satisfies the developable constraint. Second, we proposed a method for approximating target 3D surfaces using generalized waterbomb tessellations. By applying a simple numerical optimization algorithm, developable tessellations can be achieved. The validity of our methods is verified through fabrications and simulation.

7.1 Summary of Contributions

We summarize the contributions of this thesis as follows:

- **Axisymmetric 3D origami based on rotationally-symmetric crease patterns:** We have described a design method for a family of axisymmetric 3D origami folded from rotationally-symmetric crease patterns. We focused on the axisymmetric property to introduce a rotationally-symmetric crease pattern. Benefiting from the symmetric property, developable constraint can be satisfied. Then, we described the details of the calculation of the geometry. For the calculation of $P_i(i > 1)$, the two intersection points of the solution circles were selected as solution candidates. Each of them was used to create different 3D models. During the calculation, we found a special case where the two solution circles are identical; thus, the candidate solutions are not two points but all the points on the solution circle. We have applied the special case in designing origami pieces with a flat center surrounded by triangular facets.

  Furthermore, we have analyzed the effects of variations by changing two parameters: angle φ and Θ. First, we have achieved a motion that rigidly transforms one fold-state to unfold-state by continuously changing φ to 90°. Second, we introduced a way of folding called "along-arc flat-folding" by changing the value of Θ. We have showed the along-arc flat-folding sequences and practiced such folding in real origami pieces. The presented rigid motions can be potentially used for self-folding mechanism.

- **Tucking axisymmetric 3D origami:** We focused on a family of axisymmetric triangle-based 3D origami folded from the rotationally-symmetric crease patterns and proposed a computational design method for tucking such origami. The proposed method can handle the crease pattern consisting of blank spaces emerged during the 3D edition. Such blank spaces are caused by interior vertices with non-zero angle deficit. We have considered the edge symmetry of the blank spaces and divided such areas into triangles by adding additional creases and vertices. Then, we have described the calculation of the shapes folded from the areas, which are called as flaps outside or tucks inside of the edited shapes. By adding flaps or tucks, we have made the edited 3D shapes realizable through tucking. We have implemented a prototype system which supports 3D editing and demonstrated several novel 3D origami with flaps or tucks. Finally, on the application side, we have described a load-bearing experiment on a stool shape-like origami to demonstrate the potential usage.

- **Axisymmetric 3D origami with generic six-crease bases:** We have described a design method for a class of axisymmetric 3D origami with generic six-crease bases, for which the lengths of the crease lines can be regular or irregular. First, we interactively generate a crease pattern consisting of such generic bases. Then, our method analytically calculates the 3D origami shape with an axisymmetric structure. We have demonstrated various configurations to explore the variations of the calculated 3D model. We illustrated several novel 3D origami pieces, some of which can have varying curvature.

  Furthermore, we have described a rigid folding motion that can deploy or flat fold the 3D origami axisymmetrically by continually changing parameter Θ. We have described the calculation of degree of freedom and the folding process triggered by changing Θ. Then, we have shown that the 3D origami is locally flat-foldable based on the satisfaction of Kawasaki's theorem. Finally, we have analyzed the kinematic behavior by illustrating the relationship between the folding rate and dihedral angles at selected vertices on 3D origami. This rigid one-parameter motion has potential applications ranging from self-folding tessellations to deployable architectures.

- **Approximating 3D surfaces using origami tessellations:** We have proposed a method for approximating target surfaces, which are parametric surfaces of varying or constant curvatures, using generalized waterbomb tessellations. First, we have described the generation of a base mesh by tiling the target surface using waterbomb bases. Then, we have applied a simple numerical optimization algorithm to the base mesh to produce a developable approximation. Several developable approximations were presented to demonstrate the validity of our method. The implemented system enables us to generate base meshes with variable resolutions and modify waterbomb bases interactively. Our work provides a solution for the inverse-origami-design problem based on the generalized waterbomb tessellations.

Existing design methods for 3D origami have demonstrated lots of geometrically appealing designs. However, these methods are focused on specific types of origami, and thus the variations of the shapes made by these methods are still small compared to the variations of folding a piece of paper. To explore new variations, we proposed several design methods for triangle-based 3D origami. By using our prototype systems, users can design such a kind 3D origami, which could not be easily generated by using existing methods.

In addition, existing design methods have put their emphasis on creating 3D shapes but not on investigating the deformations. In this thesis, as for the axisymmetric 3D origami, we demonstrated rigid folding motions about a common axis. Besides, we illustrated various deformations by changing input configurations. These results can be the basis for creating novel foldable mechanisms.

For designing non-axisymmetric 3D origami, we use generalized waterbomb tessellations to approximate parametric surfaces. Fitting target 3D surfaces using origami can be viewed as an inverse-origami-design problem. Although several methods have been proposed, most of them are based on Miura-ori. It is the first time to use waterbomb tessellations for solving this problem. Owing to the high degree of freedom, non-orientable target surfaces can be handled. In addition, by using the same optimization process on a well-defined initial base mesh, our method can be easily extended on general 3D surfaces. Furthermore, the procedure can be applied to different origami tessellation for exploring better approximations.

The proposed methods in this thesis are mainly classified into two parts: i) design methods for axisymmetric 3D origami, ii) approximating parametric surfaces using generalized waterbomb tessellations. For designing a complex 3D origami, waterbomb tessellations with high resolution could an option. On the other hand, curved-crease origami has demonstrated its ability to form a 3D structure using a small number of creases. Besides, the tuck technique has been used for hiding a part of paper into the model. A combination of the curved-crease origami and the tuck technique could be another solution for designing complex 3D origami.

7.2 Future Work

We envision our long-term goal. Although our research provided a number of novel 3D origami, several challenges and open questions remain. Three questions are of particular important in the context of designing and applying origami:

Thickness of origami: Considering the thickness of origami in the design process is a relatively new area. This topic began with the application of origami to the engineering, in which the thickness of the material cannot be ignored. However, most of the design methods, including the methods proposed in this thesis, are based on an ideal zero-thickness condition. Adding thickness is one direction of our research, which could board of application of the proposed origami.

Fully analysis in terms of folding motion: We have demonstrated and analyzed one-parameter folding motions. Calculating the folding path is a key issue for designing a self-folding origami. Therefore, we intend to put our emphasis on the fully analysis of the rigid motion for a general case.

Function-driven design of origami: Currently, we design an origami based on the geometric constraints. Thus the design space could not match the function, which is required for specific application. In the future, a combination of geometry and function considerations is needed in the design process.

Finally, we are also noticed that kirigami, with folding and cutting, can also generate complex 3D shapes and be a solution for specific applications ranging from self-foldable robots to architecture. A survey of this subject is given by [7]. Without the developable constraint, which origami should obey, kirigami shows its flexible to some extent. Using kirigami to design 3D shapes could also be one direction of our research.

References

[1] The Waterbomb. `http://www.britishorigami.info/academic/lister/waterbomb.php`. Accessed: 2017-12-06

[2] Ahmed, S., Lauff, C., Crivaro, A., McGough, K., Sheridan, R., Frecker, M., von Lockette, P., Ounaies, Z., Simpson, T., Lien, J.M., et al.: Multi-field responsive origami structures: Preliminary modeling and experiments. ASME Paper No. DETC2013-12405 (2013)

[3] An, B., Benbernou, N., Demaine, E.D., Rus, D.: Planning to fold multiple objects from a single self-folding sheet. Robotica **29**(1), 87–102 (2011)

[4] Bateman, A.: Paper mosaic origami tessellations. `http://www.papermosaics.co.uk/software.html`. Accessed: 2016-10-06

[5] Bern, M., Hayes, B.: The complexity of flat origami. In: SODA, vol. 96, pp. 175–183 (1996)

[6] Cai, J., Deng, X., Xu, Y., Feng, J.: Motion analysis of a foldable barrel vault based on regular and irregular yoshimura origami. In: Journal of Mechanisms and Robotics, vol. 8, p. 021017. American Society of Mechanical Engineers (2016)

[7] Callens, S.J., Zadpoor, A.A.: From flat sheets to curved geometries: Origami and kirigami approaches. Materials Today (2017)

[8] Cipra, B.A.: In the fold: Origami meets mathematics. SIAM news **34**(8), 1–4 (2001)

[9] Cromvik, C., Eriksson, K.: Airbag folding based on origami mathematics. Origami **4**, 129–139 (2006)

[10] Davis, E., Demaine, E.D., Demaine, M.L., Ramseyer, J.: Reconstructing david huffman's origami tessellations. In: Journal of Mechanical Design, vol. 135, p. 111010. American Society of Mechanical Engineers (2013)

[11] De Focatiis, D., Guest, S.: Deployable membranes designed from folding tree leaves. Philosophical Transactions of the Royal Society of London A: Mathematical, Physical and Engineering Sciences **360**(1791), 227–238 (2002)

[12] De Temmerman, I.a.N., Mollaert, M., Van Mele, I.a.T., De Laet, I.a.L.: Design and analysis of a foldable mobile shelter system. International Journal of Space Structures **22**(3), 161–168 (2007)

[13] Debnath, S., Fei, L.: Origami theory and its applications: A literature review. World Academy of Science, Engineering and Technology pp. 1131–1135 (2013)

[14] Demaine, E., Demaine, M., Koschitz, D.: Reconstructing david huffmans legacy in curved-crease folding. Origami **5**, 39–52 (2011)

[15] Demaine, E.D.: Folding and unfolding linkages, paper, and polyhedra. In: Japanese Conference on Discrete and Computational Geometry, pp. 113–124. Springer (2000)

[16] Demaine, E.D., Demaine, M.L., Huffman, D.A., Koschitz, D., Tachi, T.: Characterization of curved creases and rulings: Design and analysis of lens tessellations. Origami **6**, 209–230 (2015)

[17] Demaine, E.D., Demaine, M.L., Koschitz, D., Tachi, T.: Curved crease folding: a review on art, design and mathematics. In: Proceedings of the IABSE-IASS Symposium: Taller, Longer, Lighter (IABSE-IASS2011), London, England, Sept, pp. 20–23 (2011)

[18] Demaine, E.D., ORourke, J.: Geometric folding algorithms. Cambridge university press Cambridge (2007)

[19] Demaine, E.D., Tachi, T.: Origamizer: A practical algorithm for folding any polyhedron. In: LIPIcs-Leibniz International Proceedings in Informatics, vol. 77. Schloss Dagstuhl-Leibniz-Zentrum fuer Informatik (2017)

[20] Dudte, L.H., Vouga, E., Tachi, T., Mahadevan, L.: Programming curvature using origami tessellations. Nature materials **15**, 583–588 (2016)

[21] Dureisseix, D.: An overview of mechanisms and patterns with origami. International Journal of Space Structures **27**(1), 1–14 (2012)

[22] Early, J.T., Hyde, R., Baron, R.L.: Twenty-meter space telescope based on diffractive fresnel lens. In: UV/Optical/IR Space Telescopes: Innovative Technologies and Concepts, vol. 5166, pp. 148–157. International Society for Optics and Photonics (2004)

[23] Edwards, A., Yan, H.: Dna origami. In: Nucleic Acid Nanotechnology, pp. 93–133. Springer (2014)

[24] Evans, T.A., Lang, R.J., Magleby, S.P., Howell, L.L.: Rigidly foldable origami gadgets and tessellations. In: Royal Society open science, vol. 2, p. 150067. The Royal Society (2015)

[25] Felton, S., Tolley, M., Demaine, E., Rus, D., Wood, R.: A method for building self-folding machines. Science **345**(6197), 644–646 (2014)

[26] Felton, S.M., Tolley, M.T., Shin, B., Onal, C.D., Demaine, E.D., Rus, D., Wood, R.J.: Self-folding with shape memory composites. Soft Matter **9**(32), 7688–7694 (2013)

[27] Filipov, E., Paulino, G., Tachi, T.: Origami tubes with reconfigurable polygonal cross-sections. In: Proc. R. Soc. A, vol. 472, p. 20150607. The Royal Society (2016)

[28] Fink, M., Montaldo, G., Tanter, M.: Time-reversal acoustics in biomedical engineering. Annual review of biomedical engineering **5**(1), 465–497 (2003)

[29] Francis, K.C., Rupert, L.T., Lang, R.J., Morgan, D.C., Magleby, S.P., Howell, L.L.: From crease pattern to product: Considerations to engineering origami-adapted designs. ASME Paper No. DETC2014-34031 (2014)

[30] Gjerde, E.: Origami tessellations: awe-inspiring geometric designs. AK Peters/CRC Press (2008)

[31] Haas, F., Wootton, R.J.: Two basic mechanisms in insect wing folding. Proceedings of the Royal Society of London B: Biological Sciences **263**(1377), 1651–1658 (1996)

[32] Hans, M.: Wingler, the bauhaus: Weimar, dessau, berlin, chicago, trans. Joseph Stein p. 534 (1978)

[33] Hawkes, E., An, B., Benbernou, N.M., Tanaka, H., Kim, S., Demaine, E., Rus, D., Wood, R.J.: Programmable matter by folding. In: Proceedings of the National Academy of Sciences, vol. 107, pp. 12,441–12,445. National Acad Sciences (2010)

[34] Hoffmann, R.: Airbag folding: Origami design applied to an engineering problem. In: 3rd International Meeting of Origami Science, Math, and Education, Asilomar, CA, Mar, pp. 9–11 (2001)

[35] Huffman, D.A.: Curvature and creases: A primer on paper. IEEE Transactions on computers (10), 1010–1019 (1976)

[36] Hunt, G., Lord, G.J., Peletier, M.A.: Cylindrical shell buckling: a characterization of localization and periodicity. Discrete and Continuous Dynamical Systems Series B **3**(4), 505–518 (2003)

[37] Ida, T., Takahashi, H., Marin, M., Kasem, A., Ghourabi, F.: Computational origami system eos. In: Origami 4-Fourth International Meeting of Origami Science, Mathematics and Education, pp. 285–294 (2009)

[38] Jacobsen, L.: Fra fladt papir til foldet lampeskærm (2008)

[39] Kasahara, K., Maekawa, J.: Viva! origami. Sanrio, Tokyo, Japan (1983)

[40] Kawasaki, T.: On the relation between mountain-creases and valley-creases of a flat origami. In: Proceedings of the 1st International Meeting of Origami Science and Technology, pp. 229–237 (1989)

[41] Kilian, M., Flöry, S., Chen, Z., Mitra, N.J., Sheffer, A., Pottmann, H.: Curved folding. In: ACM Transactions on Graphics (TOG), vol. 27, p. 75. ACM (2008)

[42] Kobayashi, H., Kresling, B., Vincent, J.F.: The geometry of unfolding tree leaves. Proceedings of the Royal Society of London B: Biological Sciences **265**(1391), 147–154 (1998)

[43] Kuribayashi, K., Tsuchiya, K., You, Z., Tomus, D., Umemoto, M., Ito, T., Sasaki, M.: Self-deployable origami stent grafts as a biomedical application of ni-rich tini shape memory alloy foil. Materials Science and Engineering: A **419**(1), 131–137 (2006)

[44] Lang, R.J.: TreeMaker. `http://www.langorigami.com/article/treemaker/`. Accessed: 2017-12-06

[45] Lang, R.J.: A computational algorithm for origami design. In: Proceedings of the twelfth annual symposium on Computational geometry, pp. 98–105. ACM (1996)

[46] Lang, R.J.: The science of origami. In: Physics world, vol. 20, p. 30. IOP Publishing (2007)

[47] Lang, R.J.: Computational origami: from flapping birds to space telescopes. In: Proceedings of the twenty-fifth annual symposium on Computational geometry, pp. 159–162. ACM (2009)

[48] Lebée, A.: From folds to structures, a review. International Journal of Space Structures **30**(2), 55–74 (2015)

[49] Lee, D.Y., Kim, J.S., Kim, S.R., Koh, J.S., Cho, K.J.: The deformable wheel robot using magic-ball origami structure. In: ASME 2013 International Design Engineering Technical Conferences and Computers and Information in Engineering Conference, pp. V06BT07A040–V06BT07A040. American Society of Mechanical Engineers (2013)

[50] Ma, J., You, Z.: The origami crash box. Origami **5**, 277–290 (2011)

[51] Ma, J., You, Z.: A novel origami crash box with varying profiles. In: ASME 2013 International Design Engineering Technical Conferences and Computers and Information in Engineering Conference, pp. DETC2013–13,495. American Society of Mechanical Engineers (2013)

[52] Martínez-Martín, F., Thrall, A.: Honeycomb core sandwich panels for origami-inspired deployable shelters: Multi-objective optimization for minimum weight and maximum energy efficiency. Engineering Structures **69**, 158–167 (2014)

[53] Matsukawa, Y., Yamamoto, Y., Mitani, J.: Enumeration of flat-foldable crease patterns in the square/diagonal grid and their folded shapes. In: Proc. of 17th International Conference on Geometry and Graphics (ICGG2016), Article, vol. 33 (2016)

[54] Meguro, T.: The method to design origami. Origami Tanteidan Newspaper (1991)

[55] Mitani, J.: ORIPA (origami pattern editor). `http://mitani.cs.tsukuba.ac.jp/oripa/` (2005). Accessed: 2017-12-06

[56] Mitani, J.: Development of origami pattern editor (oripa) and a method for estimating a folded configuration of origami from the crease pattern. IPSJ Journal **48**(9), 3309–3317 (2007)

[57] Mitani, J.: Rendering method for flat origami. In: Eurographics (Short Papers), pp. 107–110 (2008)

[58] Mitani, J.: A design method for 3D origami based on rotational sweep. Computer-Aided Design and Applications **6**(1), 69–79 (2009)

[59] Mitani, J.: A design method for axisymmetric curved origami with triangular prism protrusions. In: Origami 5: Fifth International Meeting of Origami Science, Mathematics, and Education, pp. 437–447. CRC Press (2011)

[60] Mitani, J.: ORI-REVO: A design tool for 3d origami of revolution. `http://mitani.cs.tsukuba.ac.jp/ori_revo/` (2011). Accessed: 2017-12-06

[61] Mitani, J.: Column-shaped origami design based on mirror reflections. Journal for Geometry and Graphics **16**(2), 185–194 (2012)

[62] Mitani, J., Igarashi, T.: Interactive design of planar curved folding by reflection. In: Pacific Graphics (2011)

[63] Miura, K.: Method of packaging and deployment of large membranes in space. In: title The Institute of Space and Astronautical Science report, vol. 618, p. 1 (1985)

[64] Miura, K.: Map fold a la miura style, its physical characteristics and application to the space science. Research of Pattern Formation pp. 77–90 (1994)

[65] Miyashita, S., Guitron, S., Ludersdorfer, M., Sung, C.R., Rus, D.: An untethered miniature origami robot that self-folds, walks, swims, and degrades. In: Robotics and Automation (ICRA), 2015 IEEE International Conference on, pp. 1490–1496. IEEE (2015)

[66] Nangreave, J., Han, D., Liu, Y., Yan, H.: Dna origami: a history and current perspective. Current opinion in chemical biology **14**(5), 608–615 (2010)

[67] Nojima, T.: Modelling of folding patterns in flat membranes and cylinders by origami. JSME International Journal Series C Mechanical Systems, Machine Elements and Manufacturing **45**(1), 364–370 (2002)

[68] Quagli, C., Ballard, Z., Thrall, A.: Parametric modelling of an air-liftable origami-inspired deployable shelter with a novel erection strategy. Mobile and Rapidly Assembled Structures IV **136**, 23–33 (2014)

[69] Resch, R.D.: The topological design of sculptural and architectural systems. In: Proceedings of the June 4-8, 1973, national computer conference and exposition, pp. 643–650. ACM (1973)

[70] Resch, R.D., Christiansen, H.: The design and analysis of kinematic folded plate systems. In: Proceedings of IASS Symposium on Folded Plates and Prismatic Structures (1970)

[71] Rothemund, P.W.: Folding dna to create nanoscale shapes and patterns. Nature **440**(7082), 297–302 (2006)

[72] Ryu, J., DAmato, M., Cui, X., Long, K.N., Jerry Qi, H., Dunn, M.L.: Photo-origamibending and folding polymers with light. In: Applied Physics Letters, vol. 100, p. 161908. AIP (2012)

[73] Schenk, M., Guest, S.: Folded shell structures. Ph.D. thesis (2012). University of Cambridge, Cambridge, United Kingdom

[74] Song, K., Zhou, X., Zang, S., Wang, H., You, Z.: Design of rigid-foldable doubly curved origami tessellations based on trapezoidal crease patterns. In: Proc. R. Soc. A, vol. 473, p. 20170016. The Royal Society (2017)

[75] Stewart, I.: Mathematics: some assembly needed. Nature **448**(7152), 419–419 (2007)

[76] Tachi, T.: Origamizer. `http://www.tsg.ne.jp/TT/software/index.html#origamizer`. Accessed: 2017-12-06

[77] Tachi, T.: 3D origami design based on tucking molecule. In: The Fourth International Conference on Origami in Science, Mathematics, and Education, R. Lang, ed., Pasadena, pp. 259–272 (2009)

[78] Tachi, T.: Freeform variations of origami. Journal for Geometry and Graphics, **14**(2), 203–215 (2010)

[79] Tachi, T.: Geometric considerations for the design of rigid origami structures. In: Proceedings of the International Association for Shell and Spatial Structures (IASS) Symposium, vol. 12, pp. 458–460 (2010)

[80] Tachi, T.: Origamizing polyhedral surfaces. IEEE Transactions on Visualization and Computer Graphics **16**(2), 298–311 (2010)

[81] Tachi, T.: Freeform origami tessellations by generalizing reschs patterns. In: ASME 2013 International Design Engineering Technical Conferences and Computers and Information in Engineering Conference, pp. V06BT07A025–V06BT07A025. American Society of Mechanical Engineers (2013)

[82] Tachi, T., Masubuchi, M., Iwamoto, M.: Rigid origami structures with vacuumatics: Geometric considerations. Paper presented at IASS-APCS Seoul, Korea, 21–24 May, 2012

[83] Thompson, J., Hunt, G., Tvergaard, V.: Elastic instability phenomena. Journal of Applied Mechanics **52**(1), 241–242 (1985)

[84] Thrall, A., Quaglia, C.: Accordion shelters: A historical review of origami-like deployable shelters developed by the us military. Engineering structures **59**, 686–692 (2014)

[85] Tørring, T., Voigt, N.V., Nangreave, J., Yan, H., Gothelf, K.V.: Dna origami: a quantum leap for self-assembly of complex structures. Chemical Society Reviews **40**(12), 5636–5646 (2011)

[86] Tsuruta, N., Mitani, J., Kanamori, Y., Fukui, Y.: A cad system for diagramming origami with prediction of folding processes. In: Origami 5: Fifth International Meeting of Origami Science, Mathematics, and Education, pp. 335–345. CRC Press (2011)

[87] Tsuruta, N., Mitani, J., Kanamori, Y., Fukui, Y.: An exploring tool for simple flat origami based on random foldings. In: International Conference on Simulation Technology (JSST2013) (2013)

[88] Tsuruta, N., Mitani, J., Kanamori, Y., Fukui, Y.: Simple flat origami exploration system with random folds. In: Origami 6: Sixth International Meeting of Origami Science, Mathematics, and Education, pp. 513–521. American Mathematical Society (2017)

[89] Wilson, L., Pellegrino, S., Danner, R.: Origami sunshield concepts for space telescopes. In: 54th AIAA/ASME/ASCE/AHS/ASC Structures, Structural Dynamics, and Materials Conference, p. 1594 (2013)

[90] Xi, Z., Lien, J.M.: Folding rigid origami with closure constraints. In: ASME 2014 International Design Engineering Technical Conferences and Computers and Information in Engineering Conference, pp. V05BT08A052–V05BT08A052. American Society of Mechanical Engineers (2014)

[91] Yamamoto, Y., Mitani, J.: ORI-RELIFE PIX. `http://www.npal.cs.tsukuba.ac.jp/projects/2017/pixel_graphics_by_tessellation/index.html` (2017). Accessed: 2017-12-06

[92] Yoshimura, Y.: On the mechanism of buckling of a circular cylindrical shell under axial compression. Reports of The Institute of Science and Technology, The University of Tokyo **5**, 179–198 (1951)

[93] You, Z., Kuribayashi, K.: Expandable tubes with negative poissons ratio and their application in medicine. Origami **4**, 117–127 (2009)

[94] Zhang, Q., Jiang, Q., Li, N., Dai, L., Liu, Q., Song, L., Wang, J., Li, Y., Tian, J., Ding, B., et al.: Dna origami as an in vivo drug delivery vehicle for cancer therapy. Acs Nano **8**(7), 6633–6643 (2014)

[95] Zhao, Y., Endo, Y., Kanamori, Y., Mitani, J.: Approximating 3d surfaces using generalized waterbomb tessellations (accepted). Journal of Computational Design and Engineering (2018)

[96] Zhao, Y., Kanamori, Y., Mitani, J.: Geometry of axisymmetric 3D origami consisting of triangular facets. Journal for Geometry and Graphics **21**(1), 107–118 (2017)

[97] Zhao, Y., Kanamori, Y., Mitani, J.: Design and motion analysis of axisymmetric 3d origami with generic six-crease bases. Computer Aided Geometric Design **59**(Supplement C), 86 – 97 (2018)

[98] Zhou, X., Wang, H., You, Z.: Design of three-dimensional origami structures based on a vertex approach. In: Proc. R. Soc. A, vol. 471, p. 20150407. The Royal Society (2015)

[99] Zirbel, S.A., Lang, R.J., Thomson, M.W., Sigel, D.A., Walkemeyer, P.E., Trease, B.P., Magleby, S.P., Howell, L.L.: Accommodating thickness in origami-based deployable arrays. In: Journal of Mechanical Design, vol. 135, p. 111005. American Society of Mechanical Engineers (2013)

[100] Zirbel, S.A., Trease, B.P., Thomson, M.W., Lang, R.J., Magleby, S.P., Howell, L.H.: Hanaflex: a large solar array for space applications. In: Micro-and Nanotechnology Sensors, Systems, and Applications VII, vol. 9467, p. 94671C. International Society for Optics and Photonics (2015)